Spatial Coupling of Biological Oscillators:
Towards a Quantitative Understanding of Mitotic Waves

by

Owen Puls

A dissertation submitted in partial fulfillment
of the requirements for the degree of
Doctor of Philosophy
(Physics)
in the University of Michigan
2023

Doctoral Committee:

Associate Professor Qiong Yang, Chair
Assistant Professor Jordan Horowitz
Associate Professor Puck Ohi
Associate Professor Kevin Wood
Professor Michal Zochowski

Owen Fischer Puls

owpuls@umich.edu

ORCID iD: 0000-0002-5097-3420

Dedication

To my mother, an everlasting fountain of love, support and guidance.

To my sister, without whose grounding example I would be a lesser man.

And to my father, for better or for worse.

Acknowledgements

Graduate school and the path to a PhD contain numerous struggles in normal times; the COVID-19 pandemic only exacerbated and expanded on them. Between months of isolation and long periods of experimental downtime, the journey to this journey's end started and stopped relentlessly, mostly outside anyone's control. As a result, while the work and knowledge presented in this document are my own, none of it would have come to be without the extensive help and support of countless individuals.

I would first extend my never-ending gratitude and love to my family. From weekly calls to any and all various care packages, to the ever-needed breaks back in Wisconsin, the Lorrigan family stood behind me with endless support. Words fail to communicate how lucky I am to have had this power at my side, and I can only imagine where I would be without it. More specifically, I must especially thank my mom and sister. In a developing theme, I am so terribly lucky to count two such strong and caring women as my rocks. The past few years have presented many obstacles outside of graduate school, as we three know acutely, and I know I made it through in no small part thanks to you both.

Second, my life would not, in no uncertain terms, be the same without my partner, Karley. She has come into my life and completely changed my concept of how happy I could be. She has provided continual support through the many ups and downs over the past years, even before we were together, but especially now. I must apologize to her for the angst and stress finishing my degree has caused us collectively, but I am excitedly looking forward to our life together moving forward.

Additionally, I must acknowledge the life-long friends who offered much-needed distraction, assurance and fun. To Johnathon and Jennifer, I cherish our weekly game nights, as well as your kindness and acceptance. To Nick and Kiegan, I look forward to each of our (almost) monthly dinners and other adventures. I will truly miss them once we move. To Harry, thank you for always joining me for coffee: these little jaunts always helped keep my spirits up. And finally, I cannot forget the DnD/boardgames/Bachelorette group who provided so many laughs over the years.

More directly relevant to the substance of this text, I would be remiss if I did not thank the Yang lab for all their help and guidance throughout my years here. Qiong warmly welcomed this physicist with no biological training and trusted me with a new project bereft of a clear ending. She has always given me support in any and all aspects of my education and research career. I cannot thank her enough. To the other members of the lab (all of whom also belong in the ”friends” section), certainly much less of this work would have seen the light of day without your help. Shiyuan, Gembu, Minjun and Franco: so much of what we frog people do comes from a strong sense of collaboration and mutual assistance, and I am so grateful for all of your help. To the other members of the lab—Usha, Chun-yen, Liam—thank you for your input and advice throughout the years. I know you all will go on to accomplish many great things. I will miss all of your knowledge and friendship.

Furthermore, I must extend sincere gratitude to our collaborators in the Gelens Lab: Lendert and Dani. Our discussions, as well as their significant theoretical and analytical contributions, helped us frame our observations in a clearer and more scientifically meaningful manner. Without them, the work presented here would likely remain less well-defined and explored.

I would also like to thank the members of my committee, Dr.'s Puck Ohi, Jordan Horowitz, Kevin Wood and Michal Zochowski, for both taking the time to help me finish out my graduate career, but also for all their insight and advice along the way. In particular, I want to thank Puck for graciously accepting me into his lab for a rotation some years ago. I learned so much from you and your group. That experience not only breathed new life into my research career, but also introduced me to a collection of wonderful people. I cannot thank you enough.

As my final personal note here, I will leave the reader with some words from the most important non-acquaintance in my life, to whom I owe much.

"**Wave on wave of life**
Like the great wide ocean's roll
Haunting hands of memory
Pluck silver strands of soul
The damage and the dying done
The clarity of light
Gentle bows and glasses raised
To the charity of night*"*
-- *Bruce Cockburn*

Table of Contents

List of Tables

List of Figures

Abstract

Over the years, various models were developed to capture the mechanism behind the mitotic clock. In short, the clock network centers on the cyclin-dependent kinase (Cdk1), such that its oscillatory rising and falling activity directs the cell through a series of steps which define one mitotic cycle. When a collection of these oscillators couple, they synchronize. In particular, early embryogenesis is marked by a series of synchronous cell divisions across the length of the embryo in various systems, e.g. *Drosophila* (approximately 0.5mm in length) and *Xenopus* (approximately 1.2mm in diameter). This synchrony allows embryos to simply grow in viability prior to differentiation, at which point, cell types diverge, and the physical form of the organism begins to take shape. However, the large size of these embryos implies a faster coordinating effect than diffusion alone.

Work in the field proposes a mechanism for such spatial coordination in the form of mitotic waves. However, this literature describes waves which fall into two categories: canonical trigger, or bistable waves, and recently proposed sweep waves. These two types of waves are separated by both the speeds at which they propagate and the biochemical mechanisms behind their formation. Nevertheless, recent work proposes a model by which sweep waves may transition to trigger waves if cycles slow heterogeneously over time. To this point, little-to-no work exists studying the time dependence of mitotic waves in either context.

Using *Xenopus* extracts and a Cdk1 FRET sensor, I exploit the slowing of oscillations in extracts to demonstrate such a transition for the first time. Moreover, I show how the addition of nuclei entrains the system to the trigger wave regime. Finally, using a novel approach utilizing

metaphase-arrested extracts, I produce one-dimensional directed mitotic waves without reconstituted nuclei. With this setup, I reinforce the notion of entrainment explicitly, as well as probe the possible differences between mitotic waves in systems with and without nuclei, finding the speed scaling of the former to be significantly slower. Additionally, my work lays the groundwork for this system to be used in the future to systematically study perturbations to these waves. In total, the presented work offers the first direct observation of mitotic waves in *Xenopus*, explains their time-dependent behavior, and displays a unique method for exploring biochemical waves experimentally.

Chapter 1

Introduction

Across the span of living organisms, the capacity to adapt and respond to the environment is essential. As a result, biological systems at all scales—cells, tissues, organisms—exist in a constant state of flux: DNA replicating, cells dividing, tissues growing, bodies moving. Such systems rely on biochemical interactions to ensure the accurate and precise execution of many of these processes. In many cases, these interactions occur cyclically and form a broad class of processes known as biochemical oscillations. Due to their ubiquity and fundamentality, it is of great importance that the timing and regularity of these processes be maintained. In fact, disturbances can lead to various diseases and maladies such as cancer or insomnia.

Thus, a significant fraction of research across disciplines focuses on understanding the design and function of such oscillators. In the Yang lab, multiple projects focus on one of two oscillating systems: the cell cycle and somitogenesis. In work on the cell cycle, almost all efforts are focused on single oscillators: cell cycles reconstituted in single micro-emulsion droplets. Through it, the lab hopes to discern the fundamental behavior of this invaluable process, including how it modulates its own function in response to environmental changes such as temperature or extraneous drugs. In the case of somitogenesis, while still considering oscillators generally, focuses more on collections of oscillators and how they communicate to form large-scale structures: in this case, somites. Here, my fellow graduate students study tissues, either intact or disassociated, to understand the coupling between different oscillatory systems over large distances.

My work sits at the intersection of these two classes of projects, focusing on how collections of mitotic oscillators couple together to form patterns and transmit information through biochemical waves. In this chapter, I will introduce the physical and biochemical history of biological oscillators and waves, laying the groundwork for my research work and its place in the field. Some of the following has been adapted from my previously published review (Puls and Yang, 2018).

1.1 Biochemical Oscillators

The nature and function of biological oscillators are very diverse. These oscillations are ubiquitous throughout nature and play a fundamental role in preserving life and fostering growth across evolutionary scales. In our own bodies for example, neurons fire on the scale of sub-seconds; single cells replicate and divide throughout the course of a day; and our inherent circadian rhythms inform our sleep schedule each night (Figure 1.1). As demonstrated in Figure 1.1, the timescales at which biochemical oscillators functions span orders of magnitude, pointing to the wide array of biological machinery at work (Li and Yang, 2018). Indeed, starting at the level of the nucleus, some oscillators involve the regulation of transcription/translation of genes; some oscillations are formed by proteins and other molecules interacting in the cytoplasm of cells; and yet others function at the cell membrane via ion-ion channel interactions (Li and Yang, 2018). Thus, both the type and scale of biological oscillators varies significantly across life.

Moreover, biological oscillations serve myriad functions depending on their nature and context (Figure 1.1). For example, some oscillators generate frequency-specific signals to inscribe regulatory information for gene expression and cell decision making processes: e.g. the signal transduction pathway of Ca^{2+} signaling (Isomura and Kageyama, 2014; Cai et al., 2008).

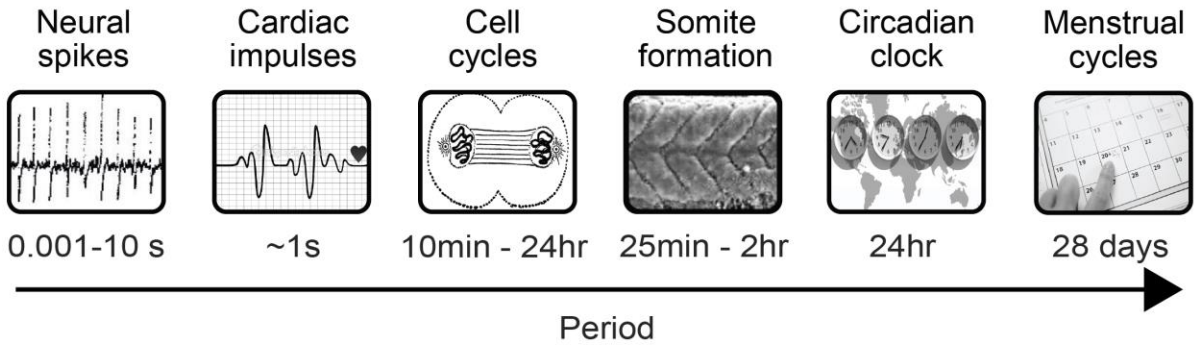

Figure 1.1 Biological Oscillators Span Orders of Magnitude in Period

Biological oscillators span orders of magnitude in period, ranging from fractions of seconds for neural spikes (left), to days for menstrual cycles (right). In order from right to left, examples of oscillators and their corresponding periods: neural spikes (Ainsworth et al., 2012), cardiac impulses (Cai et al., 2008), cell cycles (Murray and Kirschner, 1989), somite formation (Oates et al., 2012), circadian clocks (Bell-Pederse et al., 2005), and menstrual cycles (Grieger and Norman, 2020).

However, in most cases, and particularly relevant here, oscillators function as the pacemaker, or timekeeper, to control the regularity of a particular function. We are familiar with many of these pacemakers in our daily lives. Our heartbeats (Brown et al., 1979), breathing (Paydarfar and Eldridge, 1987), and sleep schedule (Bell-Pedersen et al., 2005; Forger and Peskin, 2003; Forger, 2017) all operate at regular and predictable frequencies through the function of an underlying pacemaker. To expand on the last example somewhat, the circadian clock, which regulates our sleep schedule, is found across the spectrum of organisms on earth. In short, this clock produces 24-hour rhythms in the activity of genes—one of which is aptly named the *Period* gene—which affect an organism's wakefulness and alertness (Forger, 2017). Regardless of function or makeup, biological oscillators play a critical role in biological regularity.

1.1.1 The mitotic clock and its underlying biochemical network

One of the most important processes in all of biology, cell division, is regulated by a well-studied pacemaker oscillator called the mitotic clock (Figure 1.2 B). The cell cycle (DNA-

replication-division cycle) is defined by the sequence of events by which cells replicate DNA and partition the copies into daughter cells such that each daughter receives precisely one copy of the genome (Tyson and Novak, 2015). In the case of non-growing cells (such as *Xenopus laevis* early embryos), this process(es) encompasses the entirety of a cell's lifetime and can be considered complete in that regard. Due to its importance in both development and life generally, biologists devoted much time and effort to understanding its function and control.

Like many essential well-conserved biological oscillations, including the circadian clock, the cell cycle clock shows significant evolutionary conservation, a fact which allowed early work to take place in many various model organisms. In yeast, Leland Hartwell and colleagues identified cell division genes via the use of *cdc* mutants (Hartwell, 1971; Hartwell et al., 1974); while in *Xenopus laevis* embryos, the proteins promoting cell cycle progression, collectively deemed M-phase promoting factor (MPF), were identified (Masui and Markert, 1971; Smith and Ecker, 1971). Subsequently, other work realized MPF and Cdc2 to be homologs, connecting decades of disparate intellectual threads, in different organisms (Gautier et al., 1988). Working off the foundational work in yeast, other studies revealed two *cdc* genes which regulate cell cycle length (Nurse, 1976; Nurse, 1985). These genes, as discovered later, code for the kinase Wee1 and the phosphatase Cdc25, which inhibit Cdc2 via phosphorylation and activate it via dephosphorylation, respectively (Russell and Nurse 1987; Russell and Nurse, 1986). After the discovery of two proteins which accumulate throughout the cell cycle, cyclin A/B (Evans et al., 1983), the purification of MPF led to its identification as a heterodimeric protein kinase made up of Cdc2—eventually renamed Cdk1 (cyclin-dependent kinase)—and one of these, cyclin B (Lohka et al., 1988; Dunphy et al., 1988; Gautier et al., 1988). This represented a significant breakthrough in our understanding of the cell cycle.

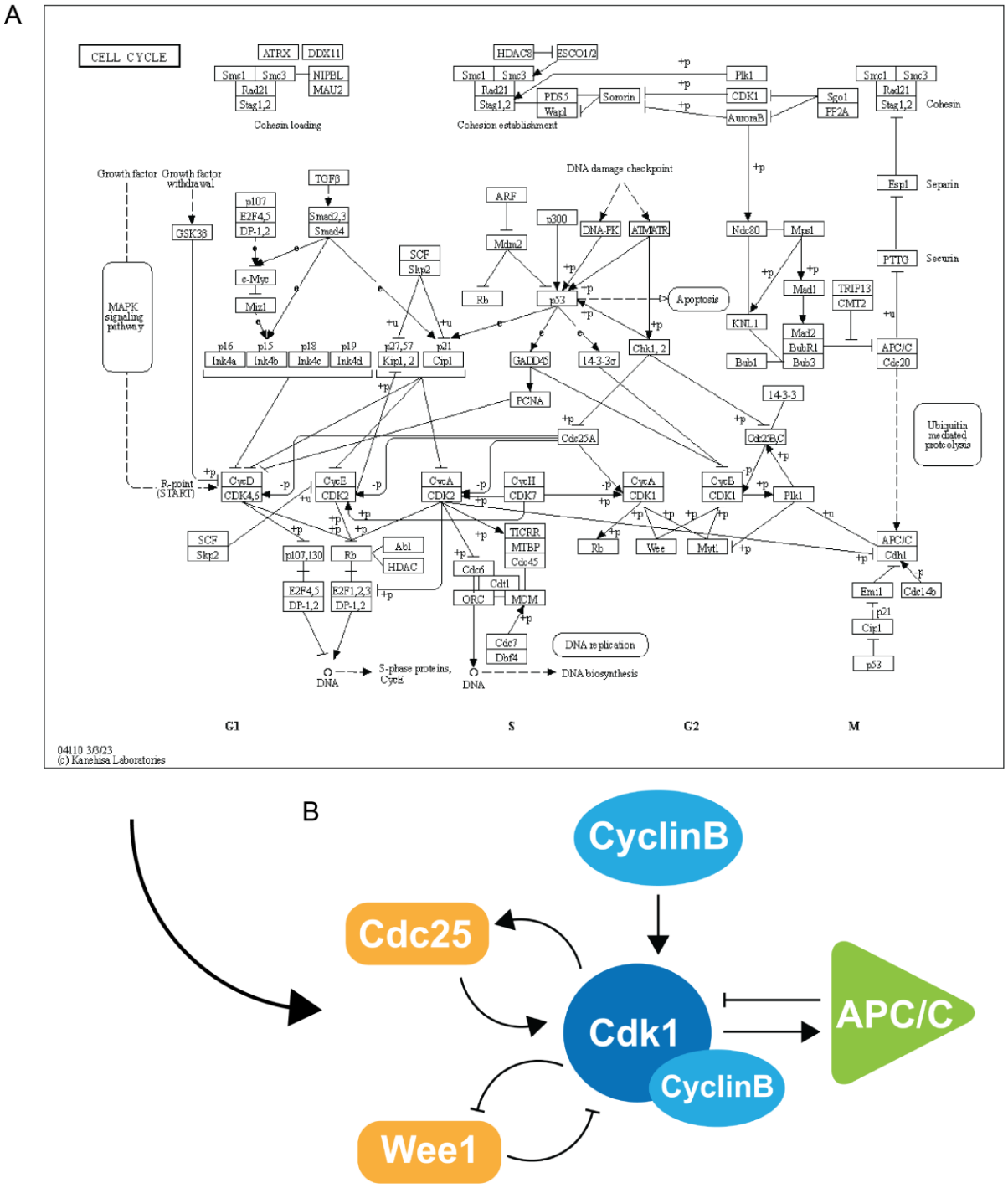

Figure 1.2 Two Representations of the Cell Cycle Network

A) Cell cycle pathway diagram of *Xenopus laevis* (adopted from Kyoto Encyclopedia of Genes and Genomes [KEGG] database. B) The central regulator of the mitotic clock, the complex Cdk1-cyclin B, is itself regulated by many other entities. Yang and Ferrell simplified the complex network to what is presented above (2013). Namely, the synthesis of cyclin B acts as a positive input by facilitating the formation of the Cdk1-cyclin B complex. The complex itself promotes its own activation by activating its activator, Cdc25, and inhibiting its inhibitor, Wee1. Finally, a negative feedback loop with APC/C controls the degradation of the complex (cyclin B) at the onset of anaphase.

For the final piece of the puzzle, *Xenopus* frog egg extracts—a technique to be described in the next section—facilitated the discovery of the specific roles of these constituent parts. In seminal and field-defining work, Murray and Kirschner (1989) used these extracts to show cell cycle progression through interphase depended only on cyclin B synthesis; and the cycle's exit from mitosis hinged on the degradation thereof through ubiquitination via the enzyme APC/C (anaphase-promoting complex/cyclosome). Yet other works in extracts crystalized the function of Wee1 and Cdc25. Both are phosphorylated by the active form of Cdk1: this inactivates Wee1, Cdk1's inhibitor, while activating Cdc25, Cdk1's activator, forming double-negative and double-positive feedback loops, respectively (Kumagai and Dunphy 1992; Tang et al., 1993; Mueller et al., 1995). Of course, the field has continued to delve deeper into the specific functions of the relevant molecules, but at this point, we can consider the fundamental network of the cell cycle oscillator to be complete (Figure 1.2 B).

In summary, as cyclin B is synthesized, it binds to Cdk1, functionalizing it for regulation (Solomon et al., 1990). Wee1 and Cdc25 interact with the Cdk1-cyclin B complex through double-negative and double-positive feedback loops, respectively. Finally, Cdk1, at some threshold of activity, activates its own inhibitor, APC/C, via multi-site phosphorylation, which in turn tags cyclin B for degradation through ubiquitination, resetting the entire cycle (Nurse, 1990; Figure 1.2 B). In reality, the biochemical network underpinning this oscillator contains numerous (hundreds) of different interacting molecules with distinct temporal and spatial functions (Li and Yang, 2018; Figure 1.2 B). Moreover, the cell cycle (if not all biological oscillators) exists in a context containing other necessary pathways and often couples or inputs to them in nontrivial ways, an innumerable number of possible factors to consider (Yang et al., 2010). However, it remains useful to consider this reduced form of the oscillator to study these specific feedback

loops in granular detail, on top of which other details can be added. Furthermore, this simplified network remains sufficient to broadly capture the behaviors we observe and dovetails with the advent of cell free extracts.

1.1.2 Recapitulating mitotic oscillations in Xenopus laevis extracts

Cell-free systems are simplified *in vitro* tools used to study the corresponding *in vivo* counterparts. Centrifugation separates cellular components by density and allows the cytosolic portion to be extracted to probe the biochemical machinery in a controlled and simplified environment. Early efforts focused on prokaryotes, most commonly *E. coli*, given their relative simplicity compared to eukaryotes (Spirin et al., 1998). To this day, bacterial cell extracts facilitate large-scale protein synthesis and pharmacological antibody development (Carlson et al., 2012). Cell extracts offer many advantages compared to working with live cells. For one, cell extracts contain the minimal components necessary for activity, reducing the complexity induced by cell-cell and membrane interactions. Further, by combining hundreds of cells together, extracts afford significantly larger volumes of material which can greatly increase the possible throughput of experiments. Finally, though the list goes on, working in extracts offer increased flexibility to introduce extraneous perturbations in the form of mRNAs, proteins, drugs, fluorescent reporters, etc. which otherwise prove difficult to introduce into live cells. As a result, this strain of synthetic biology proves invaluable for modern science.

However, this technique need not be limited to prokaryotes. As discussed in some detail previously, the frog species *Xenopus laevis* has been crucial to unraveling the intricacies of cell cycle oscillations. While early work with this model system occurred *in vivo*, Murray and Kirschner revolutionized studies in *Xenopus* by proposing a method for producing egg extracts which support multiple cell cycle oscillations (1989). By activating eggs via electrophoresis,

these extracts were capable of proceeding through a few cycles of nuclear division, establishing an environment for careful study of cell cycle biochemistry (Murray and Kirschner, 1989). This system subsequently facilitated many discoveries fine-tuning our understanding of these oscillations. In particular, quantitative measurements indicated that the Wee1/Cdc25 response to Cdk1 exhibits high non-linearity, i.e. ultrasensitivity (Pomerening et al., 2003; Pomerening et al., 2005; Kim and Ferrell, 2007), and that this ultrasensistivty makes the oscillations more robust (Ferrell, 2008). Additionally, the other leg of the network—the Cdk1-APC/C interaction—was also found to behave with a similar level of ultrasensitivity and includes an implicit time delay which also contributes to the oscillator's robustness (Ferrell, et al., 2011; Yang and Ferrell, 2013). In this way, decades of work in *Xenopus* extracts significantly expanded the working knowledge of cell cycle mechanisms: ultrasensitivity, time delay and positive/negative feedback loops.

What is more, modern advancements in microfluidics allow us to encapsulate small amounts of extract into oil droplets, creating "artificial cells" which artificially replicate single-cell experiments (Guan et al., 2018). Such droplets proceed through dozens of cycles, many more than bulk extracts and, when tracked over time, provide detailed time traces of mitotic activity through various cell cycle reporters (Guan et al., 2018). Moreover, using multiple fluidic channels and precise pressure control, extracts can be supplemented with wide, continuous ranges of perturbative factors such as drugs, recombinant mRNAs or ATP (Li et al., 2021). Maryu and Yang used this system to provide insight into the effect of nuclei on cell cycle period (Maryu and Yang, 2022). Yet other work explored the effect of cytoplasmic density dilution on mitotic oscillations and discovered a hysteretic response (Jin et al., 2020). Moving forward, the Yang lab's work continues to expand on this droplet system to probe additional details of mitotic

oscillations. Ultimately, the *Xenopus* cell free system, in its many iterations, enables relatively simple, yet meaningful, manipulation of the cell cycle.

1.1.3 A mathematical model for cell cycle oscillations

Alongside, if not in conjunction with, experimental work, efforts to capture the dynamics of cell cycle oscillations in a mathematical model began in earnest in the decades following the discovery of the central network described above. However, the seminal work on this matter came from Bella Novak and John Tyson in the form of a pair of nonlinear differential equations (1983 a, b). Through their model, loosely based on the quintessential FitzHugh-Nagumo (FHN) model, they proposed the series of feedback loops functioned as a mitotic bistable trigger (Fitzhugh, 1961Novak and Tyson, 1993 a, b). Moreover, it produced numerous novel predictions: a cyclin threshold for Cdk1 activation/inactivation, relaxation oscillations in cycling extracts, among others (Novak and Tyson, 1993 a,b). These predictions eventually all saw confirmation experimentally in various works over time, leaning heavily on the *Xenopus* extract system (Sha et al., 2003; Pomerening et al., 2003; Chang and Ferrell et al., 2013). As a result, the general conceptualization of the Novak-Tyson model captures important details of cell cycle oscillations.

Stemming from the continued work in *Xenopus* discussed above, Novak and Tyson's model underwent a series of refinements over the years, culminating in the relatively complete model we now consider the canonical model for *Xenopus* mitotic oscillations (Yang and Ferrell, 2013). As mentioned earlier, this work identified the main negative feedback loop—that between Cdk1 and APC/C—as an ultrasensitive switch with substantial time delay (Yang and Ferrell, 2013). Additionally, outside including more accurate experimental measurements of the various rate constants, the ultrasensitivity of the feedback loops was made explicit by replacing the

Goldbeter-Koshland function with Hill functions of known coefficient (Yang and Ferrell, 2013). When discussing modeling work further on in this dissertation, it is this model we considered. However, one prediction from this line of cell cycle models not yet discussed involves the propagating waves of Cdk1 activity (Novak and Tyson, 1993a), the central focus of this dissertation and that which I will now describe in the following section.

1.2 Traveling Waves in Spatially-Coupled Biochemical Oscillator Systems

Expanding on single oscillators, biological systems often exist as populations of entities and exhibit collective behavior. As our understanding of the complexity of such biological systems progresses, a substantial question arises: how do cells, tissues and other populations coordinate these complex processes in time and space over contextually relevant distances? In the simplest case, molecules spread throughout space through random diffusion, flattening peaks in local concentration. In other cases, motor proteins "carry" their cargo at distance-independent speeds throughout the cell through what is known as active transport. Faster still, pure fluid flow can achieve quite quick communication: circulation of hormones through our bodies occurs on the order of tens of seconds (Hall, 2010). However, these mechanisms, though obviously effective in some cases, pose significant limitations: diffusion is slow over long distances; whereas active transport requires specific infrastructure not universally available to all systems; and many systems do not admit fluid flow between constituents (Deneke and Di Talia 2018). In earlier embryonic development, for example, cell division events occur largely synchronously across millimeter length scales in a context lacking specific transport machinery and any substantial fluid flow between cells (Chang and Ferrell, 2013; Deneke et al., 2016).

Instead, over the past few decades, the community devoted much work to studying traveling waves as a plausible mechanism for quick, long-distance signaling. Pacemaker

oscillators embedded in an excitable medium may trigger waves that propagate over long distances (Gelens et al., 2014). In physics and chemistry, the Belousov-Zhabotinsky oscillator has been known to display propagating waves in multiple dimensions (Winfree 1972). From these observations, the mathematical theory of traveling waves in chemical reactions quickly developed (Tyson and Keener, 1988). Classically, traveling waves develop when bistable dynamics are coupled in space, primarily by diffusion. This mechanism is shared by the conventional picture of biochemical waves—deemed "trigger waves"—and observed in myriad systems: e.g. mitotic trigger waves in *Xenopus laevis*, most notably for our discussion (Chang and Ferrell, 2013). Due to their relatively fast speed and robustness, they serve their corresponding biological functions well. In this section, I will provide a brief overview of the history of biochemical traveling waves, discuss the discovery of mitotic waves, and then address lingering questions within the field.

1.2.1 Theoretical mechanisms and examples of biochemical traveling waves

Let us begin this discussion by first stepping back from biology to focus on a purely chemical system. The canonical example is the Belousov-Zhabotinskii (BZ) wave, named for the two scientists who discovered the chemical reaction in question (Belousov, 1956; Zaikin and Zhabotinskii, 1970). This system is defined by an oxidation-reduction reaction which occurs in solutions of citric (or malonic) and sulfuric acid in the presence of cerium ions (Belousov, 1956; Zhabotinskii, 1964). The cerium ions undergo autocatalytic oxidation, oscillating between oxidation states, causing the solution to change colors repeatedly over time (Zhabotinksii, 1964). If conducted in thin layers, this reaction produces spontaneous target patterns of wavefronts (backs) of oxidation and reduction (Zhabotinksii, 1970). What is more, modifications to the central reaction destroy the spontaneity of the waves but allow them to be triggered in space and

time (Winfree, 1972). In other words, the dormant media is excitable, the term now used to define this entire class of systems (Tyson and Keener, 1987). The BZ system represented the first well-known and well-studied example of such an autocatalytic oscillator, and the "BZ wave" is now considered the canonical example of traveling chemical waves.

Returning to biology, living systems exhibit realizations of a fundamentally similar mechanism in myriad contexts. Axons fire in the brain and produce action potentials which propagate at speeds upwards of ~600 m/min to initiate reflex response (Swadlow and Waxman, 2012). Waves of calcium ions move through various types of cells at slower, but still faster than diffusion, speeds of ~60 μm/min (Stricker, 1999). Of particular interest here, Cdk1 activity also propagates through suspensions of *Xenopus* egg extract at similar speeds to that of the calcium wave (Chang Ferrell, 2013; Nolet et al., 2020). The latter system is the focus of this writing and will be discussed in more detail below.

In all of these cases, despite their disparate constituent parts and contexts, the central trigger wave mechanism therein can be captured by coupling diffusion and reaction (reaction-diffusion) dynamics including positive feedback and nonlinearity (Gelens et al., 2014). These dynamics often, if not always, exhibit bistability, excitability and/or relaxation oscillations. Bistability and excitability are both dynamics with two—a high and a low activity—steady states: both stable, and one stable plus one unstable, respectively (Gelens et al., 2014). Relaxation oscillations are characterized by two slow refractory periods at low and high activity, connected by fast activation and inactivation processes, resulting in sharp, spiky oscillatory profiles (Gelens et al., 2014). Diffusion encourages mixing of molecules in space. This mixing can encourage the system to cross the threshold between steady states, after which the reaction dynamics rapidly amplify activity (Tyson and Keener, 1988). In other words, if one imagines a

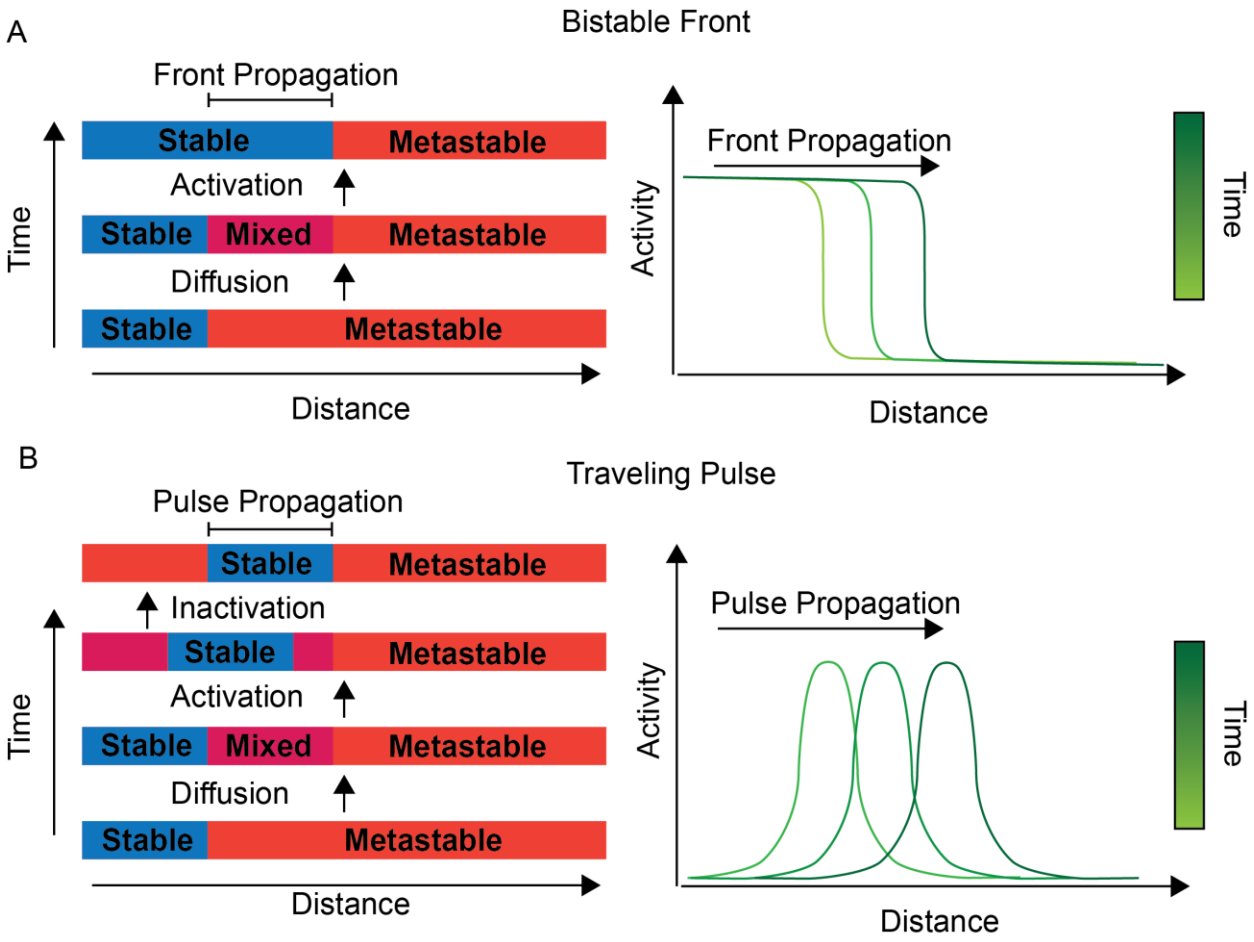

Figure 1.3 The Mechanisms of Bistable and Traveling Pulse Propagation

A) Propagation of bistable fronts. Active particles from the stable region diffuse out into the metastable region, increasing the local activity. Positive feedback causes the activation of the mixed region, broadening the stable region. This process repeats across the system, leading to stable arrest. B) Propagation of traveling pulses. In the case of traveling pulses in excitable systems, the same process governs activation at the front of the pulse. However, negative feedback leads to inactivation at the back of the pulse. Traveling wave trains follow the same logic but repeated in time.

small region in space with high concentrations of active molecules—whether through heterogeneity or some biochemical event—these molecules slowly diffuse outward and promote their neighbors' own activation (Figure 1.3). This process repeats throughout the system, leading to wavefronts.

In particular, the FHN model presents a relatively simple realization of these behaviors with careful choice(s) of parameters (Gelens et al., 2014). Reaction-diffusion dynamics of the model display propagating high-state arrest, singular traveling pulses and wave trains,

respectively (Figure 1.3) (Gelens et al., 2014). In any of these cases, theoretical predictions for the speed follow from Luther's formula $v \approx 2\sqrt{D / \tau}$, where *D* is the diffusion constant and τ is roughly the doubling time of the positive feedback (Luther, 1906). For the biological examples mentioned above, rough estimates for *D* and τ give speeds of 600-1200 m/min for action potentials, ~5 μm/s for calcium waves, and ~60-120 μm/min for Cdk1 waves, all in good agreement with observed values (Hodkin and Huxley, 1952; Stricker, 1999; Chang and Ferrell, 2013). While the FHN model does not explicitly model any of these systems accurately, it remains illustrative and qualitatively predictive as an example. However, for more specific discussion, we now turn to explore our main focus, mitotic waves.

As a brief aside, in one dimension, the picture is as depicted in Figure 1.3. However, in higher dimensions, two different topologies arise: target waves and spiral waves (spherical and scroll waves in three dimensions) (Tyson and Keener, 1988). Target waves represent the higher dimension extension of the mechanism discussed. In this case, the pulses in question materialize as rings of activity, rather than singular fronts. Alternatively, spiral waves arise due to non-zero curvature effects in higher dimensions and presents as spirals (hence the name) rotating around some central node (Tyson and Keener, 1988). Both topologies appear throughout biology, oftentimes in the same system. For example, when amebae of *Dictyostelium discoideum* (slime mold) are starved, they signal to each other through traveling waves of the molecule cyclic AMP which take on both target and spiral patterns simultaneously (Tomchik and Devreotes, 1981). In *Xenopus,* calcium signaling also emerges as plane and spiral waves (Lechleiter et al., 1991). My work presented in this dissertation is solely devoted to waves in one dimension, but it is important to point out the added complexity in higher dimensions.

At this point, it is useful to also define another class of patterning, "phase waves," and point out how they differ from the previously discussed trigger waves. In brief, phase waves arise due to an underlying gradient in the timing of a set of oscillators (Tyson and Keener, 1988). The gradient produces the visual effect of a wave-like pattern, without the physical transmission of a signal. In this way, no coupling—whether through diffusion or some other function—connects their function across space. As a result, the "speed" of these non-physical waves can be arbitrarily large and is proportional to the reciprocal of the spread in phase (Tyson and Keener, 1988). Due to the lack of spatial coupling, phase waves pass through physical barriers inserted between two parts of a system, while trigger waves are absorbed (Tyson and Keener, 1988). While present alone in many circumstances, phase waves often accompany trigger waves. For example, the wavefront of the BZ wave represents the signaling oxidation wave, while the wave back of reduction is a phase wave created by the refractory period of the reaction. Much of the focus of the work presented here rests on this distinction, as will be seen in the coming chapters.

1.2.2 Mitotic waves establish standard developmental time in embryogenesis

In early embryogenesis in organisms such as *Xenopus*, embryonic cells initially proceed through a series of fast cell divisions (Foe and Alberts, 1983; Deneke et al., 2016). These mitotic cycles lack many features of mature cells—e.g. gap phases and zygotic gene transcription—which only arise after the mid-blastula transition (MBT) (O'Farrell, 2015). In this way, such early stages correspond to proliferation alone: the organism favors pure growth towards viability, rather than the relatively complex process of differentiation and specialized function. For this reason, it is key these cycles remain roughly synchronized prior to MBT, so that they share a similar cellular state once differentiation begins. Throughout this process, mitotic events occur

within minutes of each other. However, due to the size of such embryos, diffusion alone remains far too slow to coordinate said synchrony (Chang and Ferrell, 2013; Deneke et al., 2016).

Indeed, previous work highlights the existence of waves of mitotic events—both *in vitro* and *in vivo*—which propagate at speeds sufficiently high to communicate across the lengths of the embryo (Chang and Ferrell, 2013; Deneke et al. 2016). In *Xenopus*, about 1 hour post-calcium wave, a mitotic wave transverses over the embryo, from the congressed pronuclei to the pole (Hara, 1971; Chang and Ferrell, 2013). Work in egg extracts demonstrated that the Cdk1 network eventually admits such waves, using nuclear envelope breakdown (NEB) to illustrate their propagation after a few early, largely synchronous cycles (Chang and Ferrell, 2013). In this system, late-time waves propagate as trigger waves, and not some phase wave artifact of an underlying gradient, which the authors confirmed by cutting the tube—inserting a physical barrier—and observing the absorption of the fronts at the barrier (Chang and Ferrell, 2013). However, early-time patterns remained diffuse and not easily classified by trigger waves (Chang and Ferrell, 2013). By inhibiting Wee1, the authors also disrupted the "trigger" and extracts showed decreased propensity for waves (Change and Ferrell, 2013). Moreover, by adding diffusion to the well-established Cdk1 cell cycle model, numerical simulations also exhibit wave propagation, just as in the FHN model described previously (Chang and Ferrell, 2013).

When discussing traveling waves in this light, it is often important to highlight the origination point of the fronts. We call this point the *pacemaker* of the wave, much like its namesake oscillator, in that such a point or region oscillates faster than its surroundings and drives the system at its given frequency. In their modeling work, Chang and Ferrell introduced an explicit pacemaker—introducing heterogeneity to the Cdc25 term to increase local frequency—to drive waves (2013). They argued this could represent the centrosome which

maintains a higher level of Cdc25C in the cell (Chang and Ferrell, 2013). Similarly, recent studies argued that reconstituted nuclei may act as pacemakers for mitotic waves in *Xenopus* (Afanzar et al., 2020; Nolet et al., 2020). It is proposed nuclei accumulate active clock constituents--namely Cdk1, but also Cdc25 and Wee1, among others—by importing them inside the nuclear membrane throughout the cell cycle, which leads to a local increase in the oscillatory frequency (Nolet et al., 2020; Nolet and Gelens, 2021). Nuclear spacing also impacts wave propagation as heterogenous distributions thereof can also affect local Cdk1 concentrations, leading to waves (Nolet et al., 2020; Nolet and Gelens, 2021). In follow-up work from the Ferrell lab, they showed nuclei themselves, not the earlier proposed centrosome, act as trigger wave sources (Afanzar et al., 2022).

Results from the Yang lab confirmed this. Maryu and Yang demonstrated nuclei indeed perform some concentrating effect on clock constituents (most notably Cdk1) and speed up oscillations when cyclin B concentration is not high, confirming the proposed pacemaker mechanism, at least locally. They discerned this effect when both droplets in question stem from the same bulk extract supplemented with sperm DNA; in contrast, extracts which lack sperm DNA at all oscillate even faster (Maryu and Yang, 2022). Thus, while nuclei seemingly speed up oscillations locally, the addition of sperm DNA slows oscillations globally. Furthermore, an extension of this view leads to the prediction that higher densities of nuclei (pacemakers) should facilitate faster wave propagation due to a localized boost-like mechanism (Rombouts and Gelens, 2020). These works highlight the role of nuclei both in oscillatory and wave dynamics.

1.3 Remaining open questions

In this introduction, I reviewed the history and literature surrounding mitotic oscillations and waves, with particular focus devoted to seminal papers detailing the existence of mitotic

trigger waves (Change and Ferrell, 2013) as well as the identification of nuclei as mitotic wave pacemakers (Afanzar et al., 2020; Nolet et al., 2020). While these works identify and visualize waves both *in vitro* and *in vivo*, little-to-no work exists connecting these disparate threads.

Specifically, except for minor discussion by Afanzar et al. (2020), effectively no work touches on the nature of mitotic waves in the absence of driving via nuclei. Chang and Ferrell (2013) offer a model which describes such a system, but choose to drive it artificially (i.e. with a non-physiological term, as their own future work displays) and do not utilize it to answer mechanistic questions. Relatedly, due to the choice of reporters, the field lacks explicit measurement of Cdk1 waves in *Xenopus,* and thus, do not yet fully understand their behavior. Collectively, this poses the question: without pacemakers, how do we characterize spontaneous patterns in a spatially homogenous excitable medium? How does the system go from first proceeding through a series of fast, synchronous oscillations to admitting trigger waves when cycles slow? Moreover, how do these patterns change as the oscillatory characteristics (namely, period) change over time? And as an extension, how does this picture change when the system is both compartmentalized and driven by nuclei?

With all of this in mind, my Ph.D. work strives to touch on and answer some of these questions. The work begins with a focus on the time dependence of mitotic waves and how perturbations to the extract system affect this dependence. In particular, I investigate the role of nuclei in wave propagation, and the differences between waves in systems with and without them. Stemming from lessons learned in these experiments, I then propose a novel method for generating directed waves *in vitro*¸ a setup with demonstrated efficacy in facilitating systematic tuning and investigation of wave properties. Further, I present the first direct evidence of Cdk1 waves in *Xenopus* using a Cdk1-FRET sensor. Finally, through work with our collaborators, I

offer a generalized picture of mitotic waves in *Xenopus.* Using properties of cycling extracts to describe wave behavior over time, I frame these observations in the context of a transition from phase to trigger waves over time. The vast majority of this work is currently being prepared and will be submitted for peer review in the immediate future.

Chapter 2

The Discovery of Mitotic Sweep Waves and its Impact on Our Understanding of Mitotic Waves in *Xenopus laevis* Extracts

In the introductory sections above, I outlined the theoretical predictions and subsequent experimental realization(s) of mitotic trigger waves. However, as alluded to, little work exists studying the evolution of these waves over time. Published experiments demonstrate trigger wave dynamics only after a few cycles and leave the characterization of these early cycles to future analysis (Chang and Ferrell, 2013; Nolet et al., 2020). To this point, recent work published in 2016 and 2018 addresses discrepancies between the behavior of mitotic waves in early *Drosophila* embryogenesis and the predictions from traditional bistable reaction-diffusion models (Deneke et al., 2016; Vergassola et al., 2018). In follow-up work, authors from the same group showed that this system could admit trigger waves if oscillations slowed in a particular manner or heterogeneities were introduced. In this light, trigger (or bistable) waves are not the end of the story.

In this Chapter, I will discuss the discovery of mitotic sweep waves and how they differ from the traditional picture of trigger waves. I summarized this work in a review article, the relevant parts of which are adapted to form some of what follows (Puls and Yang, 2018). Next, I address follow-up work from the Di Talia lab which proposes a possible sweep-to-trigger wave transition in *Xenopus* extracts. I will then present modeling work that I conducted with a fellow graduate student which posits the plausibility of such a transition, which I will use to motivate subsequent chapters.

2.1 Advances in the Field Highlight the Importance of Time-dependent Wave Behavior

2.1.1 Mitotic sweep waves in Drosophila melanogaster embryos

Much like *Xenopus* and other metazoans, the fruit fly embryo undergoes a series of rapid, roughly synchronous divisions post-fertilization (O'Farrell, et al., 2004). The question of coordinating this synchrony similarly highlights the need for a mechanism which travels faster than diffusion. However, in *Drosophila*, two main details separate it from our previous discussion. First, *Drosophila* embryos display waves of mitotic completion that traverse the entirety of the embryo (hundreds of microns) in mere minutes at early stages, speeds much faster than what could be achieved by traditional bistable models (Deneke et al., 2016). Second, the last few cycles preceding the maternal-to-zygotic transition exhibit slowing periods due to S-phase lengthening: this hints at a time-dependent cell cycle which traditional models of trigger waves do not consider (Daneke, et al., 2016). Together, these two facts pointed to a more careful consideration of this phenomenon. In ground-breaking work, Vergassola, et al. (2018) offered a model for waves which propagate fast enough to explain what is observed *in vivo.* Further, the authors noted distinct spatial dynamics which forgo the classical picture of a stable regime invading into and promoting a metastable regime (Figure 2.1). Instead, spatial gradients in Cdk1 activity are largely preserved (Figure 2.1), while the overall levels are swept upwards, producing what the authors deemed "sweep waves" (Vergassola et al., 2018).

To explain this distinct behavior, the authors proposed a time-dependent modification to the reaction term in the mitotic circuit. In short, the relevant biochemical reaction terms remain untouched, but an additional term that depends explicitly on time is added to the chemical force (Vergassola et al., 2018). The effect of the time dependency is to drive an initially bistable forcing term through a transition to a monostable state across the duration of one cycle. To

rigorously define this new class of waves, they break Cdk1 activation over the cell cycle into three phases: i) at low overall activity levels of Cdk1, spatial gradients develop via diffusion and reaction kinetics; ii) constant-force mechanics sweep the activity quasi-uniformly up, preserving the gradients; iii) non-linear forcing dynamics take over and push the system to the high-activity stable state in a manner which conserves spatial linearly-varying time delays (Figure 2.1) (Vergassola et al., 2018). This distinction between trigger and sweep waves is summarized in Figure 2.1.

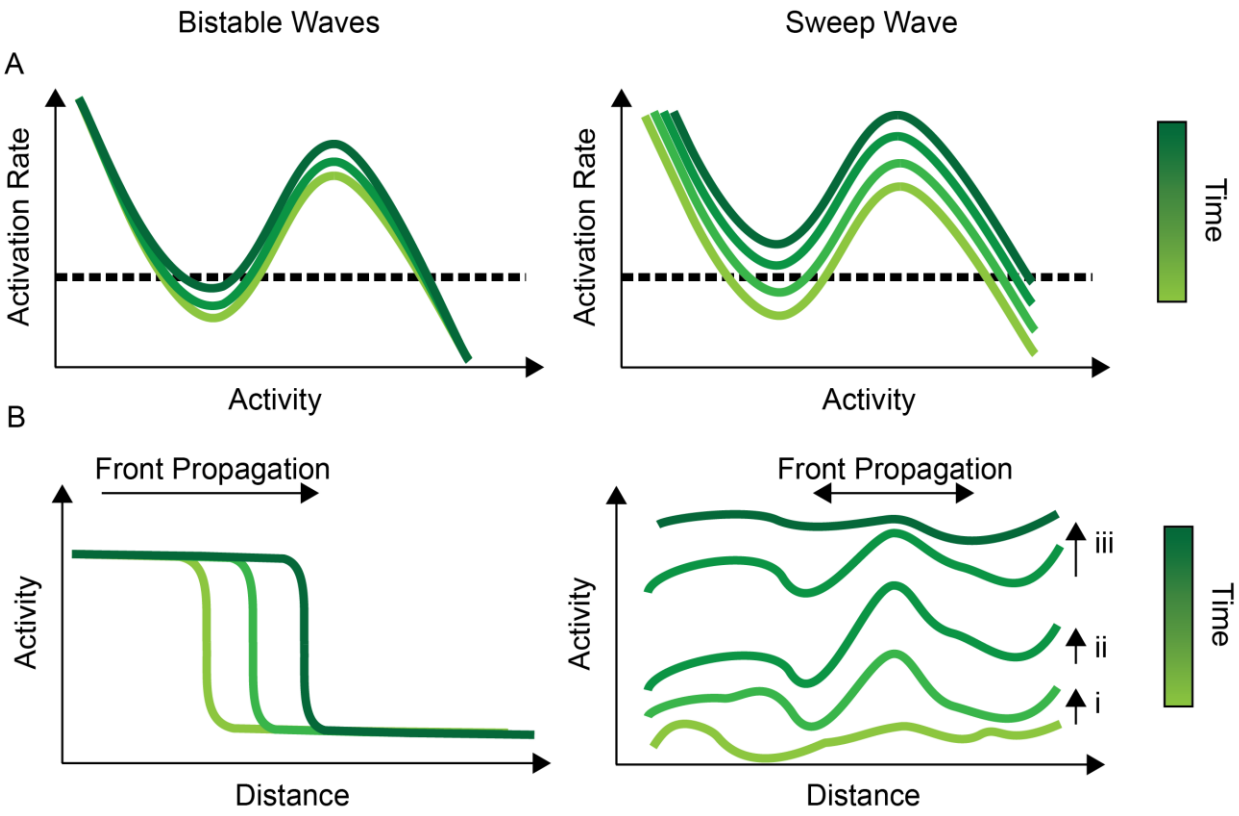

Figure 2.1 Sweep vs Trigger Wave Dynamics

A) Comparison of time-dependence of activation rates for slow, bistable cycles (left) and fast, sweep cycles (right), according to Hayden et al. (2022). The dashed line indicates the line of zero activation rate. Slow cycles retain bistability over time, as indicated by the two outer zero crossings, along with a single unstable steady state in the middle. Alternatively, fast cycles see the activation rate sweep up over the course of one cycle, losing both the low-stable and unstable steady states, leaving only the high stable steady state. B) Comparison of front propagation for the two cases. As described earlier, bistable fronts propagate through a series of diffusion-activation steps (Left). Sweep waves, conversely, follow a three-step process (Right): i) Diffusion-reaction kinetics couple to form spatial gradients of activity. ii) Constant force mechanics push activity up uniformly in space. iii) Non-linear force dynamics push the system to the remaining (high) steady state.

As the authors note, this mechanism produces waves that propagate at significantly elevated speeds compared to the bistable (time-independent) case. Moreover, this, ultimately, leads to wave-like spreading which scales faster (~7/12) than trigger waves (~1/2) with the rate of Cdk1 activation in S-phase (Vergassola, et al., 2018). They also find distinct scaling dependencies on the diffusion constant which diverge from the classical mode where the speed scales as $D^{1/2}$. Although this involves dynamics which exhibit spatial de-coupling and thus, may be akin to kinematic or "phase" waves, earlier ligation experiments (Deneke et al., 2016) and simulation results by Vergassola et al., (2018) indicate that these traveling waves are kinematic and not simply indicative of underlying phase gradients. Thus, Vergassola et al., (2018) argue that "sweep waves" represent a distinct phenomenon in which the embryo trades bistability—a once-thought necessary component—for wave speed to best facilitate rapid development of *Drosophila* embryos.

2.1.2 Genetic modifications in Drosophila embryos suggest sweep-to-trigger wave transition

In the above works, the clock itself determines the type of wave admitted. Wild-type *Drosophila* cells exhibit a mitotic clock similar to that of *Xenopus*. Importantly, however, the inclusion of the kinase Chk1 in *Drosophila* causes mitosis to slow down for late (10-13) cycles (Vergassola et al., 2018). In their original paper, the authors remarked that *Xenopus* extracts also exhibit period lengthening over time and suggested a possible link between sweep and trigger waves, as a result (Vergassola et al., 2018; Guan et al., 2018). To underline this, in more recent work, authors from the same lab questioned whether *Drosophila* embryos could, indeed, admit trigger waves if cycles were sufficiently slowed (Hayden et al., 2022). In this work, the authors identify a sweep-to-trigger transition when the characteristics of sweep waves—loss of bistability and the synchrony of said loss—are removed in *Drosohphila*.

As a first step, they utilized a temperature chamber to probe mitotic cycles and periods at a range of temperatures. They demonstrated that embryos displayed progressively slower cycles as the temperature decreased, as one might expect (Hayden et al., 2022). However, this slowing occurred homogeneously throughout the cycle, meaning Cdk1 activity profiles exhibited collapse under a rescaling of time (Hayden et al., 2022). Moreover, across all temperatures, the embryos admitted sweep waves, not trigger waves (Hayden et al., 2022). They then hypothesized a heterogeneous slowing of the cycle could unlock this potential transition.

To do so, they generated Polo kinase heterozygous embryos. Unlike the temperature-dependence, or other genetic mutations they tried, these embryos exhibited cycles which slowed only during initial activation (interphase) and largely preserved the activation time at the onset of

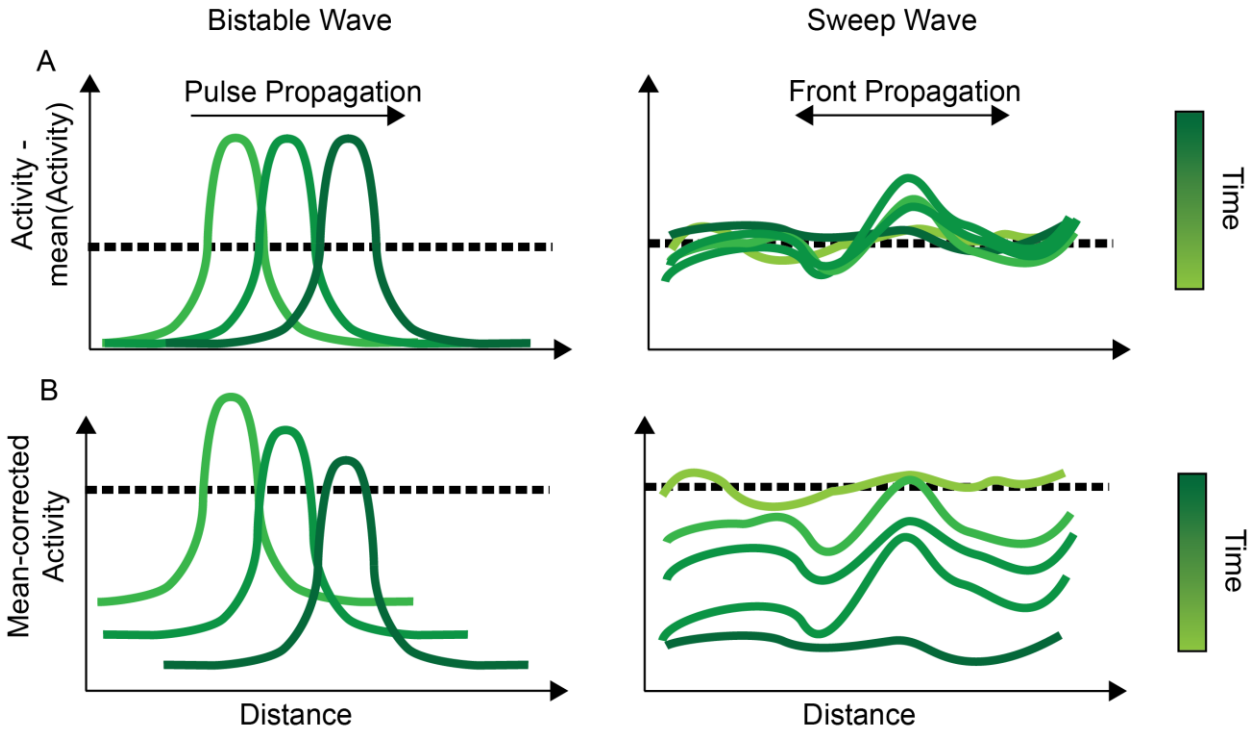

Figure 2.2 Qualitative Test for Classifying Wave Type

A) Activity profiles shifted by their means for bistable/trigger (left) and sweep (right) waves. Sweep wave profiles exhibit collapse as they preserve spatial gradients, while trigger wave profiles continue to resemble traveling pulses. Dashed lines indicate each profile is centered upon zero after mean subtraction. B) In this text, we will sometimes instead present profiles which are shifted downward linearly from the first timepoint's mean. We believe this makes traveling pulses easier to observe in noisy data.

mitosis (Hayden et al., 2022). Importantly, some of these embryos did, in fact, display trigger-like waves, instead of sweep waves (Hayden et al., 2022). As a result, the authors concluded some sort of sweep-to-trigger transition must exist as cycles slow heterogeneously. To distinguish them, they proposed a simple illustrative test, of sorts, to classify patterns as either sweep or trigger-like waves. In short, sweep-like patterns roughly collapse onto each other when their mean is subtracted off, due to the fact these waves preserve spatial gradients (Figure 2.2) (Hayden et al., 2022). Conversely, trigger-like patterns do not collapse and instead present as the classical picture of traveling pulses (Figure 2.2.). This offers the field a qualitative measure for distinguishing these two types of waves. The authors proposed such a transition could also exist in *Xenopus* and called for direct measurements of Cdk1 activity in extracts to resolve this open question. This proposal serves as the motivating force behind what follows.

2.2 Demonstrating Time-dependent Wave Dynamics in an Energy-dependent Model

Before turning to experimental data, I first offer some analysis of numerical simulations to further motivate the following chapters. In collaboration with another graduate student in the lab, Franco Tavella, I adapted the model published by Guan et al. which accounts for cycle slowing in extracts (Guan et al., 2018). Unless specified, the parameters used are the same as by Guan et al. and are given in Table 2.1. In this model, the authors include ATP consumption in the cell cycle through the parameter *r* which ultimately changes the ratio between the Wee1 and Cdc25 feedback loops with Cdk1 (Guan et al., 2018). By asserting a linear (or some other monotonically increasing function) increase in *r* over time, the system exhibits period lengthening corresponding to increased rising period, or interphase duration, while the mitotic phase remains largely unchanged, and also captures the observed cyclin accumulation of extracts (Figure 2.3) (Guan et al., 2018). This change in period, though perhaps not the mechanism itself,

mirrors what Hayden et al. reported in their *Drosophila* Polo mutants, i.e. not a simple rescaling of time, but a heterogeneous change in the underlying timescales (Hayden et al., 2022). As such, I offer it as a suitable model for comparison in *Xenopus.*

Table 1 Parameter Values for ODE and PDE Simulations of ATP-Depletion Cell Cycle Model

Parameter	Value
k_{synth}	1.0 nM/min
a_{deg}	0.0106 nM/min
b_{deg}	0.04 nM/min
K_{50_deg}	32.0 nM
n_{deg}	17.0
a_{cdc25}	0.16 nM/min
b_{cdc25}	0.8 nM/min
K_{50_cdc25}	30.0 nM
n_{cdc25}	11.0
a_{wee1}	0.08 nM/min
b_{wee1}	0.04 nM/min
K_{50_wee1}	35.0 nM
n_{wee1}	3.5
r	0.7-1.6
D	6e-4 mm^2/min

To understand this evolution, I plot the nullclines for various values of *r* along its linear trajectory (Figure 2.3). As *r* increases, the Active Cdk1 nullcline moves to the right, with the unstable steady state also moving up the cyclin B nullcline (Figure 2.3). This leads to limit cycle oscillations of increasing period referenced earlier (Figure 2.3). By *r* = 1.6 for this parameter set, the Cdk1 nullcline crosses the lower cyclin B branch, leading to the creation of two more steady states, one of which is stable, at which point the system exhibits arrest in the low-activity

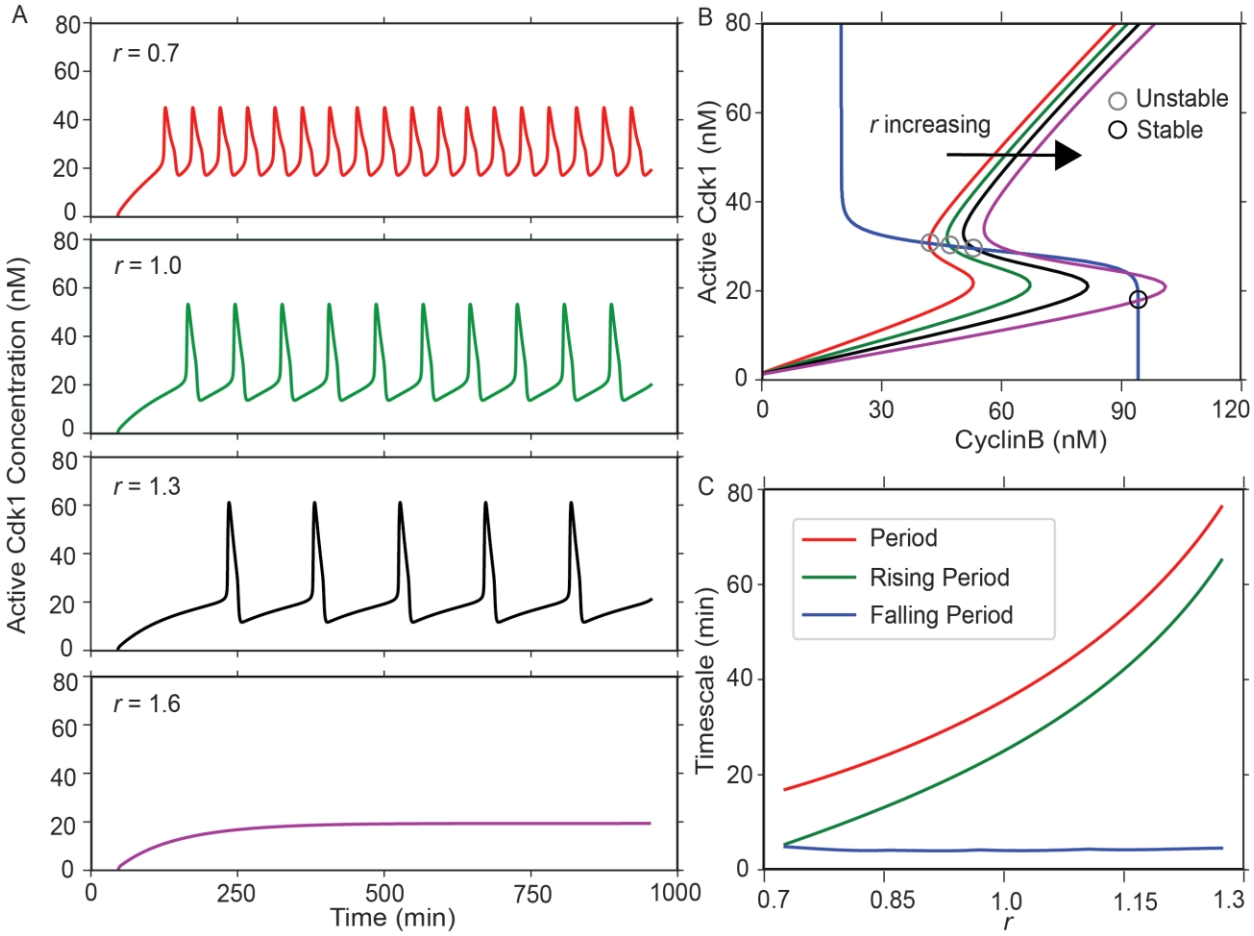

Figure 2.3 ATP-Consumption-Dependent Cell Cycle Dynamics

A) Timecourses for Cdk1 activity as the parameter *r* increases. *r* models the consumption of ATP in extracts. As ATP is consumed, the period of oscillations increases up and until cell cycle arrest in the inactive state. B) Cdk1-Cyclin nullclines for the values of *r* plotted in A. Initially, the system exhibits a single unstable steady state which admits limit cycle oscillations. As *r* increases, this nullcline shifts to the right, until it breaches the lower branch of the cyclin B, creating a stable steady state. C) The various timescales of the system as a function of *r*. The period increase is primarily, if not completely, due to an increase in the rising period, or interphase duration. This mirrors what Hayden et al. reported when they observed a sweep-to-trigger wave transition.

(interphase) state (Figure 2.3). In this regime, the system exhibits excitability, where single pulse-like "oscillations" can be generated if the system is kicked out of its stable point. Thus, the increase in *r* can be viewed as a transition of the system from an oscillatory to an excitable state.

To capture wave dynamics in this model, I added a diffusion term and solved the resulting PDE with Gaussian noise using the Python package py-pde (Zwicker, 2020). Beginning with stationary values for *r*, I solve the system for small *r*, where the system is far from excitability. In this case, one can observe roughly synchronized oscillations with clear patterning

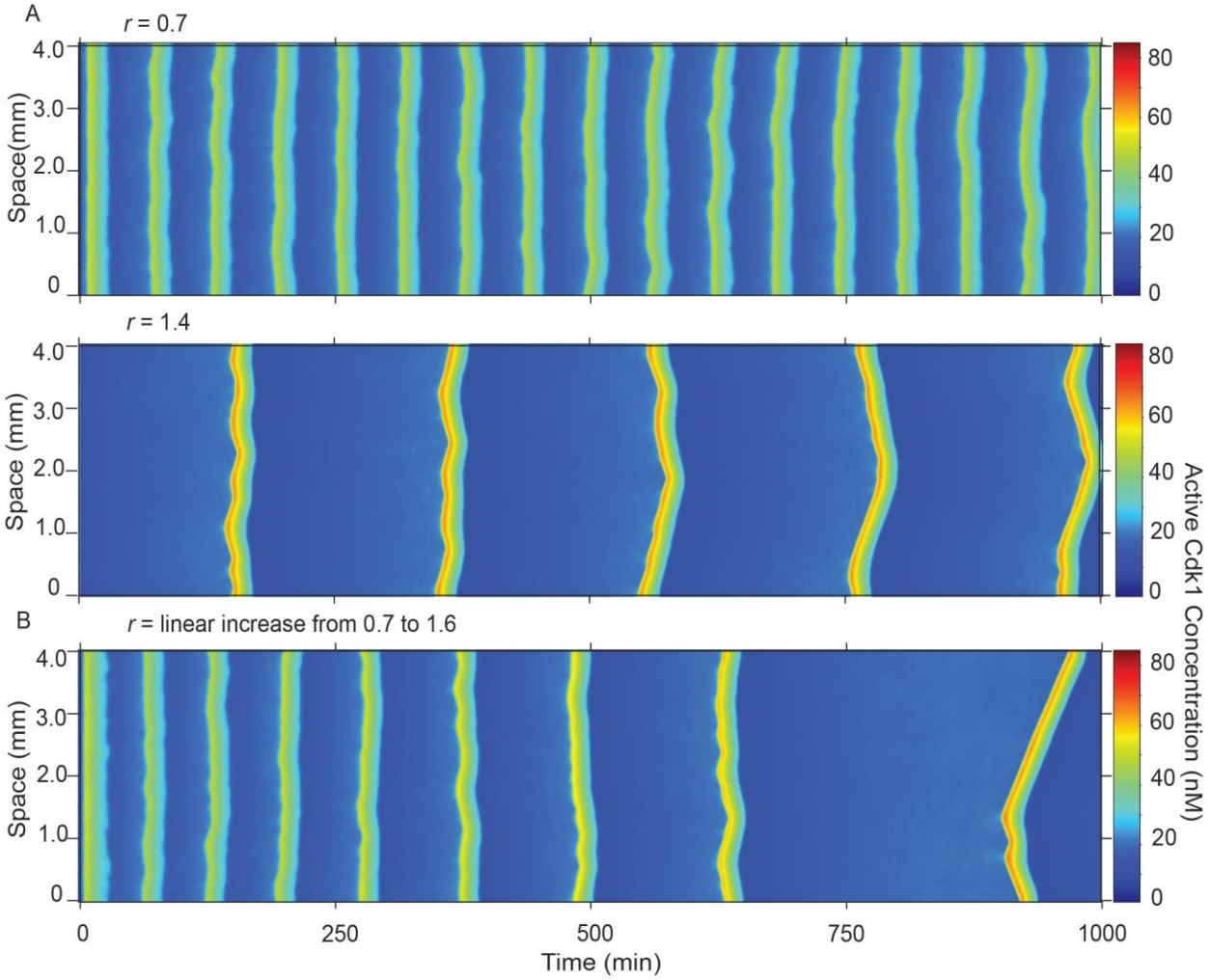

Figure 2.4 Wave Dynamics in an ATP-Depletion Model of the Cell Cycle

A) Kymographs at fixed values of *r*. Top: At low values of *r*, the system exhibits fast, largely synchronous oscillations. Bottom: At high values, conversely, the system displays trigger-like pulses. B) Kymograph for *r* linearly increasing in time. In this case, the system transitions from fast, quasi-synchronous oscillations at early times, to trigger waves at late times.

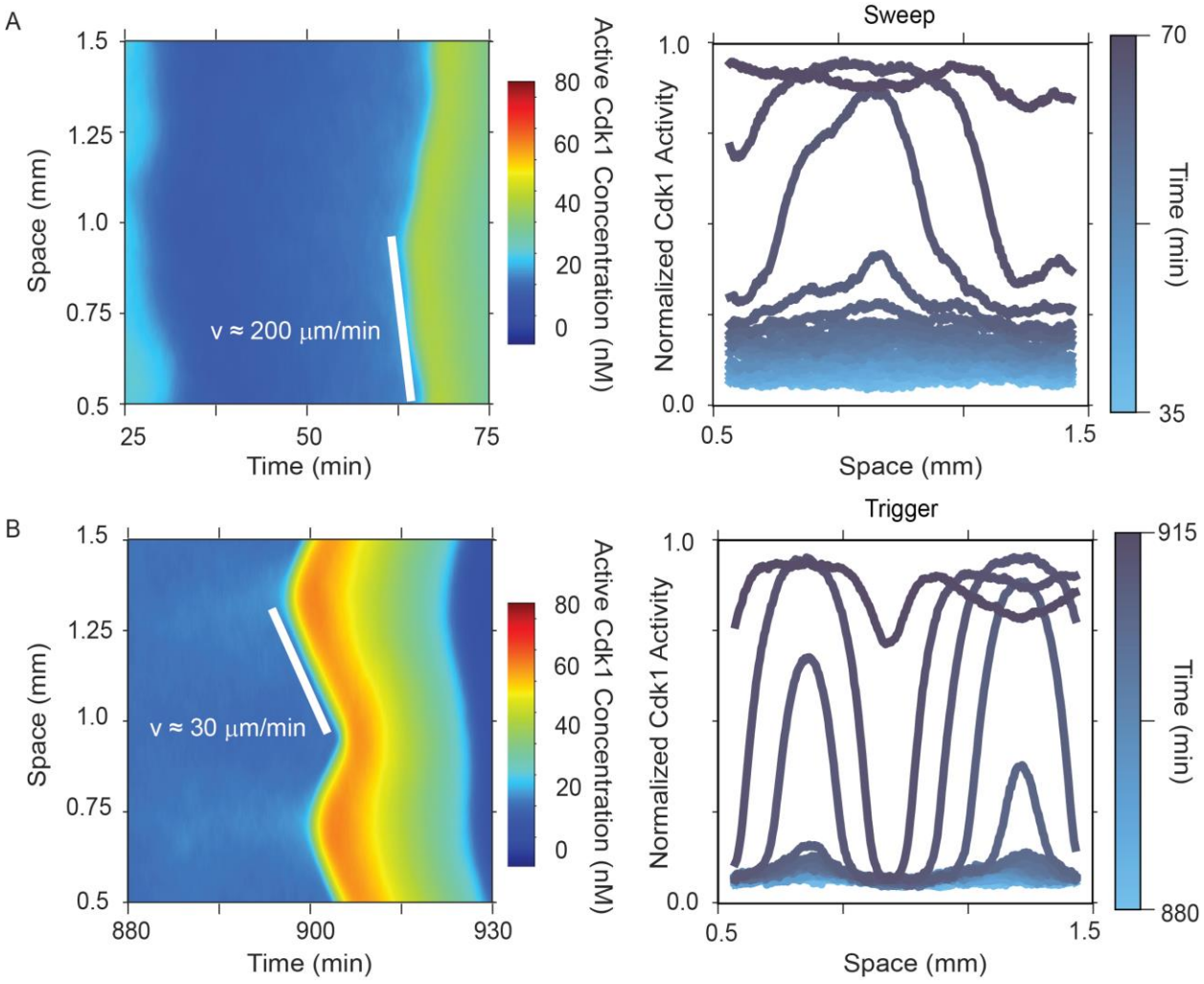

Figure 2.5 Spatiotemporal Patterns Confirm Sweep-to-Trigger Transition in the Model

A) Zoomed-in snapshots of early-time fast waves (Left) and the corresponding spatial profiles (Right) of the normalized Cdk1 concentration over time from the kymograph in Figure 2.4, B. These are sweep waves, confirmed by the preservation of spatial gradients. B) The same for late-time slow, trigger waves.

at small timescales (Figure 2.4, A, Top). Conversely, if I solve the system at a given level of *r* near this excitable state, but importantly still oscillatory, then the system admits trigger-like waves from early times onward (Figure 2.4, A, Bottom). This implies that when the system exhibits excitability, noise is sufficient to kick the system out of the steady state, causing pulses to propagate as described previously. If I, instead, allow *r* to increase over time, as in the energy-depletion model, we observe patterns that transition from one regime to the other (Figure 2.4, B).

Unsurprisingly, repeating this simulation, but without Gaussian noise, the system oscillates synchronously (not shown).

Indeed, zooming in to the scale at which sweep waves are relevant—hundreds of microns—then I find the apparent speed of these patterns to be on the order of sweep waves (Figure 2.5, A). Conversely, the clear trigger waves propagate at speeds one would expect (Figure 2.5, B). The spatial profiles plotted as in Hayden et al. (2022) confirm this observation. As such, this model appears to capture a phase/sweep-to-trigger-like transition over time in a *Xenopus* model, just as suggested by the literature (Hayden at al., 2022). This is possibly not surprising since the time-dependence of r both creates a time-dependent potential as is seemingly required for sweep waves, but also matches the form of said time-dependence Vergassola et al., used in their original model. Though implicit, rather than explicit, here, the accumulation of cyclin that this model recapitulates mirrors their reasoning behind including a time-dependent potential in the first place (Vergassola, et al., 2018). In theory, similar behavior could exist in the real system.

Moreover, to lend more credence to this model, I modeled Wee1 inhibition to test whether this exhibits a similar phenomenon to what is observed experimentally in Chang and Ferrell, 2013. Indeed, as Wee1 inhibition increases, one can observe two main behaviors. First, the lifetime of oscillations increases (Figure 2.6). This corresponds to Wee1 inhibition broadening the range of values of r for which oscillations are sustained. Second, and more importantly, Wee1 inhibition lengthens the time for trigger waves to appear (Figure 2.6). This matches what was presented experimentally and again, lends credence to the behaviors we observe using this model (Chang and Ferrell, 2013).

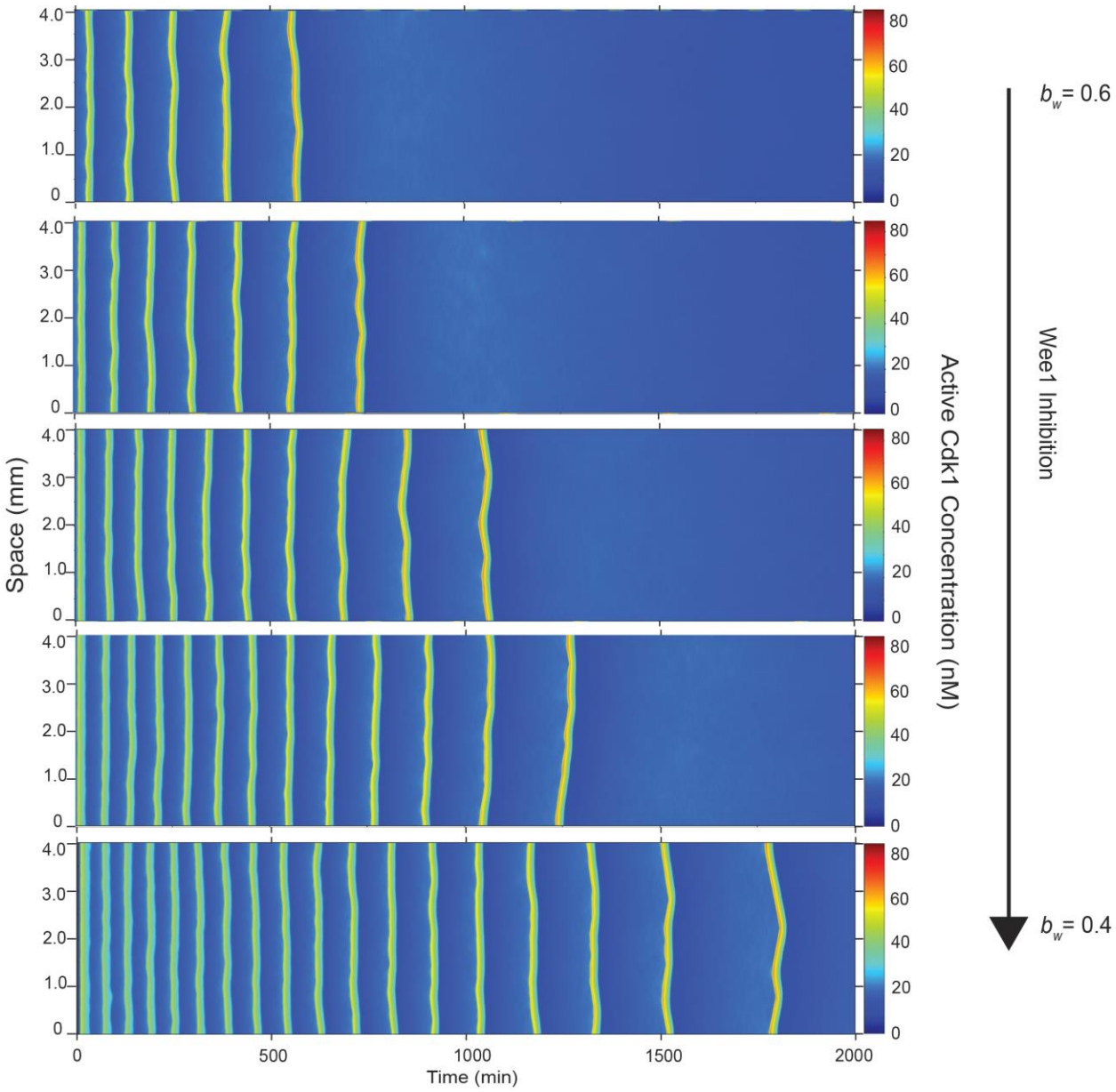

Figure 2.6 Wave Dynamics as Wee1 Inhibition Increases

Wee1 Inhibition Lengthens Cycle Lifetime and Delays Trigger Wave Formation. As the strength of the Wee1feedback loop decreases—as simulated by the model parameter b_w—the time for which cycles exist (their lifetime) increases. Additionally, this inhibition, possibly as a result of the former effect, delays the appearance of trigger waves. Both of these observations match what was previously shown experimentally (Chang and Ferrell, 2013)

Though illustrative, I do not intend this to necessarily depict the actual mechanisms at work. Nevertheless, the experimental evidence for slowing oscillations and wave speeds is clear (Chang and Ferrell, 2013; Guan et al., 2018; Nolet et al., 2020), implying some network-level time dependence, but no analysis or meaningful discussion thereof exists. Moreover, no

consideration has been paid to what early-time patterns represent, nor how they give way to definable trigger waves. In the data and analysis I will present in the following chapters, we will offer more precise measurements and discussion of this possible transition, as well as offer a generalized picture of time-dependent wave dynamics in *Xenopus.*

2.3 Conclusion

In this comparatively brief chapter, I outlined the mechanisms and behavior of proposed mitotic sweep waves in *Drosophila* embryogenesis. These waves are argued to act fundamentally differently than trigger waves and as a result, manage to coordinate development on a significantly faster scale. However, *in vitro* experiments in *Xenopus* extracts also display patterns which cannot be explained by a trigger-like mechanism. Thus, Hayden et al., proposed a sweep-to-trigger transition in *Xenopus* stemming from genetic modifications of embryos that slowed oscillations heterogeneously and admitted trigger waves.

Using an existing energy-dependent cell cycle model, I demonstrated such a transition, indeed, could exist in a model of mitotic oscillations in *Xenopus*. This model qualitatively recapitulates the behavior of the extract system where trigger waves develop over time while oscillations slow down due to interphase lengthening through some yet-unconfirmed mechanism. In the following chapters, I will report experiments on this general behavior, and with our theory collaborators, will provide a detailed explanation for time-dependent wave behavior in *Xenopus* extracts.

Chapter 3

In vitro Mitotic Waves Exhibit a Phase or Sweep-to-Trigger Transition

As discussed, much of our focus rests with elucidating the details of time-dependent wave behavior, the motivating details of which are contained in Chapter 2. However, our interest extends to the purpose and role of reconstituted nuclei in wave formation and propagation. At the time we began this project, the only existant research in the field illustrated the existence of mitotic trigger waves *in vitro* (Chang and Ferrell, 2013) and calcium waves *in vivo* (Gerhart, 1980). The former work relied on extract experiments supplemented with sperm DNA to reconstitute nuclei, and offered a model which presupposed the existence of pacemakers within the system (Chang and Ferrell, 2013). The latter demonstrated the import of coordination of the mitotic clock in early embryogenesis, but merely suggested the possible existence of mitotic waves in embryos with only a pronucleus (Gerhart, 1980; Chang and Ferrell, 2013). Future work would identify nuclei as pacemakers (Afanzar et al., 2020; Nolet et al., 2020). The former briefly touched on waves without nuclei, highlighting their existence, but did not delve too deeply into their behavior (Afanzar et al., 2020). Thus, I set out to investigate both time-dependent wave behavior, and whether a compartamentalized system behaves differently than a spatially homogeneous system as a function of time.

First, I will outline the basics of our experimental setup, including extract preparation, choice of reporters and imaging details. Second, I will present data depicting how mitotic waves develop and evolve from phase-like to trigger-like as cycles slow down. Third, I will discuss data which suggests nuclei act to entrain the system to the trigger-like regime.

This work was completed in collaboration with Lendert Gelen's lab, in particular his post-doc Daniel Ruiz Reynés. To note the contributions, I performed all experiments, processed the images, created the initial data analysis pipeline and assisted with the subsequent analysis. Daniel refined the pipeline, helped with theoretical framing and conducted numerical simulations which will appear in our manuscript. The majority of this work (Sections 3.3 and 3.4, specifically) is adapted from a manuscript which will imminently be submitted for review.

3.1 Experimental Setup and Methods

3.1.1 Extract preparation

To capture mitotic waves *in vitro*, I made cell-free cycling extracts from *Xenopus laevis* eggs following a published protocol (Figure 3.1, A) (Murray, 1991) with one main modification (Guan et al., 2018). In brief, I replaced electrical shock activation with the addition of calcium ionophore A23187 (200 ng/μL), as previously demonstrated (Guan et al., 2018). Extracts were then supplemented with various reporters, drugs and/or sperm DNA, depending on the experimental conditions desired (Figure 3.1, B). Historically, the field tended to restrict the dilution of extract —i.e. added reporters, drugs, etc.—to no more than 10%: where dilution here means [1 – Volume Extract/Total Volume] (Murray, 1990). However, during the course of my thesis research, work from the Yang lab demonstrated increased dilution can improve the number of cycles, with the best activity coming around 20% dilution (Jin, et al. 2021). As a result, the data described here come from extracts of different dilution levels. For data taken before the above revelation, the dilution never exceeds 10% but is not constant; for data acquired after, the dilution is kept constant at 20%. Due to a fortuitous confluence of timings, for data presented throughout this publication, experiments using the FRET sensor were conducted with extracts at 20% dilution; otherwise, the <10% rule applied. Importantly, in this small range, dilution appears

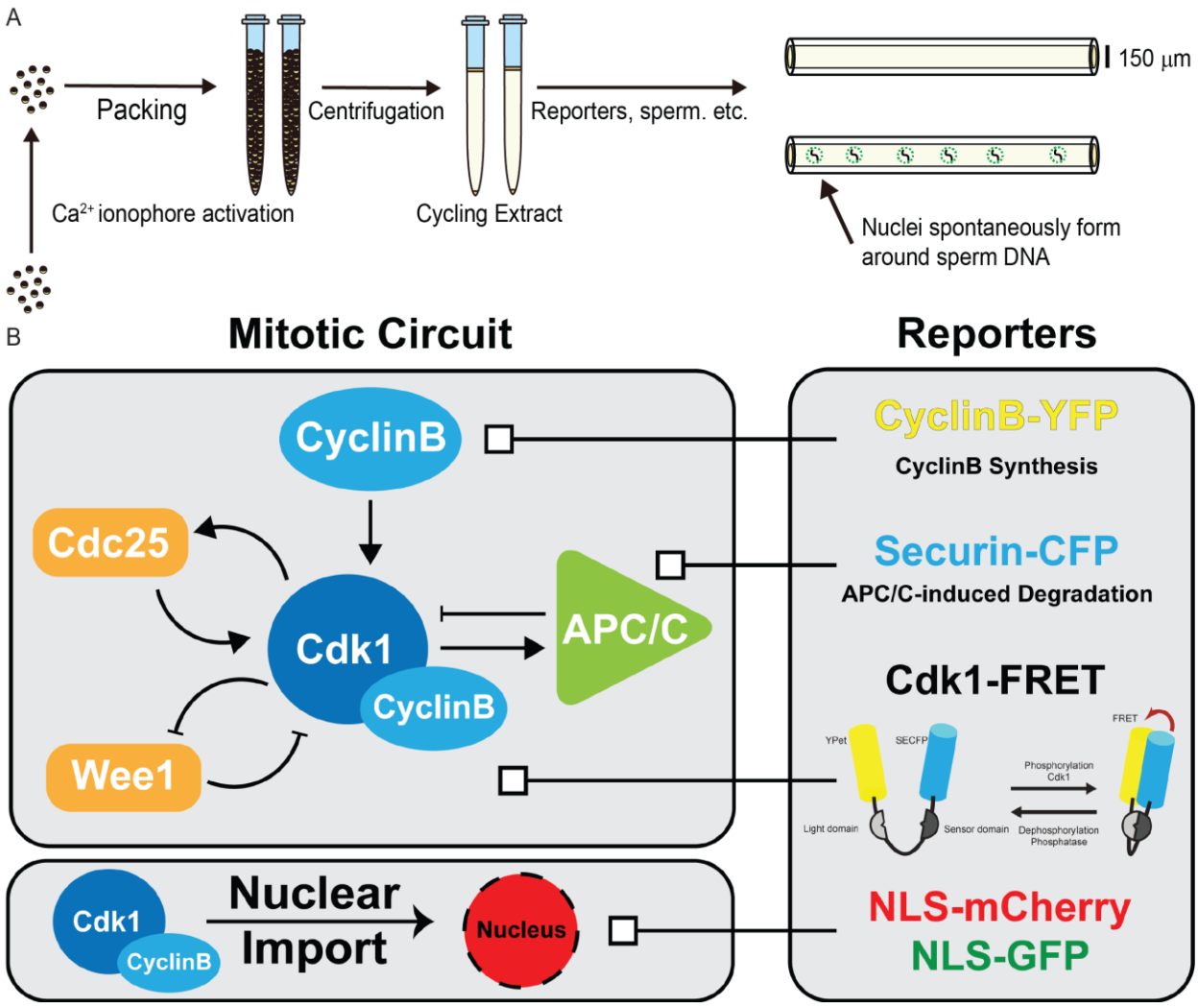

Figure 3.1 Experimental Procedure for Generating Mitotic Oscillations in 1D Tubes

A) Schematic of extract preparation. In general, we follow published protocols (Murray, 1990; Guan et al., 2018) with the singular change of replacing electro-shock activation with calcium ionophore. Cycling extracts are then loaded into quasi 1D Teflon tubing using a syringe, cut under oil to the desired length, and then imaged. B) The mitotic network and a selection of reporters. In the lab, we have access to many different reporters which capture different information about the clock. Cyclin B-YFP reports cyclin synthesis; Securin-CFP reports APC/C activity; the Cdk1-FRET sensor directly reports Cdk1 activity; and various NLS signals report the downstream event(s) of nuclear-envelope breakdown.

to only affect the lifetime and number of cycles, not any other physical property such as period (Jin, et al., 2020). Regardless of this fact, extracts were subsequently loaded into long (~30mm) sections of Masterflex PTFE tubing (inner diameter 150 μm) via aspiration, cut with a razor into 2-3mm sections while submerged under mineral oil, and then recorded using time-lapse epifluorescent microscopy [Olympus IX-83]. Given the dimensions of the tubing used, tubes

were organized into, at most, groups of five in one direction. We did not observe any significant contamination between tubes, even when forcing them into such close proximity.

To capture both oscillation and wave dynamics, I added various combinations of cell-cycle reporters and nuclei-markers plus sperm chromatin (Figure 3.1, B). The general setup mirrors what others from the Yang lab previously demonstrated in droplets (Guan et al., 2018). To summarize, de-membranated sperm chromatin (sperm DNA) was prepared according to previously published methods (Murray, 1990) and stored at -80˚C. I added sperm DNA in various dilution factors ranging from 50-200x, resulting in roughly 5 nuclei/mm along the length of the tube, though this number varied significantly tube-to-tube. Some literature exists regarding the spacing of nuclei in extract (Cheng and Ferrell, 2019), though I did not necessarily observe similar behavior in our experiments. For reporters, I used green fluorescent protein- nuclear-localization signal (NLS-GFP), NLS-mCherry, Securin-CFP nRNA, Cyclin B-YFP mRNA and a Cdk1-FRET sensor. Both NLS sequences visualize the formation and breakdown of nuclear membranes over the course of mitosis. During interphase, nuclei spontaneously form around exogenous sperm DNA, into which NLS-GFP(mCherry) translocates through nuclear pores (Figure 3.1, B). At the beginning of mitosis, this membrane breaks down, resulting in rapid diffusion of NLS-GFP to an approximately uniform distribution (Figure 3.2, A). The NLS-mCherry protein functions similarly but can be imaged simultaneously with other non-red reporters, as seen in Appendix X. To capture biochemical dynamics, Both Securin and cyclin B are substrates of APC/C: they both accumulate during interphase, peak at metaphase, and then quickly degrade at the end of mitosis (anaphase) (Figure 3.3, B; Figure 3.4, A). Therefore, both reporters indicate the progression of the mitotic cycle. One significant difference between these two reporters is their interaction with nuclei. Due to cyclin B's binding to Cdk1, it also

translocates into the nucleus throughout the cycle (Figure 3.4, A). As a result, cyclin B-YFP enables simultaneous detection of nuclei and the biochemical signal (Figure 3.4, A).

However, these reporters also exhibit some undesired properties. For one, mRNA-based reporters require accumulation over time. This fact makes early cycle detection difficult and often impedes any observation whatsoever (Figure 3.3, B). Further, synthesis of new protein outpaces degradation, so these signals exhibit significant amplitude and baseline increases over the course of the extract's lifetime (Figure 3.3, B; Figure 3.4, A). Moreover, since neither of these tagged proteins (cyclin B and Securin) display sensitive response throughout the cycle, the oscillatory waveform appears quite broad. While not precisely problematic, this distorts the kymographs and adds complexity to parameter selection for analysis pipelines. Moreover, they cannot provide any information regarding the relative (or absolute) durations of interphase and mitosis, possibly relevant information. Additionally, a downside particular to using cyclin B to report oscillations comes from its role as a positive input to the clock (Pomerening et al., 2003). As work from the Yang lab utilized to great effect, cyclin B-mRNA tunes the clock period downward (Maryu and Yang, 2022). In my experiments, cyclin B-YFP-mRNA was added at concentrations of 6-10 ng/μL. Since I was not considering the effect of cyclin B tuning in any given experiment, I did not take care to regulate the possible effect on period thereof. However, these experiments did exhibit faster periods, as a result. Finally, none (including NLS-based reporters) offer any information at all regarding Cdk1 activity.

A post-doc in the Yang lab, Gembu Maryu, designed a Cdk1 FRET sensor for precisely this purpose (Maryu and Yang, 2022). A full description of the biosensor can be found in their publication, but here I present a short summary. The sensor relies on a donor-acceptor fluorescent protein pair and a Cdc25C sequence as a phosphorylation site for Cdk1 in the active

(mitotic) state (Maryu and Yang, 2022). When Cdk1 becomes activated, the sensor and ligand domains bind, and the resulting conformational change modulates the FRET efficiency which can be quantified by calculating the ratio of donor-to-acceptor emission intensities (Maryu and Yang, 2022). This sensor is specific to Cdk1 activity and demonstrates efficacy across many cycles (Maryu and Yang, 2022). Results using this novel sensor will be displayed below.

3.1.2 Analysis methods

Both fluorescence time series and kymographs were then analyzed to obtain the cycle period (frequency), number of cycles, and wave speed. For early experiments, I generated kymographs using Fiji's stack montage feature with individual tubes cropped manually using the bright-field images as a guide. I then binned (average) over the width of the tube to reduce edge-effects. If only NLS-based reporters were used, periods could be calculated manually using the frames of nuclear envelope breakdown (NEB) in consecutive cycles to denote the endpoints of one cycle. Otherwise, peaks in the mean intensity (across the entire tube) of the reporter were used similarly. Peaks were detected in either Matlab or Python, depending on the analysis pipeline in question. Wave speeds were also handled separately. In experiments with NLS-based reporters, lines were drawn manually, following the fronts of NEB. The slopes of these lines give the speed. Otherwise, the detected peaks were used, and lines were fit to subsections of each cycle which were deemed wave-like by eye. The fitted slope similarly gives the speed.

For later experiments, when the length of the tube exceeded the field of view of the microscope (~3mm), grids of images were captured and subsequently stitched together using ImageJ's Grid/Pairwise Stitching plug-in (Preibisch et al., 2009), in conjunction with my own pipeline code written in Fiji/Java. The wavefronts do not display sufficiently recognizable characteristics for the purposes of stitching. As a result, I used bright-field images from the first

frame to generate stitching parameters, then fed these parameters to ImageJ to stitch each channel at each frame consecutively. While capturing grids of images in this way results in a non-zero timestep between subsequent sections along a tube—and thus, some multiple of this dt between the first and last sections—this gap amounts to a few seconds, much smaller than the scale of the overall imaging timestep which is on the order of minutes. As such, this can be and is ignored for the purposes of analysis. The stitched stacks are then straightened using Fiji and a manually selected curve from the bright-field images as an input. This curve is unique to each tube, though the profiles of the tubing sections often followed roughly the same shape, so not much distortion is expected. Afterwards, the tubes are cropped so as to only include the inner dimension, again using the bright-field images as a guide.

Additionally, calculation of the FRET ratio is handled separately. This Fiji code is summarized and given in Maryu and Yang (2022). I will briefly outline the procedure here. Images for the CFP-CFP (CFP) and CFP-YFP (FRET) channels are stitched separately, as previously discussed. Once assembled as individual stacks, the background is subtracted from each using Fiji and the "rolling" method. These channel signals are then divided at each frame: FRET/CFP. The resultant stack is the FRET Ratio which is ultimately used for any and all analysis. We do observe baseline decay over time, likely due to photobleaching (Maryu and Yang, 2022). This is corrected in post-processing for the purposes of analysis. Due to noise, this can result in some pixels of undefined and/or infinite intensity. This is handled later in post-processing. For visualization purposes only, the CFP and FRET channels' min and max values are determined manually and are used to generate the heatmaps displayed throughout. As indicated in each following figure, active Cdk1 corresponds to warm colors; inactive, cool colors. Due to the photobleaching-induced decay mentioned above, these heatmaps cool over

time. As stated in Maryu and Yang, 2022, they do not believe this represents an intrinsic signal reduction, but it should be noted.

For the analysis of experiments conducted with the FRET sensor, a rotation student in our lab, Yeonghoon Kim, and I designed an object-orientated algorithm in Python to analyze spatial profiles of observed patterns. I will outline the procedure here. First, individual kymographs are corrected for the decaying baseline trend, and any NaN pixels are filled using the scikit-image function inpaint. Afterwards, I detect peaks for each time series at each pixel along the tube. The peaks themselves are then clustered into individual cycles using stock clustering algorithms (DBSCAN) in Python. Once cycles are identified and separated, the collection(s) of peaks are fitted and/or smoothed in space and time, after which slopes (and speeds) are calculated along each front by taking the numerical derivative of the fits at each point. Periods follow directly from the detected peaks, as discussed previously with other reporters. Additionally, the shapes of the first cycles are used as inputs to the noise distribution for numerical simulations that will appear in our manuscript. As mentioned, our collaborating post-doc Daniel Ruiz Reynéz would ultimately refine and implement this pipeline, from which the analysis that follows stems.

3.2 Early Attempts to Realize Mitotic Waves With and Without Reconstituted Nuclei Provide Preliminary Evidence For Discrepancies in Time-Dependent Wave Propagation

I began by capturing the dynamics of extracts with reconstituted nuclei using NLS-GFP to confirm previously published results (Figure 3.2). As shown, tubes containing nuclei demonstrate similar behavior as previously reported in the field (Chang and Ferrell, 2013; Nolet et al., 2020). Early cycles display noisy synchrony, to such an extent that classifying the patterns is non-trivial and after a short time, linear trigger wave fronts develop from a source nucleus(nuclei)—matching what has been reported previously (Figure 3.2, A). Tracking the

speed of these waves over time, I find an initially rapid decay in speed from roughly 50-60 μm/min (as previously reported) up and until a much slower decay or leveling at around 20 μm/min (Figure 3.2, B). This lower speed persists for many cycles, over long periods of time (Figure 3.2, C). Moreover, such speed slowing coincided with period lengthening consistent with our lab's work in droplets (Figure 3.2, C) (Guan et al., 2018). As in droplets, I find an effectively monotonic increase in period over time (Figure 3.2, B, D). This results in the dispersion relation shown in Figure 3.2, D. I observe waves traveling at speeds seemingly independent of period at late times (Figure 3.2, D). This represents the first attempt in the field to quantify the dispersion relation for mitotic waves and I will expand on this notion later. This phenomenon remained

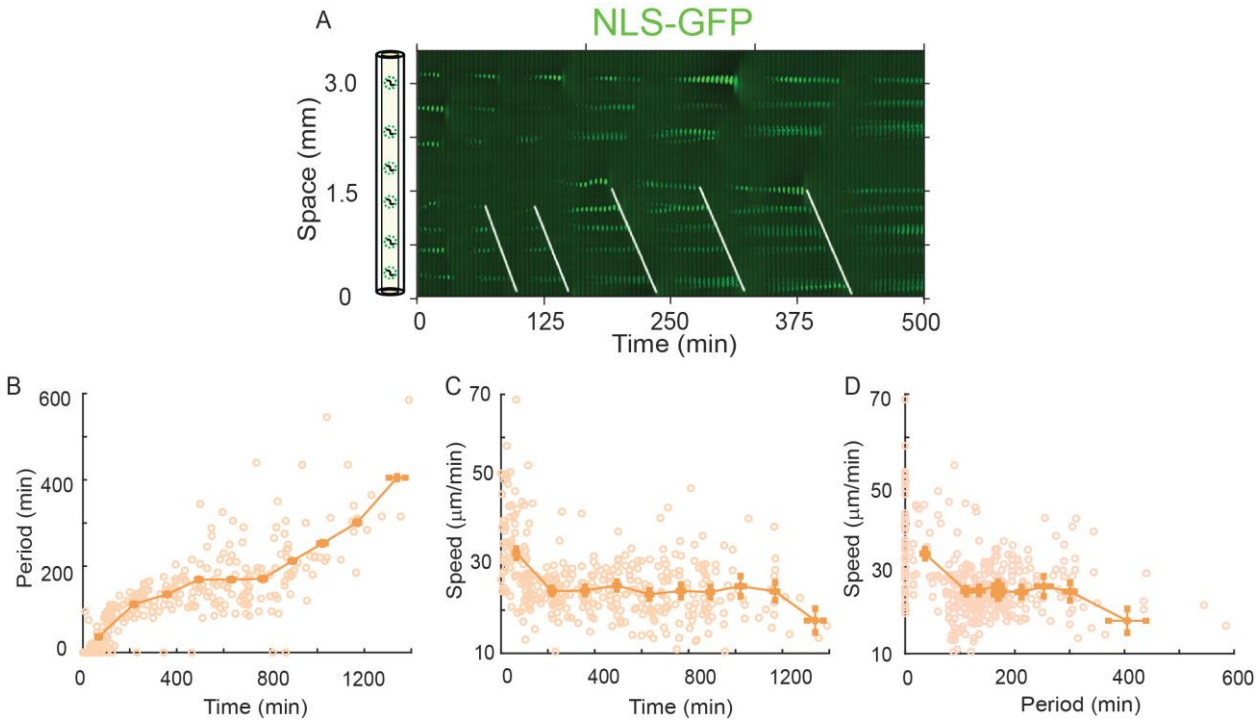

Figure 3.2 Recapitulation of Mitotic Waves, Reported by NLS-GFP and Reconstituted Nuclei

A) Representative kymograph. Nuclei spontaneously form around added sperm DNA, and NLS-GFP transolcates into the membrane(s). Waves appear as fronts of nuclear envelope breakdown (NEB) as indicated. B, C) Period and Speed plotted as a function of time. Scatter plot points represent individual wavefronts while the solid lines correspond to time-binned data. Error-bars give standard error. D) Dispersion relation. The tail of roughly constant speed as period lengthens implies a speed plateau for mitotic waves. Both period lengthening and speed slowing have been reported previously (Chang and Ferrell, 2013; Nolet et al., 2020). However, we are the first to consider the implications of the dispersion relation

consistent over multiple experiments and was not affected by small changes in sperm DNA dilution, indicating a general response.

However, tubes without reconstituted nuclei display drastically different spatial patterns. For one, I do not observe clear linear wavefronts with any regularity; instead, these tubes oscillate roughly synchronously, with minimal or ambiguous patterning (Figure 3.3, A). As mentioned previously, early cycles largely averted detection due to low signal amplitude (Figure 3.3, B). Occasionally, wave-like fronts would be observed emanating from the boundary, but these were few and far between, and when present, routinely arose at late cycles of long periods (Figure 3.A). As such, I lack sufficient statistics for representations of these fronts. Other patterns observed in the bulk almost always appeared non-linear in shape and significantly more diffuse in contour (Figure 3.3, A). Ultimately, I found these ambiguous patterns and the dearth of

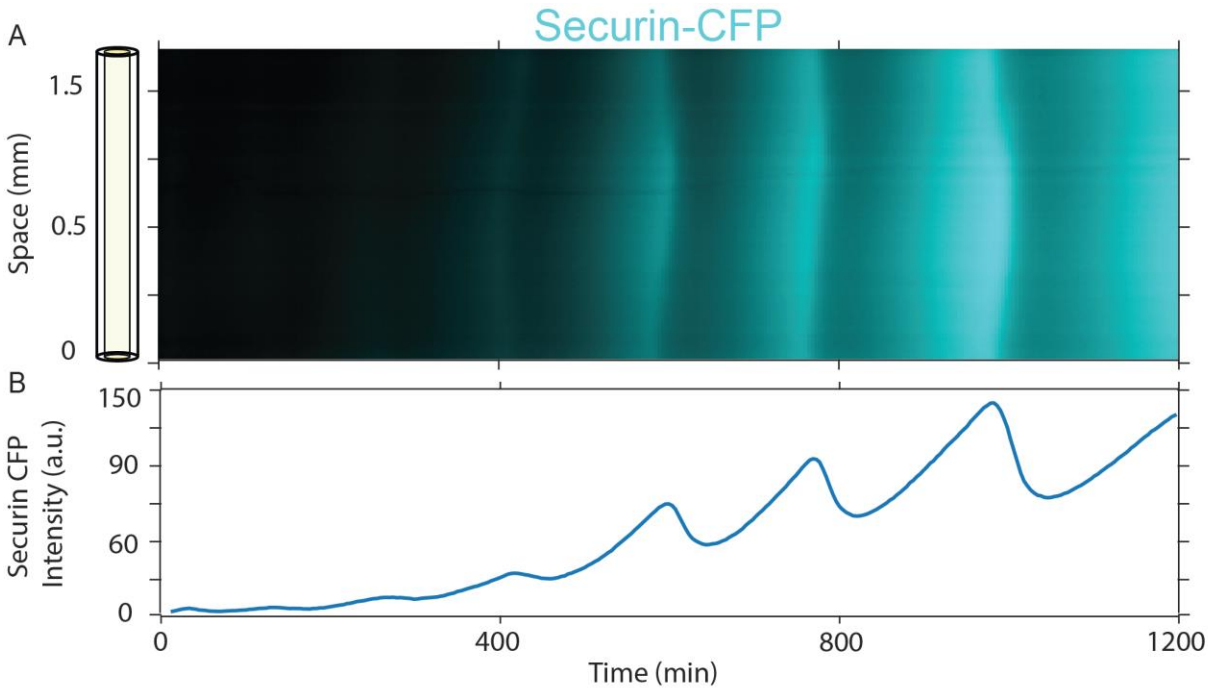

Figure 3.3 Recapitulation of Mitotic Waves, Reported by Securin-CFP

A) Representative Kymograph. Early are difficult to characterize both due to the low amplitude of the signal, as well as their indeterminate shape. Wave-like patterns sometimes arise at late times when periods are long. B) Securin-CFP intensity over time for the kymograph shown. Both the amplitude and baseline intensity increase from low values over time.

easily identifiable wavefronts frustrating. However, the visual discrepancy between systems with and without nuclei, particularly their disparate time dependence, was stark.

To probe this further, I turned to cyclin B-YFP to capture wave dynamics in systems with and without nuclei in the same experiment. In these experiments, extracts were prepared as usual, with similar amounts of added sperm DNA as before (dilution ~100x). Reproduction of the nucleus-non-nucleus comparison yielded similar qualitative results as discussed above (Figure 3.4). Tubes with nuclei demonstrated more easily classifiable wavefronts, at earlier times, while tubes without displayed less clear patterning (Figure 3.4, A). However, for these

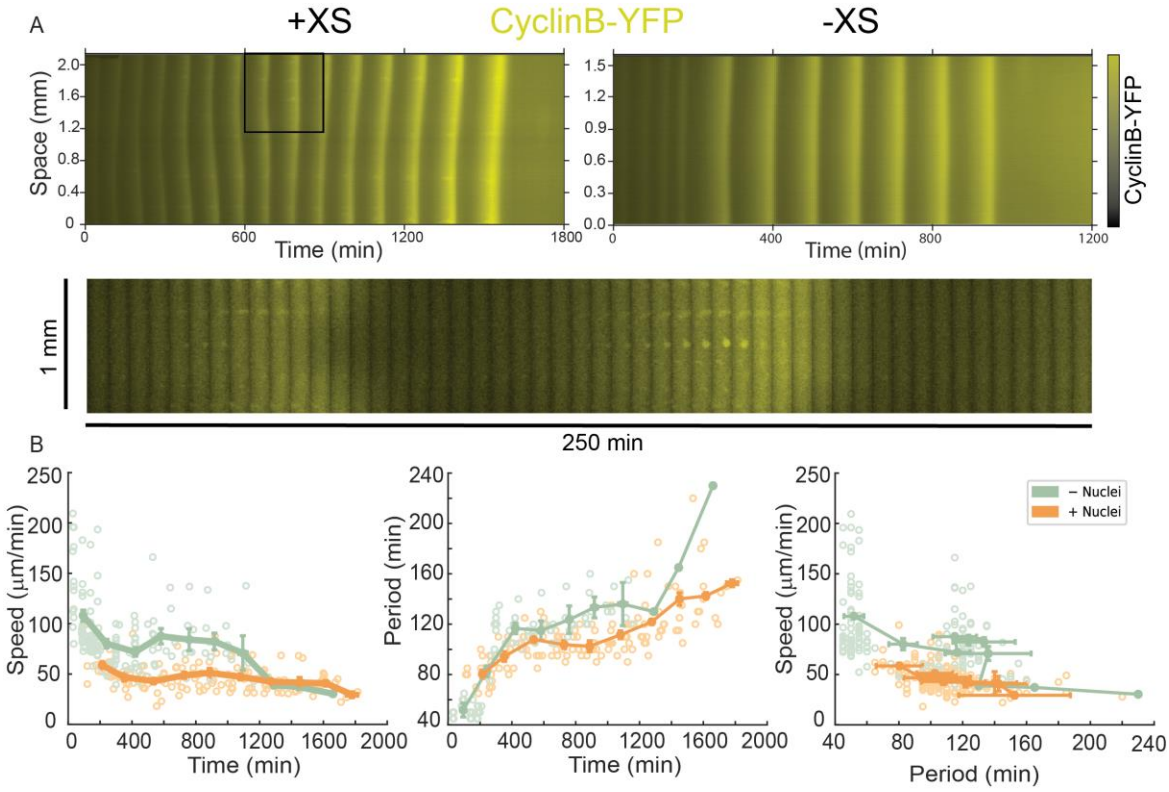

Figure 3.4 Reconstituted Waves with and without Nuclei, Reported by Cyclin B-YFP

A) Representative kymographs for tubes with (left) and without (right) reconstituted nuclei. The highlighted square region corresponds to the zoomed in snapshot below the full kymographs. The addition of nuclei seemingly increases the propensity for clear linear wavefronts. B) Quantification(s) of the speed (left) and period (middle) over time, as well as the dispersion relation (right). As before, we observe speed slowing coinciding with period lengthening over time. The dispersion relations mirror what can be observed qualitatively. Tubes without nuclei exhibit patterns of high speeds at shorter periods and are slower to decay to the observed speed plateau.

data, I had sufficient early-time amplitude to (at least roughly) quantify speeds in both conditions. As can be seen below, waves with nuclei exhibit significantly slower speeds than those without, especially initially (Figure 3.4, B). In particular, experiments with added sperm DNA display speeds which again decay quite quickly to this plateau. However, those without sperm DNA decay more slowly and persist at higher speeds for longer (Figure 3.4, B). This suggested to me, along with the clear qualitative dissimilarities, a meaningful difference between how waves with and without nuclei behave in time. However, I still lacked sufficient detail from these experiments to truly capture how, exactly, this difference manifests.

3.3 Extracts without Reconstituted Nuclei Begin as Phase-like (or Sweep-like) Waves which Transition to Trigger Waves as Cycles Slow

As well as remedying the myriad practical issues described above, the Cdk1-FRET sensor allows me to generate the first visualizations of mitotic waves as a biochemical signal of activity, rather than relying on downstream events such as NEB or APC/C-induced degradation. For these experiments, I used sections of tubing 2-5 times longer (~5-10mm) than those used previously, as indicated by the scale in the relevant figures. In part, this stems from my experience with the driven system (to be discussed in Chapter 4), but I also wanted to visualize patterns on larger length scales. As shown in previous sections, I found the patterns observed in early experiments, those in short (2-3mm) tubes, were often of wavelengths on the order of the system length itself, and thus difficult to distinguish. As such, the data presented below will hopefully present a clearer representation of the observable patterns.

Beginning with the system without nuclei, I offer a representative kymograph for such an experiment in Figure 3.5, A. For presentation purposes, I present the FRET signal as a heatmap with cool colors corresponding to low Cdk1 activity, and warm colors similarly for high activity

(Figure 3.5, A). The explicit FRET donor-to-acceptor ratio is also given for a small slice (~10 pixels) of the tube in Figure 3.5, B. Peaks in this signal are what allow me to cluster wavefronts (Figure 3.5, A). Periods (peak-to-peak) are also measured from these signals and are given in Figure 3.6. However, even visually, from both the kymograph and the FRET ratio trace, one can identify typical period lengthening due to a noticeable increase in interphase (cool regions in the kymograph). This trend matches what I observe in extracts generally. Additionally, I calculate the maximal time derivative of the activity (dA/dt) for each cycle. The purple points in Figure 3.5, B represent these maxima for this kymograph, at that slice.

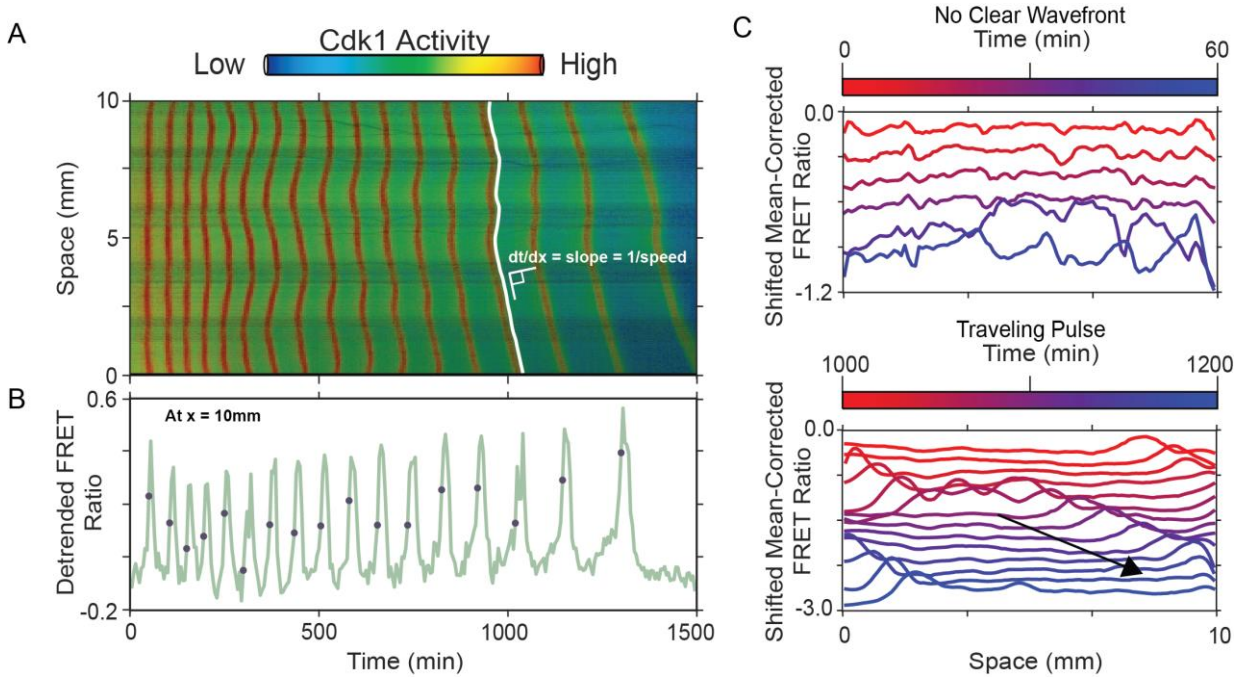

Figure 3.5 Reconstitution of Mitotic Waves without Nuclei, Reported by Cdk1-FRET Sensor

A) Representative kymograph. With the Cdk1-FRET sensor, Cdk1 activity is given by the heatmap where cool colors indicate low activity, and warm colors indicate high activity. In this way, wavefronts of Cdk1 activity appear as red/warm bands across the tube. The dark stripes are relics of stitching. The white line corresponds to a representative isolated front. B) Cdk1-FRET donor-to-acceptor ratio. This quantifies the heatmap in A). This trace corresponds to the activity at x = 10mm in A). As can be seen visually, the period lengthens over time, primarily due to the interphase duration increasing. The purple points are where dA/dt is measured. C) Mean-shifted spatial profiles, a la Hayden et al., 2022, for early (Top) and late (Bottom) cycles. At early times, the system exhibits phase (or sweep) waves, as indicated by the roughly conserved spatial gradients. Conversely, at late times, clear and obvious pulses travel through the system, indicating the presence of trigger waves. Take together, this points to a transition from phase/sweep to trigger dynamics over time as cycles slow.

I also observe obvious changes in spatial profiles over time. At early times, the patterns I observe resemble the so-called sweep waves highlighted in *Drosophila* embryos (Figure 3.5, C, Top). Taking a cue from Hayden et al. (2022), when I plot the FRET ratio spatial profile over consecutive frames for early cycles, we see a roughly uniform upswing in activity, with local peaks preserved, largely preserving spatial gradients (Figure 3.5, C, Top). While this does not equate to a strict proof for the existence of sweep waves in *Xenopus*—higher time resolution and parameter scaling are required to be certain—the similarity is striking. Additionally, early

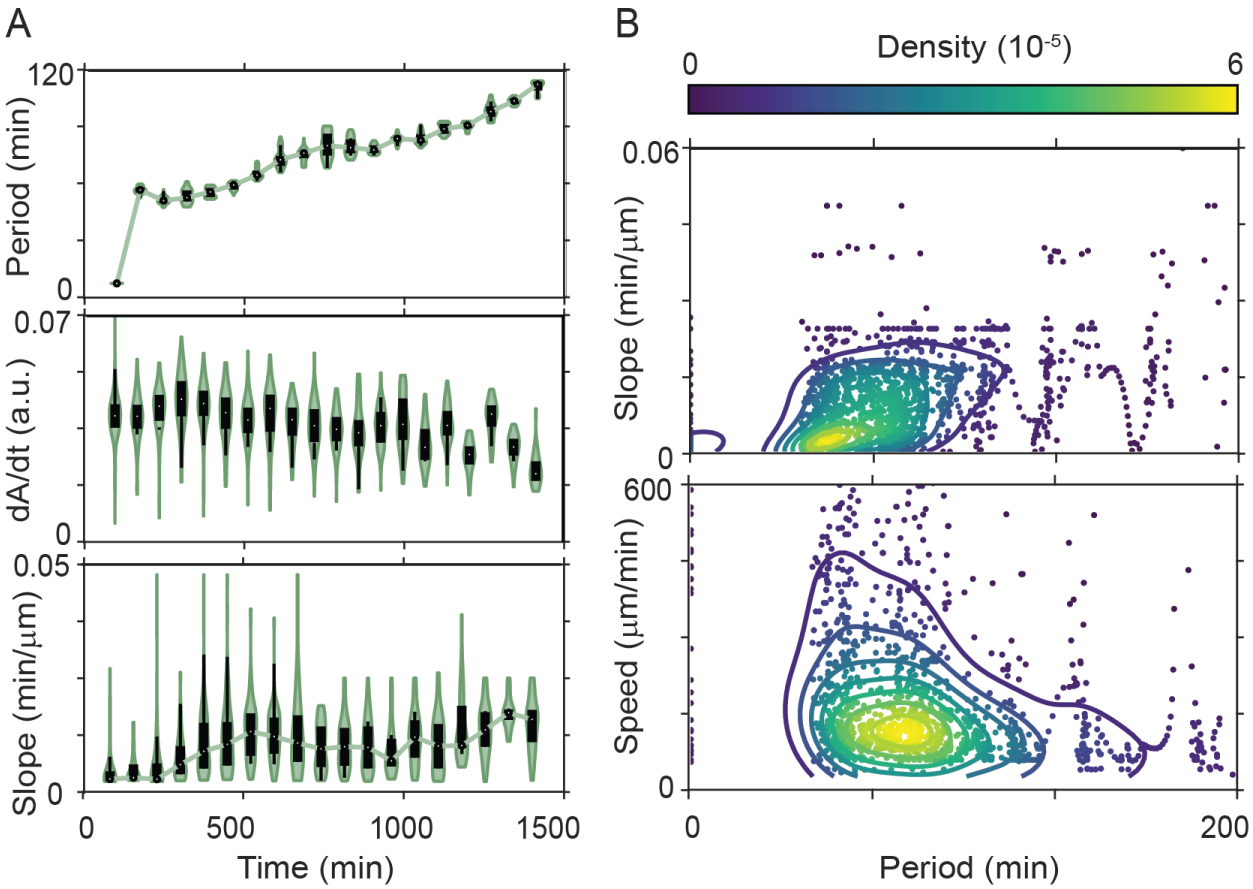

Figure 3.6 Quantification of Wave Properties for the Kymograph in Figure 3.5

A) Period (Top), dA/dt (Middle) and Slope (Bottom) over time. Each quantity is calculated at each point in space and the resulting data is presented here binned, in time. We observe period lengthening (Top), roughly constant dA/dt (Middle) and slope which initially increases and then plateaus at later times. As early-time patterns often exhibit infinite speeds at this resolution, we instead calculate the slope = 1/ C) Slope (Top) and Speed (Bottom) densities as a function of period. We observe small (large) slope (speed) are early times and small periods that increase (decrease) to apparent plateaus as time and period increase.

experiments without the FRET sensor largely obscured this information due to prohibitively low reporter amplitude. As such, this represents the first clear look at early-time patterns in extracts.

Conversely, at late times, the system exhibits clearly linear, trigger-wave-like fronts, usually emanating from one of the boundaries (Figure 3.5). Occasionally, waves originate from points in the bulk, but these are normally transient over a few cycles, at most. This behavior is consistent with results published previously (Alfanzar et al., 2020). The propensity for such boundary-driven waves appears much higher in my experiments in longer tubes than before in the smaller system. However, any possible system size dependence remains unknown. Nevertheless, when I repeat the process of plotting the spatial profile for successive frames, these trigger wave-like fronts appear as clear and obvious moving pulses (Figure 3.5, C, Bottom). As a result, this implies some sort of transition from sweep (or phase) waves at early, fast cycles, to trigger waves at late, slower cycles. However, I can also quantify this transition.

Using the analysis pipeline I designed, I can isolate wavefronts and analyze them individually (Figure 3.5, A). To begin, I plot various quantities for the single kymograph presented in Figure 3.6 to familiarize the reader with the relevant trends. However, the trends hold for the complete dataset presented in Figure 3.7 and will be what I discuss in the text. As in droplets, I observe a roughly linear increase in the period over time, with some divergence at late times when extracts die (Figure 3.7, A, Top). Here, and for all future data presented in this way, a period of 0 minutes corresponds to the first cycle. While these data cannot fit into any subsequent analysis, I present them for completeness' sake. As shown in Figure 3.7, A, Bottom, this increase in period is largely due to an increase in the rising period, or the duration of interphase, much like what Hayden, et al. (2022) report in their *polo* mutants. The rising period goes from representing 57% of the cycle duration at cycle 1, to 80% at the last cycle. This

suggests the system primarily experiences a slowing of the activation dynamics, rather than increased time spent in the active state. This all is consistent with the Yang lab's analysis of cycles in droplets and our model of ATP depletion (Guan et al., 2018).

I hypothesized that this may be accompanied by a decrease in the speed of activation, dA/dt, and a shift away from relaxation dynamics. To test this, I calculated the maximal derivative between wavefronts at each point, for each cycle. As can be seen in Figure 3.7, B, Top, this quantity remains fairly constant, or slightly decreasing, over time, suggesting the underlying oscillatory dynamics—that of a relaxation oscillator—do not change much. Instead, this again points to a time-dependent change in the ratio of the relative positive and negative feedback loop strengths. This idea will be used in the numerical work presented in our manuscript, agnostic of any biophysically specific mechanisms, such as ATP depletion.

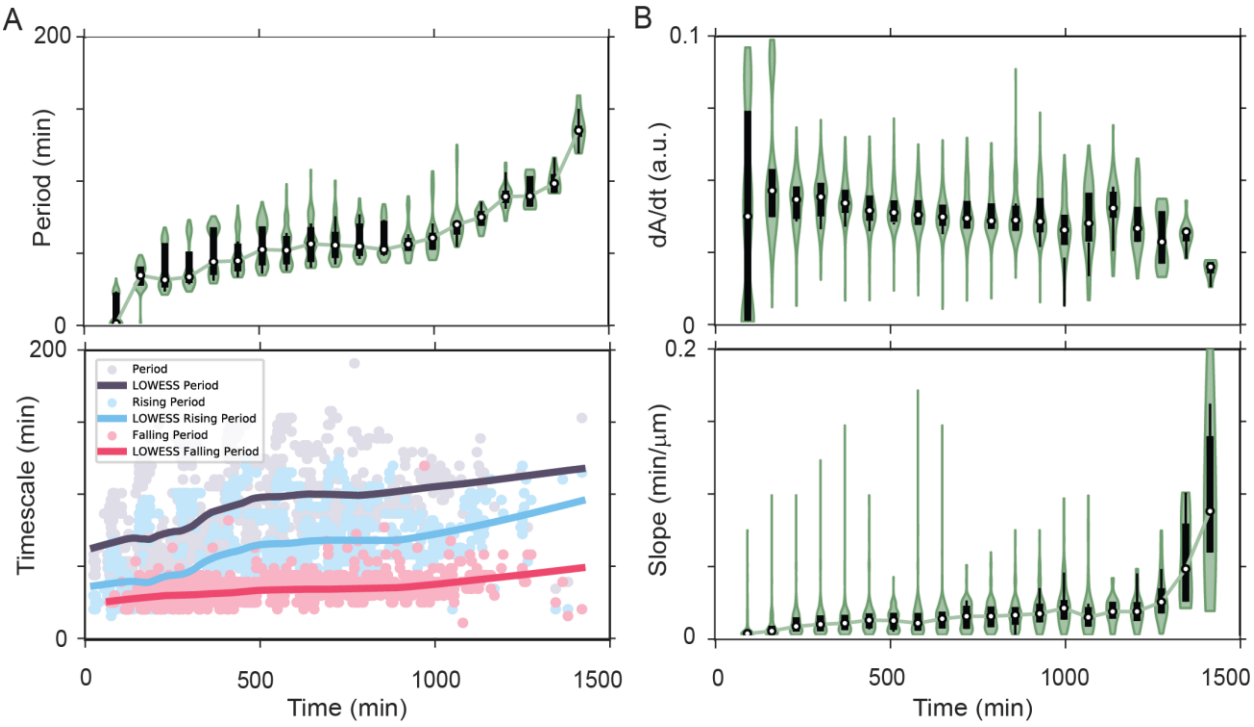

Figure 3.7 Time-dependent Measurement of Oscillation and Wave Properties for Extracts Sans Nuclei

A) Period (Top) and period broken down into rising and falling portions (Bottom). Period monotonically increases over time, primarily due to an increase in the rising period. B) The maximal activation rate dA/dt (Top) and the slope (Bottom) over time. The activation rate is roughly constant, while the slope initially increases and then plateaus, corresponding to early, short periods and late, long periods, respectively.

For wave speeds, I calculate the derivative of the fronts in Time-Position space—the flipped orientation from the kymographs—because the patterns at early times often exhibit effectively infinite speed, at this resolution. As a result, I instead measure the slope in min/μm. As shown in the violin plot in Figure 3.7 B, Bottom, the slope generally increases over time, corresponding to a slowing of the speed. Again, the divergence at late time corresponds to disparate behavior as cycles end. When combined, these measurements allow me to construct a Slope-Period relation which presents as a monotonically increasing function, when allowing for

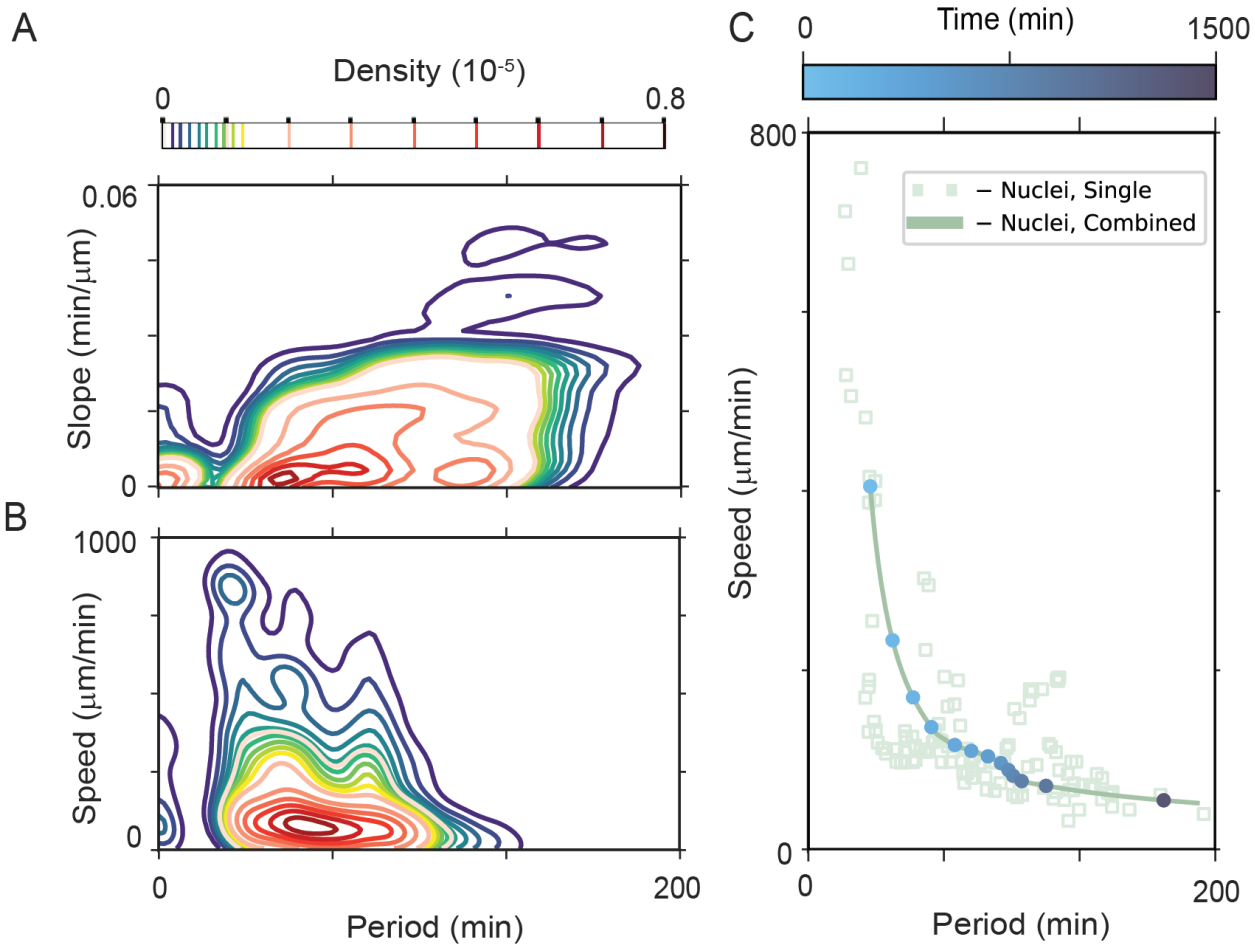

Figure 3.8 Mitotic Wave Dispersion Relation Shows Phase-Trigger Wave Transition

A) Slope-Period contour plot. The general trend combines those depicted in Figure 3.7. B) Speed-Period contour plot. C) Mitotic wave dispersion relation. This visualization highlights the existence of a transition from fast, short period patterns to slow, long period trigger waves: the first evidence for such a transition in *Xenopus*. Light-colored open squares correspond to LOWESS fits for individual experiments (connecting lines omitted for clarity), while the dark plot corresponds to the same for all the data combined. The colored points are taken from dark green curve and are meant to denote how the system moves along it in time.

late-time discrepancies (Figure 3.8, A). For the pooled data, I present the densities as contours due to the large number of data points (Figure 3.8, A, B). Converting from slope to speed, we can then create a dispersion relation for mitotic waves (Figure 3.8, B, C). To capture the trend in time, I apply LOWESS (locally weighted scatterplot smoothing) to both slope (speed) and period in time and then plot these against each other (Figure 3.8, C). This quantifies what I observe visually. At short periods (read: early times), the system exhibits phase or sweep waves of speeds much faster than trigger waves; however, these transients eventually die off as the system transitions to a regime dominated by trigger waves (Figure 3.8, C). To guide the reader in following this curve in time, a subset of points is plotted with their color indicating time (Figure 3.8, C)

This dispersion relation also appears to confirm what Hayden et al. report regarding a sweep-to-trigger transition (Hayden et al., 2022). Namely, a system which exhibits period lengthening due to heterogeneously changing time scales (interphase and mitosis) might also exhibit a transition from sweep to trigger waves. I cannot prove early-time patterns truly represent sweep waves. This would require much higher time resolution to facilitate accurate measurements of the activation rates and sweeping action Vergassola et al. use to justify their theory (Vergassola et al., 2018). However, these data offer the first quantification of the time-dependent behavior of mitotic waves in extracts and point towards a bridge between our understanding of mitotic waves in different model systems and at different time scales. Numerical simulations of this system recapitulate our experimental findings. The details of the model will be available in our manuscript.

However, this also poses the question: how does this transition change, if at all, when the system is perturbed? Specifically, as discussed, nuclei appear to play some role in wave

formation by acting as pacemakers (Afanzar et al., 2020; Nolet et al., 2020). Modeling work by the same labs demonstrates explicit and implicit inclusion of pacemakers drives waves at the pacemaker frequency, and that the response wave speed depends on this driving frequency (Rombouts and Gelens, 2020; Chang and Ferrell, 2013). This suggests that compartmentalizing the cytosol and/or introducing pacemakers might affect how the system transitions over time. The question then becomes, if so, how can we characterize this change?

3.4 Reconstituted Nuclei Entrain the System to the Trigger-Wave Regime

To answer this question, we reconstituted nuclei by supplementing extracts sperm DNA, as before. We begin our analysis at late times when trigger waves are easily identifiable. Since the FRET sensor contains an NLS-tag, I observe active Cdk1 import, as indicated by the nuclei flashing brightly red without the need for an additional NLS-specific sensor (Figure 3.9, A, Bottom). This occurs during interphase and coincides with a local depletion of active Cdk1

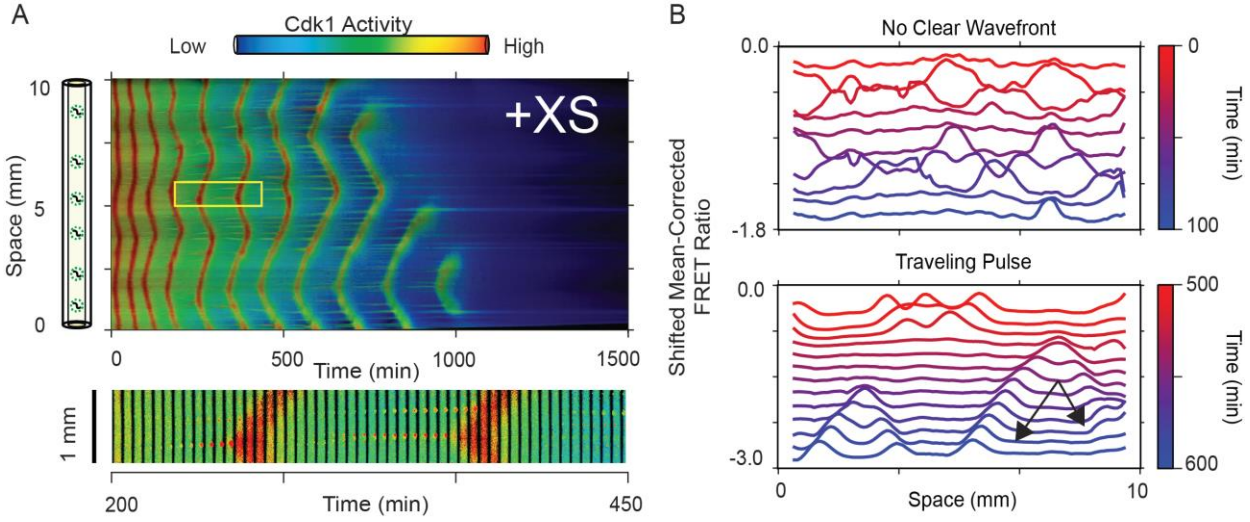

Figure 3.9 Reconstitution of Mitotic Waves with Nuclei, Reported by Cdk1-FRET Senor

A) Representative kymograph. The outlined rectangle corresponds to the zoomed-in slice below which shows how the nuclei import active Cdk1 during interphase. B) Spatial profiles for early (Left) and late (Right) cycles. As in the case without nuclei presented before, early cycles remain largely synchronized. The peaks in the profiles here correspond to the nuclei themselves which import active Cdk1 in interphase. Late cycles, alternatively, exhibit the traveling pulses of trigger waves.

outside the membrane, indicated by the cooler-colored regions surrounding the nucleus in question (Figure 3.9, A). Furthermore, even at a relatively coarse timescale, the pacemaker nucleus imports and contains more active Cdk1 earlier than its neighbors, as expected (Figure 3.9). After NEB, active Cdk1 fills the local region and pulse-like waves propagate as usual (Figure 3.9, B, Bottom). As in the case without nuclei, the spatial profiles clearly indicate propagating pulses (Figure 3.9, B, Bottom). At early times, however, the picture looks qualitatively similar to what I see in tubes without nuclei. That is, despite nuclei visibly forming, I observe a comparable sweeping up of activity, though the effect is much noisier and punctuated by peaks associated with the nuclei themselves throughout the tube (Figure 3.9, B, Top). The *Drosophila* embryo also contains nuclei, as it is syncytial, but the data from the Di Talia group does not show any semblance of nuclei-dependent aggregation as we observe. This makes it difficult to compare spatial profiles across the two systems.

Regardless, repeating the same workflow described previously to this compartmentalized system, I find qualitatively similar behavior for each of the relevant quantities: the period and slope both increase over time (Figure 3.10, A). While the periods do not differ significantly between the two conditions, the slope for these waves containing nuclei is persistently higher than that measured for tubes without nuclei (Figure 3.10, A). Moreover, the distribution of measured slopes as a function of period appears much broader (Figure 3.10, B). This discrepancy is made all the clearer when considering the dispersion relation. As shown, the transient phase/sweep patterns give way to trigger waves much more rapidly than in the systems without nuclei, as indicated by the quicker decay in speed (Figure 3.10, C). Again, the reader should equate the movement towards longer periods with the forward progression of time, as indicated by the timepoints plotted (Figure 3.10, C). The slight increase at late times is likely due to extract

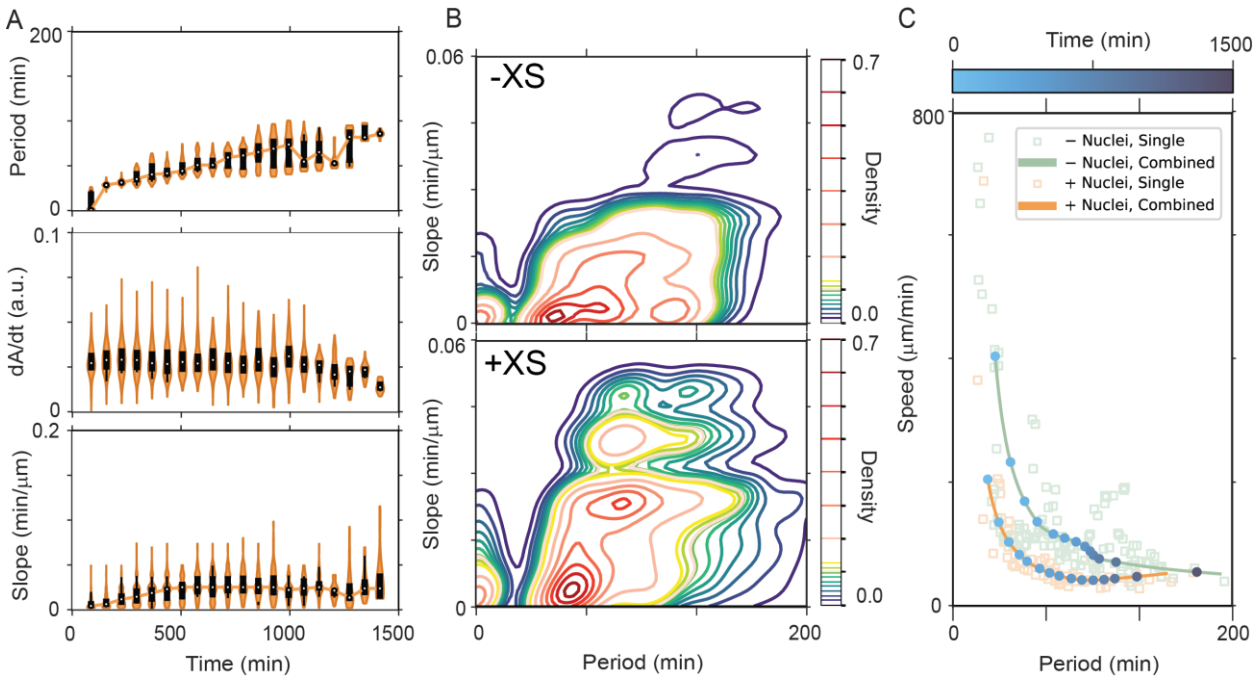

Figure 3.10 Nuclei Entrain the System to the Trigger Wave Regime

A) Period (Top), dA/dt (Middle) and Slope (Bottom) over time for experiments with reconstituted nuclei. Generally, this system behaves similarly to that without nuclei, except for exhibiting higher (slower) slopes (speeds). B) Slope-Period contour plots for both conditions. Experiments with nuclei display broader density profiles. C) Dispersion relations for both conditions. The addition of nuclei entrains the system to the trigger wave regime, as indicated by the faster decay to a slow-speed trajectory as period increases. Timepoints show evolution in time. As in Figure 3.8, light-colored open squares correspond to LOWESS for individual experiments (connecting lines omitted for clarity), while the dark trajectories represent all of the data for each condition, respectively.

death. Despite this, it is clear the addition of nuclei causes the system to admit trigger waves earlier in time, but also "earlier" in period (Figure 3.10, C).

To quantify this difference, we can perform LOWESS smoothing to our slope density data over time and fit the decay to capture a characteristic entrainment time τ using the fitting equation $y = s_f - a\, e^{-t/\tau}$. Here, the parameter s_f gives the long-term speed plateau. Comparing the results between systems with and without nuclei, I clearly observe a more abrupt decay in the latter (Figure 3.11). Additionally, the entrainment time is significantly shorter for the data with nuclei—280 ± 5 min vs 940 ± 15 min—confirming what one observes visually. Interestingly, both fits produce a plateau slope around 0.02 min/μm implying similar long-period behavior and confirming each eventually follows the same dispersion relation. The resulting

speed of roughly 40 μm/min is higher than what we had observed previously, but that likely reflects batch-to-batch differences in extract. As before, numerical simulations which treat nuclei as heterogeneous sinks of cyclin B synthesis also recapitulate these findings, the details of which will be available in our manuscript.

To summarize, I consider this phenomenon to represent the nuclei entraining the system to the trigger wave regime. As mentioned in the introduction, previous work(s) identified nuclei as the pacemakers of mitotic trigger waves (Afanzar et al., 2020; Nolet et al., 2020). In that sense, the nuclei offer a nucleation point for singular wavefronts. In light of my work here, I extend this notion to argue that the nuclei perform a global role of bringing the system out of the phase/sweep wave regime and into the trigger wave regime. To be complete, these data generally follow the trends I and others in the field observed in past work. In systems without nuclei, patterns remain diffuse and exhibit fast speeds. Over time, trigger waves do develop, albeit slowly. Conversely, systems with nuclei develop trigger waves early and often. The result, in

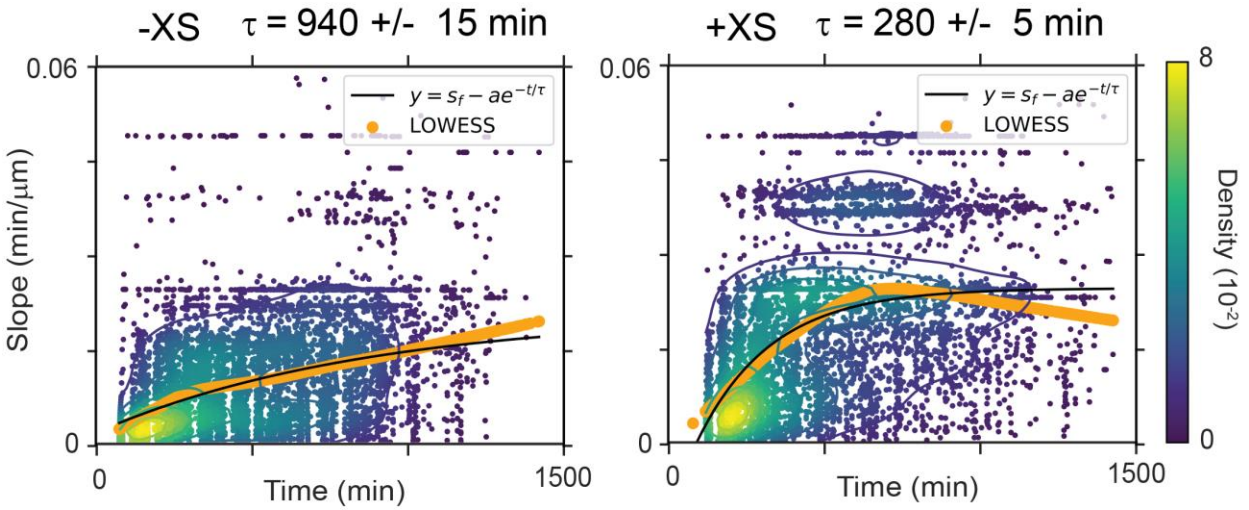

Figure 3.11 Nuclei Entrain the System to the Trigger Wave Regime

Slope-time density plots with LOWESS smoothing (orange line) for experiments without (Left) and with (Right) reconstituted nuclei. The fitted plateau decay gives both the entrainment time τ and the slope plateau s_f. The entrainment time for experiments with nuclei is a factor of three faster than for those without, but the speed plateaus are similar.

terms of measurables, is that the former display fast speeds that slowly decrease as the period increases, while the latter display speeds that quickly decay and follow a trigger wave dispersion relation. My early data pointed to this conclusion, but the imprecision of the reporters I used at the time obfuscated this fact.

3.5 Conclusion

Throughout this chapter, I demonstrated the capacity to realize mitotic waves and patterning *in vitro* using cycling *Xenopus laevis* egg extracts. Using a broad spectrum of reporters, I first reproduced initial results from the field, including realizing mitotic waves using nuclear-localization-signal-based reporters. With these data, I demonstrated how these waves slow down over time until they reach a speed plateau, after which waves continue to propagate at a constant speed, despite persistent period lengthening. I also realized waves sans nuclei. These experiments produced qualitatively distinct patterns and when measured, displayed significantly faster speeds and less drastic decay to said speed plateau.

I then expanded on these early results with the use of the Yang lab's novel Cdk1 FRET sensor. In this way, I produced the first direct observation of Cdk1 waves in *Xenopus* extracts. Additionally, using the FRET sensor, I distinguished between early-time, phase or sweep-like patterns and late-time, trigger waves, in systems both with and without nuclei. This result ties my work into the larger picture of the field: the developing two-class picture of wave propagation. Taken together, I provide evidence for mitotic waves in two distinct systems: a purely 1D biochemical environment, and one compartmentalized by the presence of spatially relevant nuclei. These results demonstrate nuclei are not required for the existence of mitotic waves and qualitatively coincide with my preliminary work using other reporters. Instead, along with collaborators, I showed nuclei also function to organize wave propagation and entrain the system

to follow the trigger wave dispersion relation. In the next chapter, I will underline and reinforce the notion of entrainment by introducing an explicit driving force.

Chapter 4

A System for Driving Mitotic Waves Confirms Entrainment and Increases the Feasibility of Systematically Studying Waves under Tuning Conditions

To confirm and reinforce this notion of entrainment in mitotic waves, I turned to focus on driving waves explicitly. Furthermore, I wanted a way to control wave propagation systematically in order to perturb the oscillator without disrupting wave formation. Such a system could provide a direct test of mitotic waves in these two distinc contexts: that of a homogenous cytosol and one compartamentalized by nuclei. To accomplish this, I took inspiration from published work on driving apoptotic waves *in vitro* (Cheng and Ferrell, 2018). In this work, the authors utilized a reservoir of extract arrested in apoptosis (cell death) to drive an apoptotic signal through a tube filled with extract arrested in interphase (Cheng and Ferrell, 2018). They distinguised between reservoir material diffusing into the tube using a fluorescent dye and the resulting apoptotic wave (Cheng and Ferrell, 2018). After reading this work, I realized that I could accomplish something functionally similar but with cyclcing extract.

In this chapter, I will first describe the reasoning behind and the design of this novel experimental procedure, including the extracts used and their function. Then, I will demonstrate its efficacy in driving mitotc trigger waves with and without reconstituted nuclei, demonstrating that they may not function in the same manner. Finally, I will present some forward-looking data which provides evidence for the efficacy of this system for studing the effects of tunability on wave proapgation. The vast majority of this chapter is adapted from the same soon-to-be submitted work in collaboration with the Gelens laboratory.

4.1 CSF Extracts Drive Mitotic Waves in Tubes of Cycling Extract

The reservoir in question is cytostatic-factor (CSF) extract which is derived from inactivated embryos arrested at meiosis-II (Masui and Market, 1971; Murray, 1991). The biological details of CSF arrest remain somewhat in question, though the field largely agrees most signs point to the Emi family of proteins serving a critical role through their inhibition of APC/C (Schmidt et al., 2005), with possible additional function provided by the Mos-MAPK pathway (Yamamoto et al., 2005). Regardless, CSF extracts exhibit and maintain high Cdk1 activity unless released from arrest by treatment with Ca+2 as we do in the cycling extract protocol (Good and Heald, 2018). Moreover, these extracts can be reliably frozen and stored for many months, giving us a reliable source of stable high-activity extract. Due to the self-promoting activity of Cdk1 in the mitotic circuit, supplementing oscillating extract with CSF ought to result in forced activation and resulting traveling fronts.

4.1.1 Design of a novel method for driving mitotic waves

The CSF extracts were made following established protocols (Good and Heald, 2018) which are minimally adapted from the originals (Murray, 1991). Using laid eggs, I produced large quantities of extract (on the order of mL), vastly more than necessary for a single experiment (10-20 μL). To preserve said large quantities of extract, I implemented a freezing protocol adopted from Takagi and Shimamoto, 2017. Fresh extracts are centrifuged through a 100 kDa-membrane filter in a bench-top rotor, producing concentrate and flow-through fractions (Takagi and Shimamoto, 2017). The individual fractions are then aliquoted, flash frozen with liquid nitrogen, and stored at -80˚C for many months.

On the day of an experiment, one aliquot of each CSF fraction is allowed to thaw on ice, and when combined, are ready to be used. To maintain conditions across the reservoir and the

cycling extract, CSF extracts were also diluted to 20% with extract buffer. No reporters or drugs were added. I cut PTFE tubing into individual sections of ~10mm lengths and loaded each via aspiration such that the extract filled the tube in excess: visual inspection of the syringe adapter showed the fluid line exceeding the tube opening. I then dipped the tube into the CSF reservoir syringe-end first for 5-10 seconds to ensure fluidic contact between the cycling and CSF extracts. While the original apoptotic wave paper described maintaining contact between the reservoir and tubes for many minutes, I observed any contact longer than ~10 seconds resulted in mitotic arrest overtaking most, if not all, of the tube (Cheng and Ferrell, 2018). In fact, even at short dipping times, this sometimes occurred regardless. As such, care was taken to minimize the contact time.

4.1.2 CSF-dipping creates an arrested region which drives waves

To test this hypothesized mechanism, I first conducted a few proof-of-concept experiments with reliable reporters we had on hand in the lab (the FRET sensor, at the time, remained in testing), the results of which can be seen in Figure 4.1. Tubes (of length ~10mm) filled with cycling extract tube were dipped into a reservoir of CSF extract for a few seconds and then imaged as previously described. I first observe a roughly diffusive region growing from the dipped end (Figure 4.1, C, D). This is likely due to diffusion of the cytostatic factor itself. In the case of the tube with reconstituted nuclei reported by NLS-GFP, this materializes as a region without nuclei (Figure 4.1, C); in experiments without nuclei, this appears as a bright region of roughly uniform distribution, as indicated by the uniformly bright Securin-CFP signal (Figure 4.1, D). Both signals are indicative of a high-Cdk1-activity-arrested (mitotic) state, supporting my hypothesis for the setup. Second, the system exhibits waves emanating from the arrested region (Figure 4.1, C, D). Finally, these fronts eventually take over the entirety of the tube,

propagating for multiple millimeters at a time. In total, these preliminary experiments proved the plausibility of this driven-wave setup.

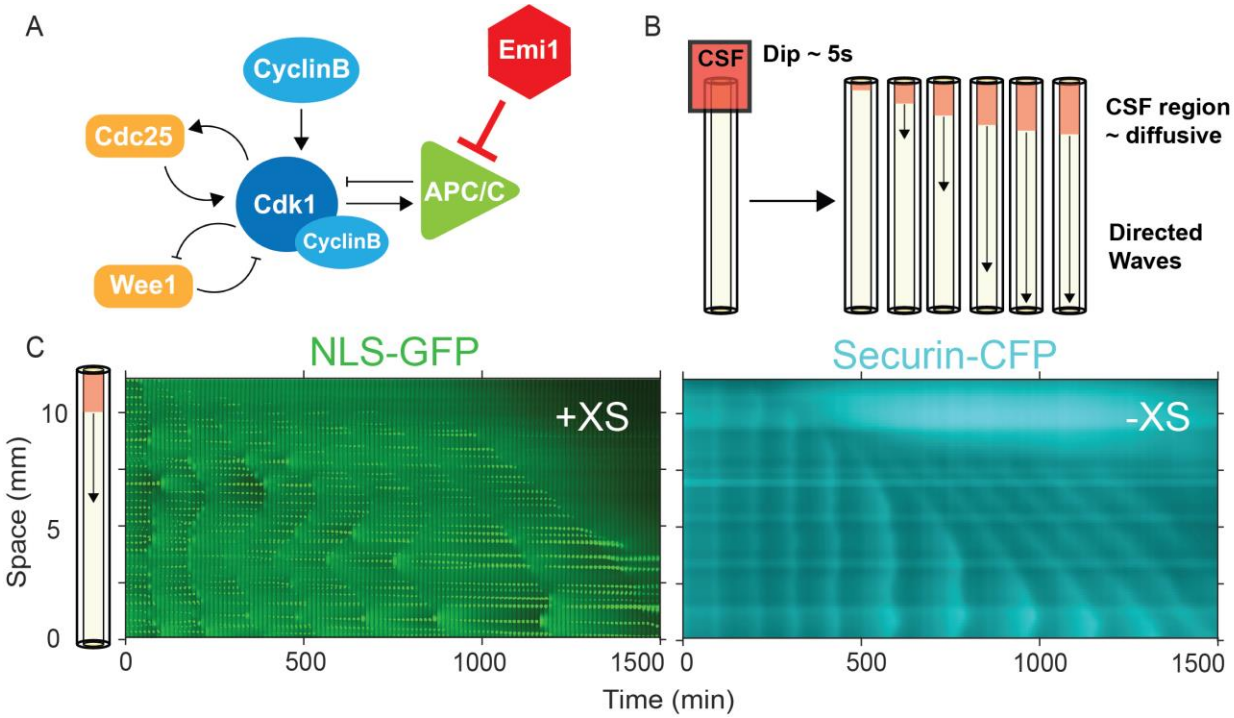

Figure 4.1 Design and Proof of Concept for CSF-Driven Mitotic Waves

A) Schematic of CSF extract's proposed effect on the cell cycle network. The field believes the cytostatic factor belongs to the Emi family and that it maintains arrest through inhibition of APC/C (Schmidt et al., 2005). B) Schematic of the CSF driving setup. 10-12mm sections of Teflon tubing are filled with cycling extract as before. The syringe-end, which was over-filled, is then dipped into a reservoir of CSF extract for at most 5 seconds. Tubes are then submerged under oil and imaged as before. C) Representative kymographs for proof-of-concept experiments in extracts with reconstituted nuclei reported by NLS-GFP (Left) and without nuclei reported by Securin-CFP (Right). The arrested region appears as a growing region absent nuclei (Left) or of high-fluorescence intensity (Right). As can be seen, the trigger waves generated by the CSF quickly take over the system.

4.2 Driven Mitotic Waves Display Fast and Permanent Entrainment

After this early work, and in conjunction with the proven stability of the FRET sensor, I turned my focus to experiments combining these novel developments. As shown in Figure 4.2, the mitotic arrested region is confirmed by high FRET signal, indicating persistent high Cdk1 activity. Although literature suggests cyclin B synthesis persists under CSF arrest (Schmidt et al., 2005), I observe initially increasing Cdk1 activity as arrest sets in, but otherwise constant activity until extract death (Figure 4.2, A). This detail remains unexplained but does not impact the

efficacy of the setup. As alluded to previously, the mechanisms behind CSF arrest continue to evade complete understanding by the field, so this is not entirely surprising.

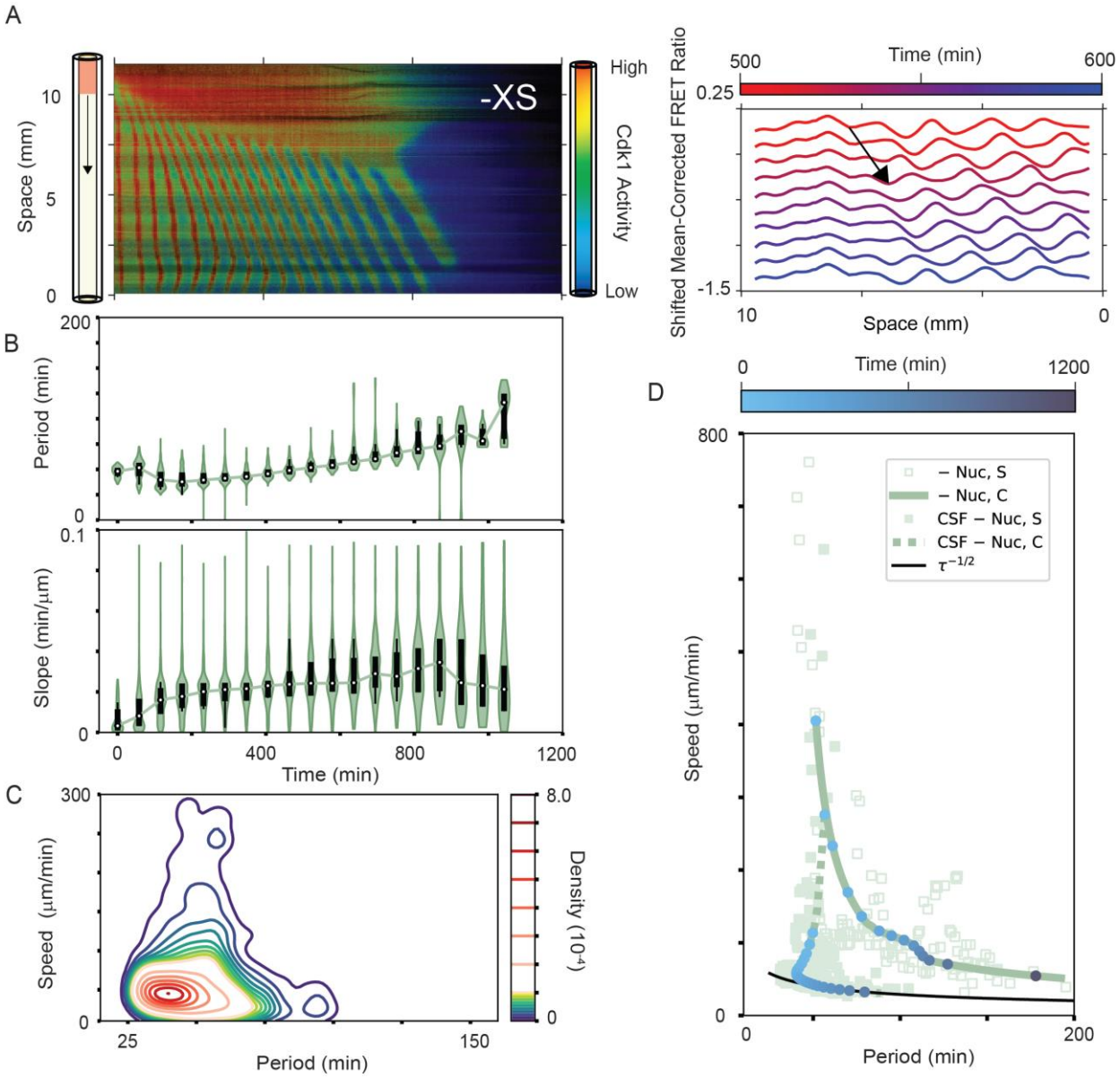

Figure 4.2 Driven Mitotic Waves Exhibit Trigger Waves that Dominate the System

A) (Left) Representative kymographs for the CSF-driven system without reconstituted nuclei, as reported by the Cdk1-FRET sensor. In this case, the high-activity arrested region can be confirmed as such due to the persistent high FRET ratio. As before in Figure 4.1, the source generates trigger waves which dominate the system. The dark stripes are relics of stitching. (Right) Spatial profiles for late times. Traveling pulses are easily identifiable in each case. B) Period and slope over time. C) Slope-period relation. D) Comparison of dispersion relations for the undriven (solid) and driven (dashed) cases. Timepoints show how the system evolves in time. Light-colored open (solid) squares correspond to LOWESS fits for individual undriven (driven) experiments (connecting lines omitted for clarity). The solid black line is an eye guide, not a fit.

Turning to driven waves, as previously shown, the mitotic arrested region persistently drives waves of Cdk1 activity throughout the tube (Figure 4.2, A). As in the undriven experiments with FRET sensor, wavefronts appear as pulses of high Cdk1 activity (Figure 4.2, A). Importantly, the pulse-like nature of the fronts confirms them as trigger waves, distinct from early-time patterns in bulk extracts, and similar to both boundary-driven and nuclei-facilitated wavefronts. It is noteworthy the dominance that the driving exerts on the system and it highlights the efficacy of trigger waves at disseminating biological information large distances. Applying the same analysis workflow from the previous chapter, I again observe that the oscillation period monotonically increases over time (Figure 4.2, B). Additionally, and as before, the slope (speed) increases (decreases) over time, leading to the dispersion curve(s) shown (Figure 4.2, D).

Importantly, driving the system in this way explicitly entrains the system to the trigger wave regime, quickly and permanently (Figure 4.2, D). The phase/sweep waves of early times quickly—within two or three cycles—give way to trigger waves which propagate across the entirety of the tube. These waves appear to follow a clear dispersion relation, distinct from the undriven case (Figure 4.2, D). One can consider this curve to represent the real trigger wave speed-period relationship, free of any effect from transients. Indeed, if I plot an eye-guide of a $\tau^{-1/2}$ dependence, this falls on top of the data nicely (Figure 4.2, D). In this way, driving the system elucidates a clear difference between the transients—and possible sweep waves—of early times and trigger waves.

4.3 Under Driving, Waves with and without Nuclei Obey Different Dispersion Relations and Display Different Entrainment Times

Next, I deployed this system to discern any fundamental difference(s) in wave propagation in systems with and without nuclei. For these experiments, the same procedure was followed as described above, with sperm DNA added at a dilution factor of 150x. The same CSF reservoir was used for each condition on any given day. As before, the mitotic-arrested region drives waves predictably throughout the system (Figure 4.3. A). In this case, despite experiencing the same driving force, the induced frequency was smaller for tubes containing nuclei (Figure 4.3, B). While I consistently observed the phenomenon of lower bulk frequencies

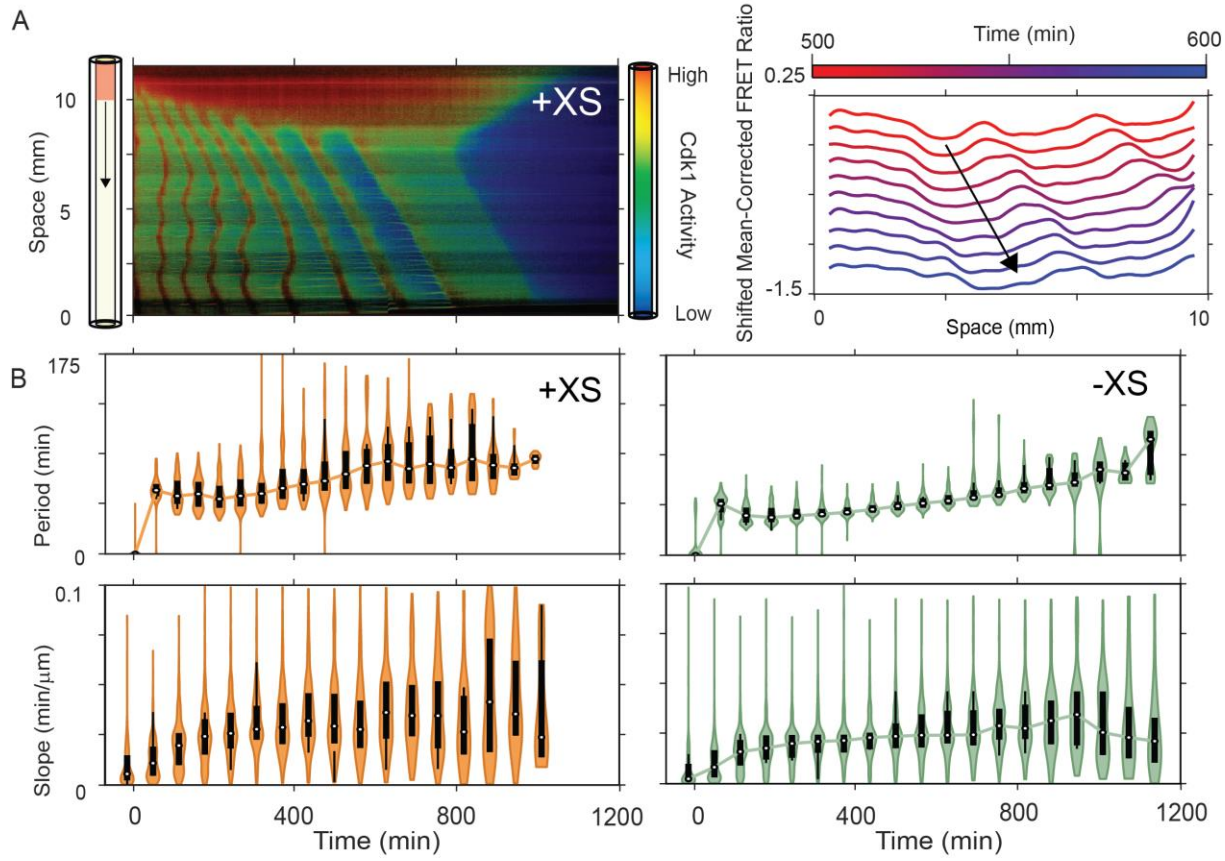

Figure 4.3 CSF-Driving Entrains the System

A) (Left) Representative kymographs for the CSF-driven system without reconstituted nuclei, as reported by the Cdk1-FRET sensor. (Right) Spatial profiles for late-times. B) Period (Top) and Slope (Bottom) plotted over time for experiments with (Left) and without (Right) reconstituted nuclei. Despite experiencing the same driving force, the latter exhibit significantly longer periods, a trend true in droplets generally (Maryu and Yang, 2022).

for oscillators with nuclei, it is nevertheless surprising the driving frequency appears affected. Seemingly as a result, the systems also exhibit different cycle numbers, with nuclei systems oscillating fewer times and over shorter lifetimes (Figure 4.3, A).

When measuring the wave speed, I observe two main phenomena. First, slopes for the systems with nuclei remain higher than their non-nuclei counterparts, matching what I observed in the non-driven system (Figure 4.3, B). This is likely due, in part, to the longer periods I observed, but also suggests a possible difference in the systems at the level of wave propagation. Importantly, the apparent plateau of speed = 1/slope ~ 1/0.05 min/μm = 20 μm/min appears to be conserved from what I observed in our initial experiments (Figure 4.3, B). Notably, the

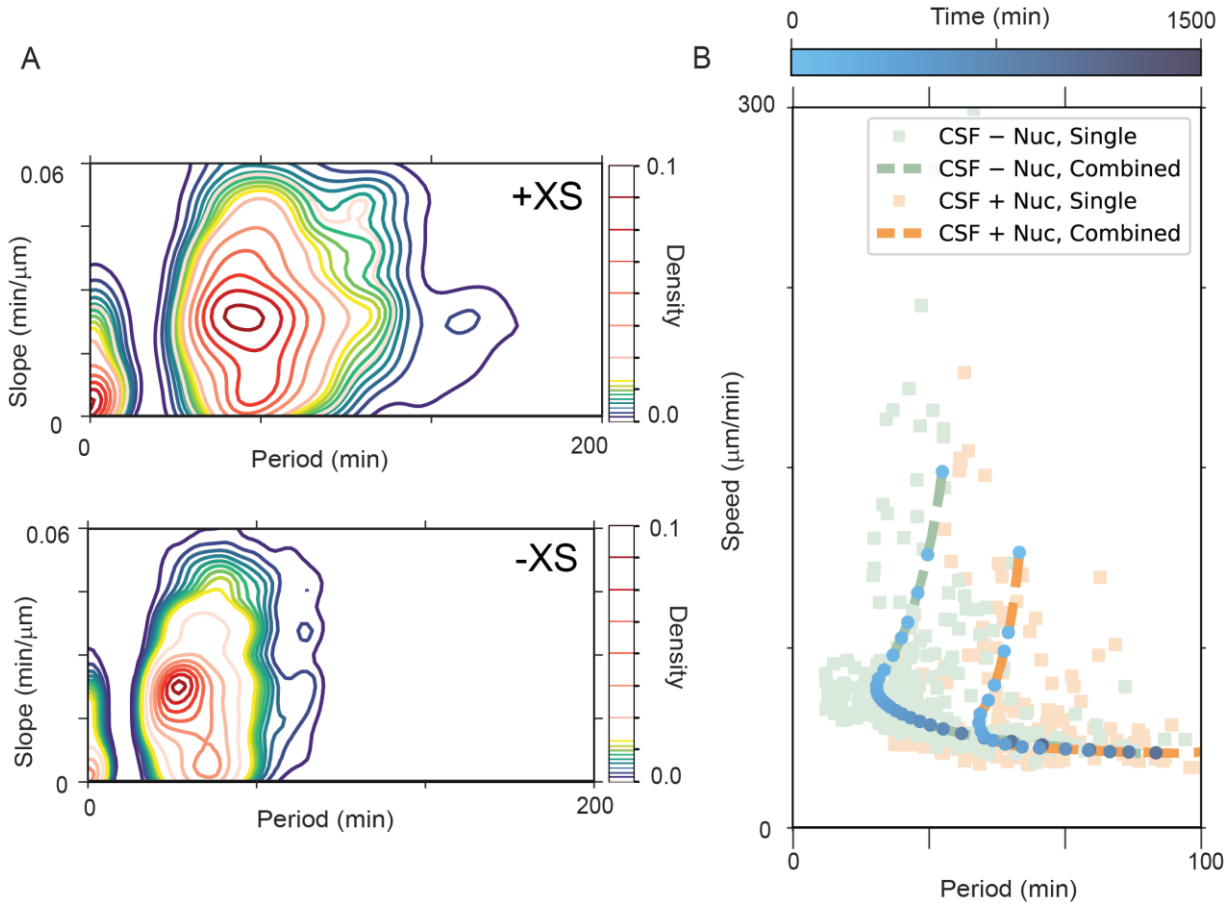

Figure 4.4 Comparison of CSF-Driven Dispersion Relations for Non-Nuclei/Nuclei Systems

A) Slope-Period relations for systems with (Top) and without (Bottom) reconstituted nuclei. B) LOWESS fits for the dispersion relation for the conditions in A). As before, the timepoints are selected to show how the system evolves in time. Light-colored solid squares correspond to LOWESS fits for individual experiments (connecting lines omitted for clarity), while dashed lines correspond to pooled data.

average speed of these known trigger waves is lower than the late-time speeds from undriven experiments (Figure 4.3, B). The precise reasoning for this discrepancy remains unknown, though it is possible that the entrainment in the former case could be incomplete, resulting in some contribution of remaining transients to the average behavior.

Using the same fitting equation from the previous section, I can again compute the entrainment times for these conditions. As before, I find the entrainment time for data with nuclei remains shorter than those without (Figure 4.4). This could point to some cumulative effect from multiple pacemakers: both the CSF and nuclei terms contribute to the entrainment. Regardless, both entrainment times are significantly faster than their undriven counterparts (Figure 4.5). Interestingly, the entrainment time for the CSF-driven case without nuclei is still slower than the undriven case with nuclei. It is plausible a set of multiple, but theoretically weaker, pacemakers could entrain the system faster given a distributed effect throughout space. Future work could probe this effect more carefully. Additionally, the fitted speed plateau of

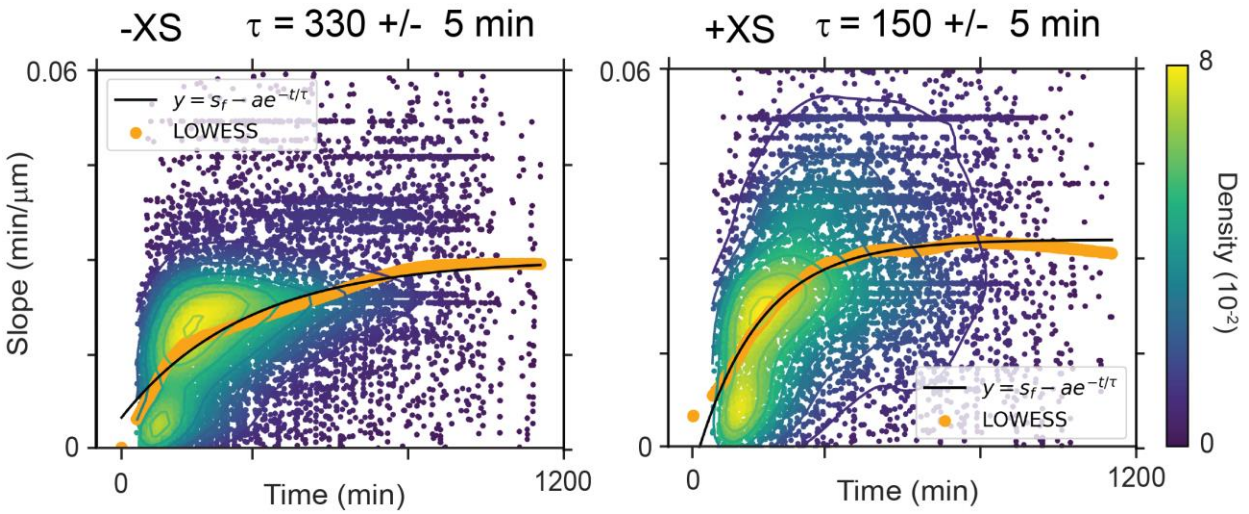

Figure 4.5 CSF Entrains the System to the Trigger Wave Regime Faster and Explicitly

Slope-time density plots with LOWESS smoothing (orange line) for experiments without (Left) and with (Right) reconstituted nuclei when driven by CSF. As before, the entrainment time for experiments with nuclei is faster than those without. Interestingly, CSF-driving does not seem to entrain faster than nuclei alone. The plateau speed of 30 μm/min closely matches reported speeds for mitotic trigger waves.
.

1/slope = 1/0.03 = 30 μm/min closely matches what I and others have observed previously for known trigger waves.

Second, while the data plotted in Figure 4.3 might suggest otherwise, upon closer inspection, I observe a significant difference in the dispersion relations for each condition once entrainment has set in (Figure 4.6). By plotting each dispersion curve on a log-log scale and fitting a line to the entrained segment, I can estimate the scaling exponent *m* for each (Figure 4.5). Unsurprisingly, for the case without nuclei, I find $m = -0.5 \pm 0.1$, as predicted by Luther's formula for trigger waves (Luther, 1906). However, for the system with nuclei, $m = -0.3 \pm 0.1$, suggesting this system exhibits sub-trigger wave scaling (Figure 4.5).

This is, perhaps, unsurprising. Before performing these experiments, and after witnessing the behavior of the undriven system, I hypothesized that the cycle-dependent import-export

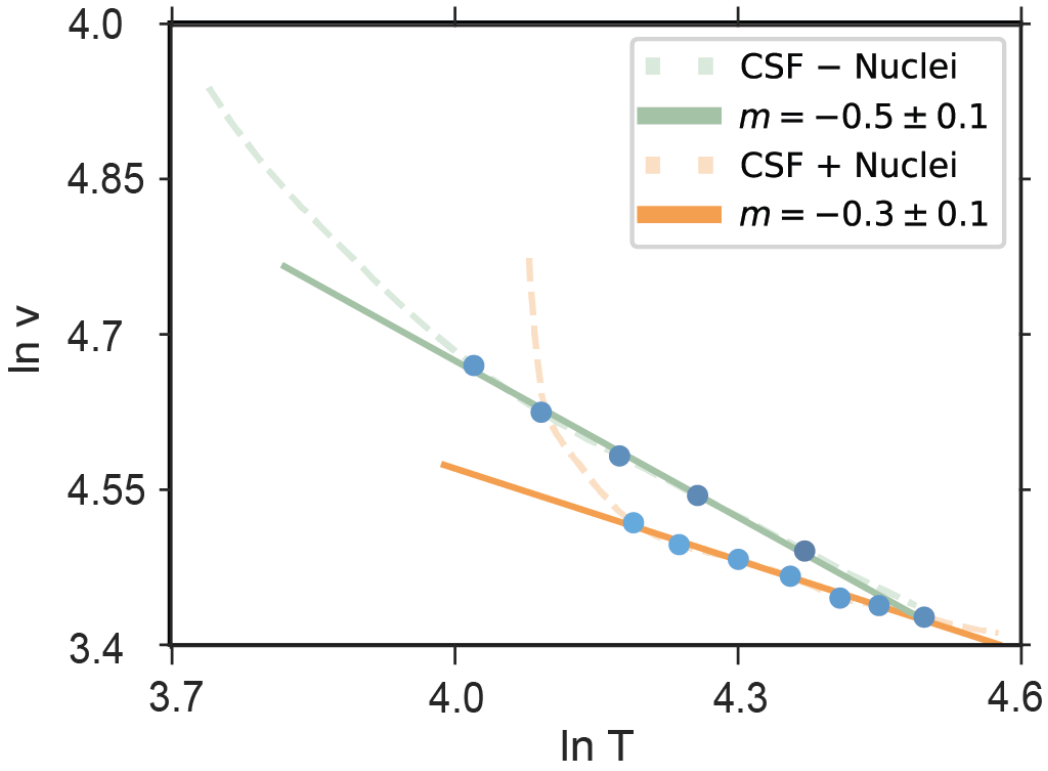

Figure 4.6 Non-Nuclei and Nuclei Systems Display Disparate Entrained Dispersion Relations

Linear fits of post-entrainment dispersion curves for systems with and without nuclei. These fits reveal different scaling exponents for the two conditions.

function of nuclei presented a fundamentally different environment in which waves could be realized, related to, but outside their apparent role as pacemakers or entrainers. Namely, I envisioned a measurable difference between a compartmentalized environment with a constantly modulating heterogeneous distribution of particles, and that of a quasi-homogenous fluid. Though I do not yet provide a careful analysis or propose a theory for this behavior, the data indicate such a hypothesis remains plausible. Future work—especially using the system outlined in Section 4.5—could focus on both more precisely determining the respective scaling laws and explaining their disparity physically. For now, by driving waves in this manner—with what constitutes a strong driving force—these data reinforce the notion of entrainment and highlight that function of nuclei in the non-driven case.

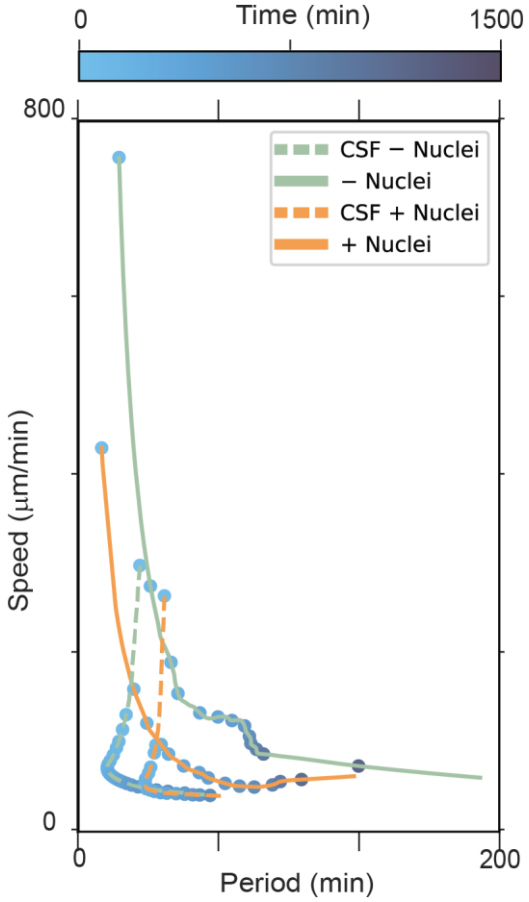

Figure 4.7 Comparison of all Dispersion Relations for each Experimental Condition

LOWESS fits of the dispersion relations for each experimental condition presented. The CSF-driving underlines the concept of entrainment.

To summarize, I demonstrate four distinct dispersion relations for mitotic waves in *Xenopus* extracts (Figure 4.7). Undriven extracts without nuclei experience a slow decay from phase waves to trigger waves. The addition of nuclei speed up this process by entraining the system to the trigger wave regime. Driving the system with a source such as CSF explicitly entrains the system to admit trigger waves, reinforcing this notion. The addition of nuclei to this driven system even further speeds up the entrainment likely due to some cumulative effect of multiple sources.

4.4 Introduction of a Known Pacemaker Allows for Systematic Perturbation of the Oscillator while Maintaining Wave Dynamics

Changning focus slightly, one of the main motivations behind creating the CSF-driven framework was to establish a method for analyzing wave dynamics in parameter space without worrying over the nature of the pacemaker. In this light, viewing the addition of sperm DNA as a perturbation of sorts, this system also admits other, more clock-specific, perturbations. From the Yang lab's work in droplets, I have access to numerous drugs to affect various pieces of the mitotic clock, as well as baseline(s) for how they affect cycling extracts (Jin et al., 2020; Maryu and Yang, 2022; Ye et al., 2018). Here, I focus on two such drugs: the Cdk1 inhibitor Roscovotine and morpholinos (MOs), antisense oligonucleotides against *Xenopus* cyclin B. Roscovotine inhibits cyclin-dependent kinases (CDKs) through direct competition at the ATP-binding site and sees broad use for both fundamental biology and clinical studies (Cisenas, et al., 2015). To perturb endogenous cyclin B mRNA translation, the relevant MOs bind to repress the target gene sequence and block further protein production (Maryu and Yang, 2022). As mentioned, work from the Yang lab indicated MOs significantly affect oscillatory dynamics in

the droplet system (Maryu and Yang, 2022). In both cases, these drugs allow me to observe changes in wave propagation as I modulate the clock.

4.4.1 Inhibiting Cdk1 tunes both the period and speed of driven waves

To perturb the central mitotic regulator, I added increasing amounts of Cdk1 inhibitor to cycling extracts used in conjunction with the CSF-driven system. I expected this to slow oscillations and possibly affect induced arrest. As shown in Figure 4.4, increasing amounts of added Cdk1 inhibitor results in reduced Cdk1 activity, as indicated by smaller peak FRET response (cooler colors) at early times when the effect is most easily seen. This reduction is evident in the bulk, but not in the arrested region, indicating an effect on the oscillating term, while mitotic arrest remains unchanged (Figure 4.8). Moreover, if I track the progression of the arrested region over time, Roscovotine-treated extracts exhibit slower arrest advancement

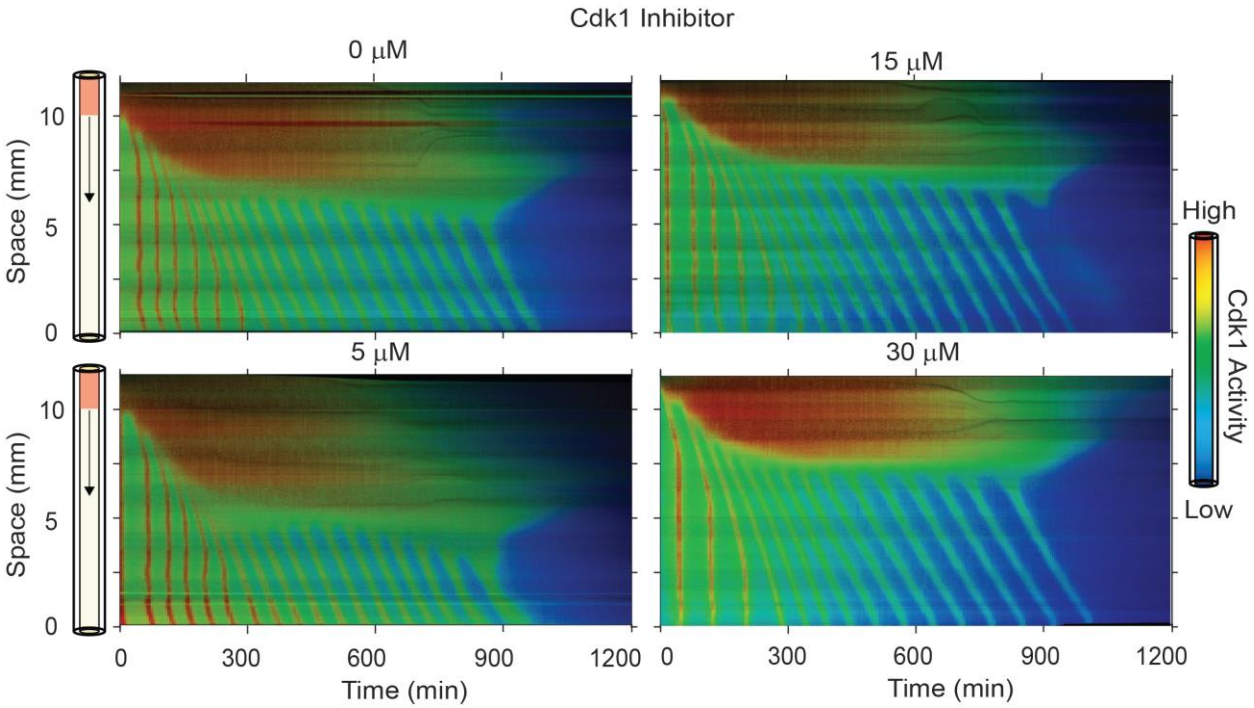

Figure 4.8 Representative Kymographs for CSF-Driven Waves under Cdk1 Inhibition

Cdk1 inhibition via the drug Roscovotine visually lengthens the period of driven oscillations. Additionally, the arrested region appears to progress shorter distances as the drug concentration increases. Finally, the intensity and relative warmth of the peaks at early times decreases as inhibitor concentration increases.

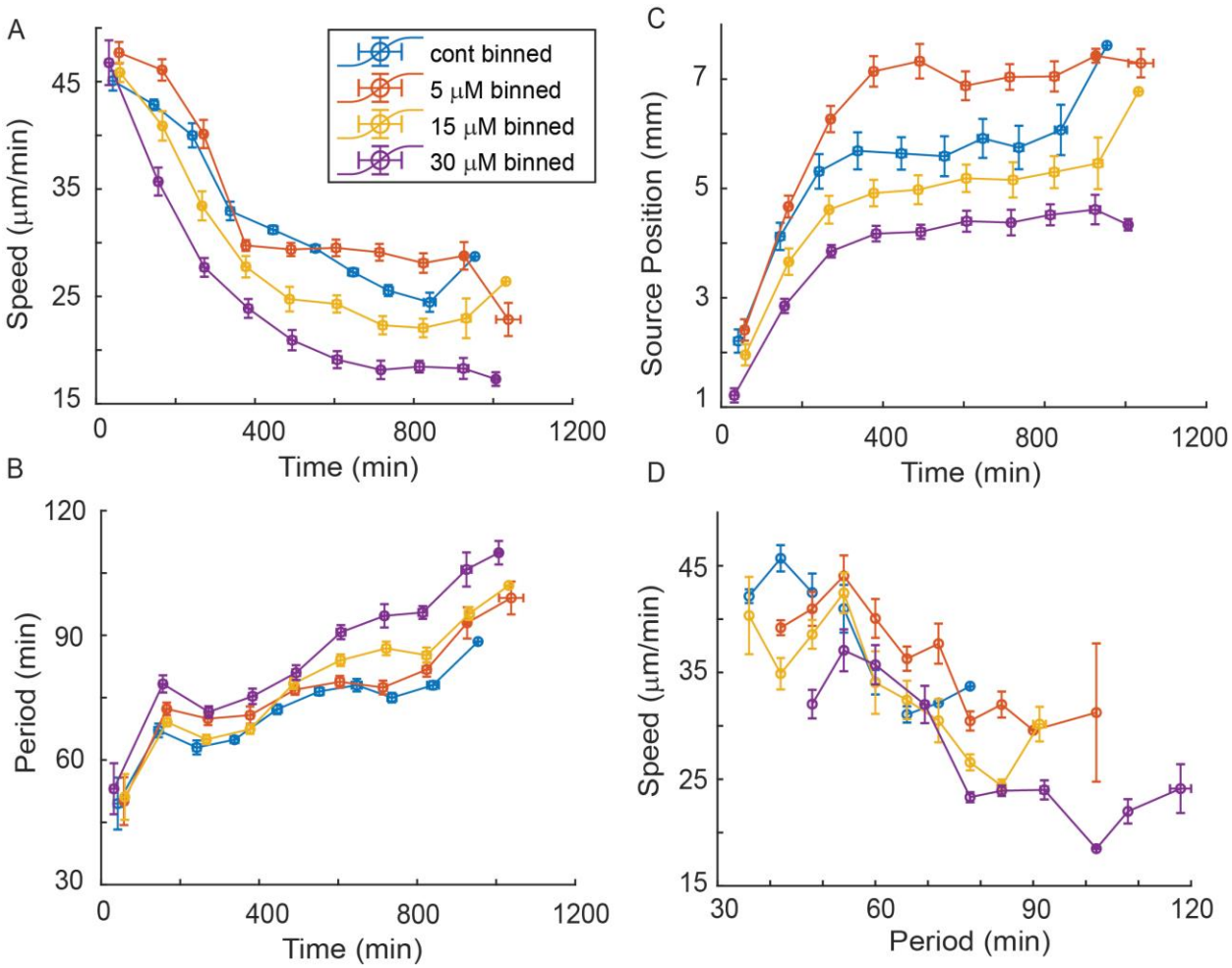

Figure 4.9 Cdk1 Inhibition Effectively Tunes the Cycle Period and other System Properties

A) Speed as a function of time. Cdk1 inhibition slows the waves and increases the rate at which the speeds decay to the apparent plateau. B) Period as a function of time. Inhibiting Cdk1 increases the cell cycle period. C) Progression of the arrested region over time. As Cdk1 inhibition increases, the arrested region effects less of the system's length. We believe the 5 μM condition does not represent significant inhibition and thus its behavior relative to the control is not indicative of the trend. D) Dispersion relations for each condition. Inhibiting Cdk1 does not appear to fundamentally change wave propagation.

(Figure 4.8). This indicates the system is more robust to induced active-state arrest when Cdk1 is inhibited, which makes intuitive sense. Moreover, increasing the inhibitor concentration slowed both periods and speeds, broadening the dynamic range for wave propagation (Figure 4.9). Similar period slowing is observed in the control (non-driven) tubes (not shown). Additionally, I observe a faster decay in the speed, again to an apparent plateau of roughly 20 μm/min, as I showed previously (Figure 4.9). However, I pointedly do not observe any significant variance in

the dispersion relation across conditions, suggesting that this inhibition merely affects rates, not fundamental mechanisms (Figure 4.9). Future experiments could be directed at expanding the range of added inhibitors, as it would be interesting to analyze data up and until inactive arrest.

4.4.2 Morpholino-induced degradation of endogenous cyclin B-mRNA translation results in transient high-speed,-slow-period wavefronts

With morpholinos, I instead choose to inhibit an input to Cdk1, rather than the main regulator itself. By blocking cyclin B-mRNA translation, only endogenous levels of the cyclin B protein remain for complexing with Cdk1. As a result, I expect longer periods, specifically due to an increase in interphase duration (Maryu and Yang, 2022). Indeed, upon treatment with MOs, undriven tubes exhibit progressively longer periods as MO concentration increases (Figure 4.10, B). Similarly, I observe elongated first and second cycles when driven, compared to control (Figure 4.10, A). Interestingly, the effect is most obvious at the lowest concentration of MOs, though due to the transience of this effect, it is possible I missed acquisition thereof due to the nonzero loading time. However, this effect largely disappears after the second or third cycle, and the conditions follow a similar trend in the period afterwards (Figure 4.11). This suggests the source truly drives the system, at least somewhat irrespective of the bulk conditions. Nevertheless, despite longer periods for the first two cycles, I do not observe a corresponding decrease in the speed (Figure 4.11). Indeed, across all cycles, each condition's average speed largely follows the same trend as time progresses (Figure 4.11). More work remains to understand these phenomena.

Regardless, I also note the drastic increase in the size of the arrested region as the morpholinos concertation increases (Figure 4.11). This indicates knockdown of cyclin B reduces the system's robustness to arrest. Moreover, the progression of arrest loses its roughly diffusive

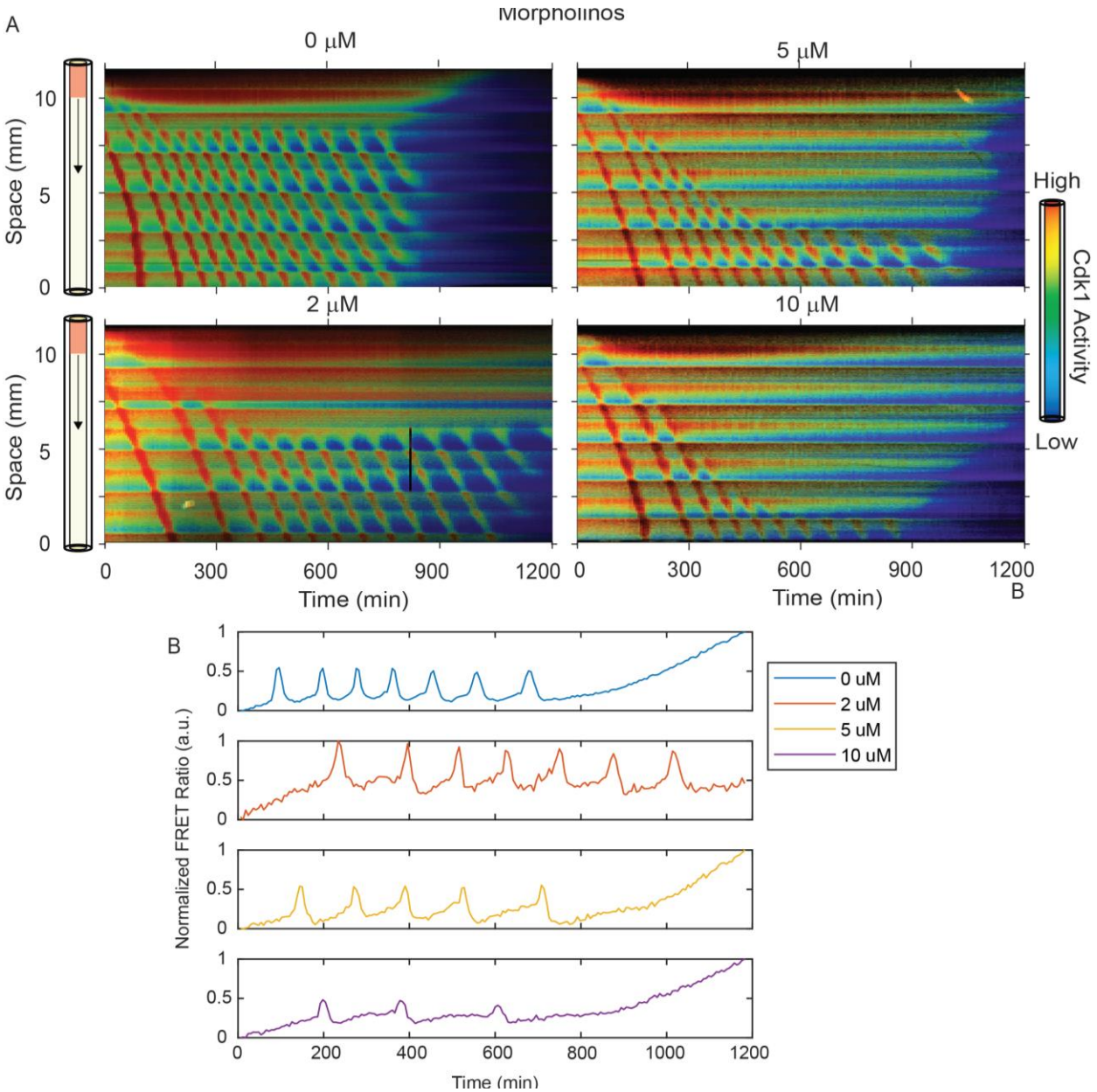

Figure 4.10 Morpholinos Lengthen First Cycle Period and Perturb Dispersion Relation

A) Representative kymographs for different amounts of added morpholinos. Though not quantified, increased morpholino concentration appears to lead to larger swaths of the tube arresting in the active state. The dark stripes are relics of stitching, and the black segment in the 2μM kymograph reflects a microscope issue within one frame at that position. B) Timeseries of the normalized FRET ratio to indicate the MO effect on undriven extracts.

profile at higher levers of MOs, suggesting that the arrest spreads in a manner more akin to a bistable front, rather than diffusion alone (Figure 4.11). If so, the speed at which arrest propagates lags that of the mitotic waves themselves. This highlights the interplay between the source's function of arrest and the quasi-bistability of the cycling extract.

Together, these results from two methods demonstrate the efficacy of the system for analyzing wave dynamics under clock perturbations. I expect other data from other drugs, as well as expansions on these proof-of-concept experiments, will help elucidate finer details on mitotic waves. Additionally, this setup will prove useful for confirming future model predictions on trigger wave properties.

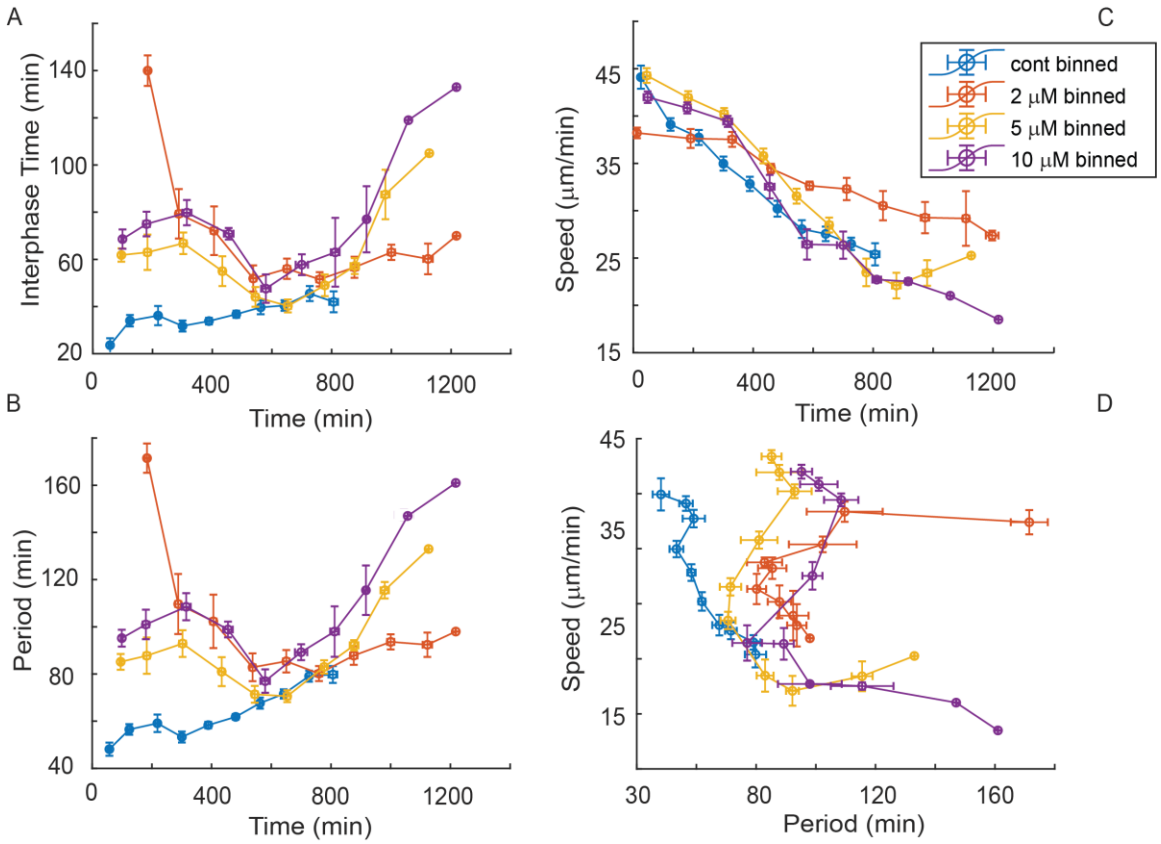

Figure 4.11 Morpholinos Cause Waves the Propagate Faster but at Slow Period

A) Interphase duration over time for each condition. Added morpholinos increase the duration of interphase for early cycles. We believe the effect appears greatest for the 2 μM case because we missed the first cycle in the other two drug conditions. D) Period over time. Due to, in part, the increase in interphase duration, morpholinos also increase the period of early cycles. C) Speed over time. Morpholino concentration does not appear to significantly affect the speed, despite the effect on period. E) Dispersion relations. The relatively longer first few cycles lead to drastically perturbed dispersion curves for the drug conditions. We observe a regime where speeds slow but periods remain constant, followed by a return to the expected trend.

4.5 CSF Drives Singular Wavefronts in Interphase Extracts

An extension, or rather a simplification, of the work above involves replacing cycling extracts with interphase extracts. Much like CSF extracts, interphase extracts are arrested, but in the low-activity state, hence the name. In principle, dipping an interphase-extract-filled tube into a CSF reservoir should produce a singular wavefront emanating from the source region. This is functionally similar to what we observed with added morpholinos. Such a setup eliminates both the time-dependence and spatial heterogeneity factors present in the work presented so far. [Note: the spatial distribution of molecules could very well exhibit non-homogeneity, but the activity thereof should be homogenously arrested]. As a result, this would allow us to investigate the nature of pure bistable fronts and the role of activation alone in this system.

To do so, interphase extracts were prepared using the standard protocol in the field (Deming and Kornbluth, 2006). Like CSF extracts, interphase extracts can be frozen at -80˚C for many months without losing potency, though less care need be taken for separating fractionated parts. Thawed interphase extracts are then loaded into Teflon tubing, as before, and dipped into a reservoir of CSF, also as before. As expected, I observe a single traveling front of high Cdk1 activity propagating from the dipped end of the tube (Figure 4.12). Interestingly, I did not observe the same arrested region moving into the tube as we did in the case of cycling extracts, a detail which still needs to be explained. Nevertheless, these fronts consistently propagated at 40 ± 2 μm/min across each tube, in agreement with what is predicted sans time-dependence (Tyson and Keener, 1993). This gives a baseline for the speed of bistable fronts in extracts. Unfortunately, due to a scarcity of time, resources and focus, I was only able to produce this proof-of-concept experiment. However, it demonstrates the efficacy of this approach and paves the way for a diverse set of follow-up experiments that will be described in the Discussion.

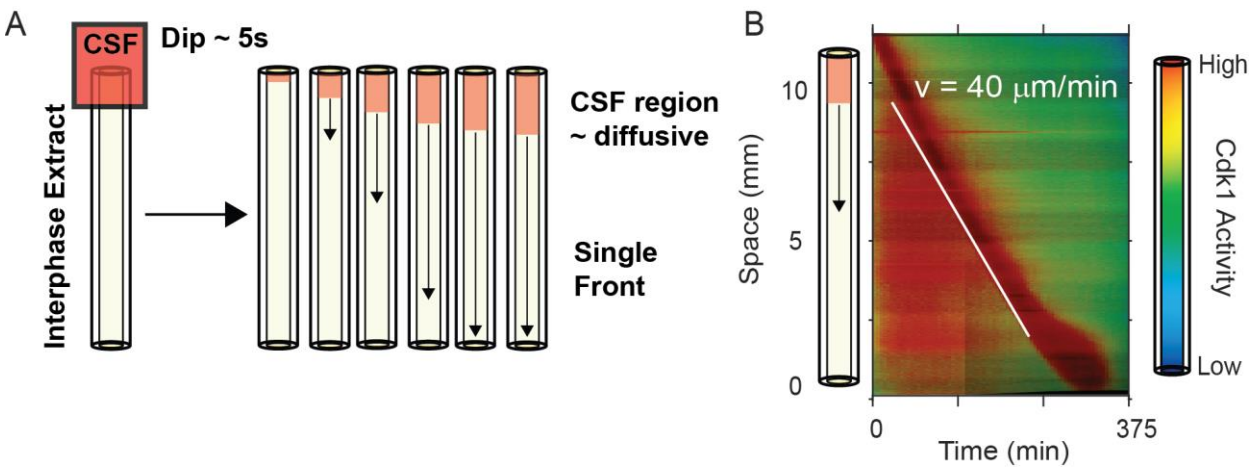

Figure 4.12 Bistable Front Propagation in CSF-driven Interphase Extracts

A) The procedure for this setup mirrors that described throughout this chapter, with interphase extracts replacing cycling extracts. B) Representative kymograph for this experiment, displaying a singular bistable front propagating from the dipped end of the tube. The lack of arrested region remains unexplained.

4.6 Conclusion

Previous work on mitotic waves in *Xenopus* focused on the role of nuclei and pacemakers generally (Chang and Ferrell, 2013; Nolet et al., 2020; Alfanzar et al., 2020). In this chapter, I demonstrated the design and efficacy of an experimental setup for implementing an explicit pacemaker to drive mitotic waves *in vitro*. This novel method combines two types of *Xenopus* extracts—cycling and metaphase-arrested—to instigate mitotic waves over long distances and many cycles. With this system, I showed how it can be used to study wave properties in various contexts. In particular, I used it to demonstrate explicit entrainment through a strong driving force, reinforcing the concept introduced in the previous chapter. Moreover, I probed possible differences in waves with and without nuclei, showing the compartmentalized exhibits a distinct dispersion relation; analyzed wave properties as a function of Cdk1 inhibition; used morpholinos to visualize waves in cyclin B-knockouts; and demonstrated the use of interphase extracts to drive singular bistable fronts. By coopting the natural period slowing of cycling extracts, I was able to present a quantitative description of the dispersion curve for mitotic waves. Moving

forward, this experimental design affords innumerable opportunities to continue this line of work in this way.

4.7 Appendix

4.7.1 Modeling the CSF source expedites quantification of wave speed throughout the relevant parameter space

In conjunction with this experimental work, I also compiled a relatively simple partial differential equation (PDE) model of CSF-driven waves to support these data. In short, I added a third species to the existent mitotic trigger wave model offered by Chang and Ferrell in 2013. This species—CSF—acts to turn off the oscillator when its concentration is above a threshold via an ultra-sensitive feedback loop which takes the form of a decreasing Hill function with $K_{csf} = 1.0$ and $n_{csf} = 50.0$ (also given in Table 2), values that were chosen somewhat arbitrarily to make the interaction sufficiently switch-like and ensure abrupt and permanent arrest. This term thus takes the form $F_{CSF} = \frac{{K_{CSF}}^{n_{CSF}}}{{K_{CSF}}^{n_{CSF}} + {CSF}^{n_{CSF}}}$. The degradation term in the model is then multiplied by this CSF term to shut it off when the CSF species is above the threshold. To mirror the dipping performed in experiments, I set the initial condition at one end of the tube to include

mitotic levels of active Cdk1 and the CSF species, after which all species are allowed to diffuse as normal. Unless specified, the parameters used are the same as outlined in Table 1.

Additionally, to avoid substantial phase slipping, the initial concentration of active Cdk1 was set to the high stable state for the parameter set, which was solved independently using Matlab. Interestingly, despite it occurring persistently in the model, I observed effectively no

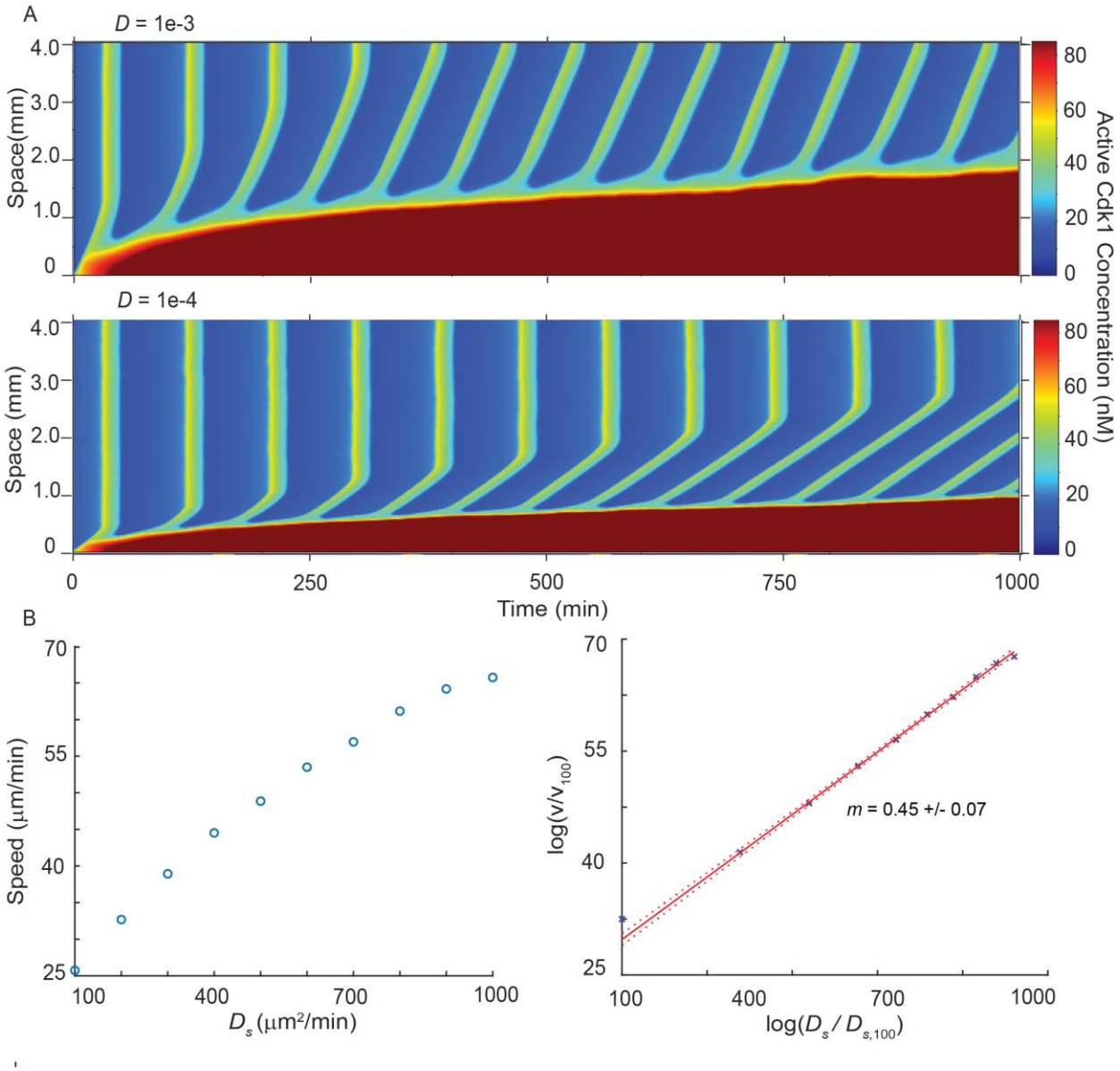

Figure 4.13 Model of CSF-Source Confirms Diffusion Constant Speed Scaling

A) Numerical simulations of the CSF-driven system at two diffusion constants (Top: high; Bottom: low). Visual speed slowing can be observed. B) Speed vs Diffusion constant (Left) and the same on a log-log scale (Right). A linear fit of the latter gives a scaling law of around 0.5, in rough agreement with theoretical predictions.

instances of phase slipping over the course of all experiments. It remains an open question as to how the real system appears to be much more robust to driving than the model system. Nevertheless, with this model, I performed a discrete sampling of reasonably tunable parameters in the model: namely, the diffusion constant (Figure 4.13), the positive-negative feedback ratio, R (Figure 4.12, B), and the synthesis rate of cyclin B (Figure 4.14, A). After simulating, periods, wave speeds and other parameters were calculated in Matlab via peak detection.

Table 2 Parameter Values for PDE Simulations of CSF-Source Model

Parameter	Value
K_{50_CSF}	1.0 nM
n_{CSF}	50.0
D	6e-4 mm^2/min

As a first step, I tested the simplest of theoretical predictions, namely that trigger waves' speed exhibits a roughly $D^{1/2}$ scaling (Luther, 1906). As can be seen in Figure 4.13, increasing the diffusion constant by an order of magnitude results in minimal change in period, but a significant (roughly a factor of 3) increase in the speed, as expected. Moreover, a linear fit of these data on a log-log scale leads to a scaling exponent of 0.45 ± 0.01, which is in rough agreement with the theory (Luther, 1906). As a result, I can confirm this model sufficiently recapitulates expected wave dynamics. I then moved on to attempt to capture the wave slowing, coupled with period lengthening, we observe experimentally.

To do so, I focused on two sets of parameters: the positive-negative feedback ratio, *R*, and the synthesis rate k_s. As shown in Figure 4.14, k_s non-monotonically modulates the period, and while this is associated with changes in speed, it results in a non-physical dispersion relation. Alternatively, *R* effectively tunes the speed but does not display any significant effect on the

period. This struck me as surprising, given what I know both about the cell cycle in general, but also the ATP-depletion model and how it recapitulates period lengthening precisely by perturbing these feedback loops (Yang and Ferrell, 2013; Guan et al., 2018). To that point, and to bring everything full circle, I also combined this driving model with the aforementioned ATP-depletion model, fully expecting something resembling what we see experimentally. Surprisingly, while this captures the period lengthening of the ATP model, it fails to generate any meaningful wave slowing (Figure 4.42, C). As a result, it remains an open question what causes the driven waves to slow, or rather, how period lengthening and speed slowing are tied, in practice.

Taken together, this modeling work presents a functional step towards understanding mitotic wave dynamics, but does not offer a complete picture thereof. Further work is required on elucidating the intricacies of both wave dynamics, generally, and the mechanisms of this driven system, specifically.

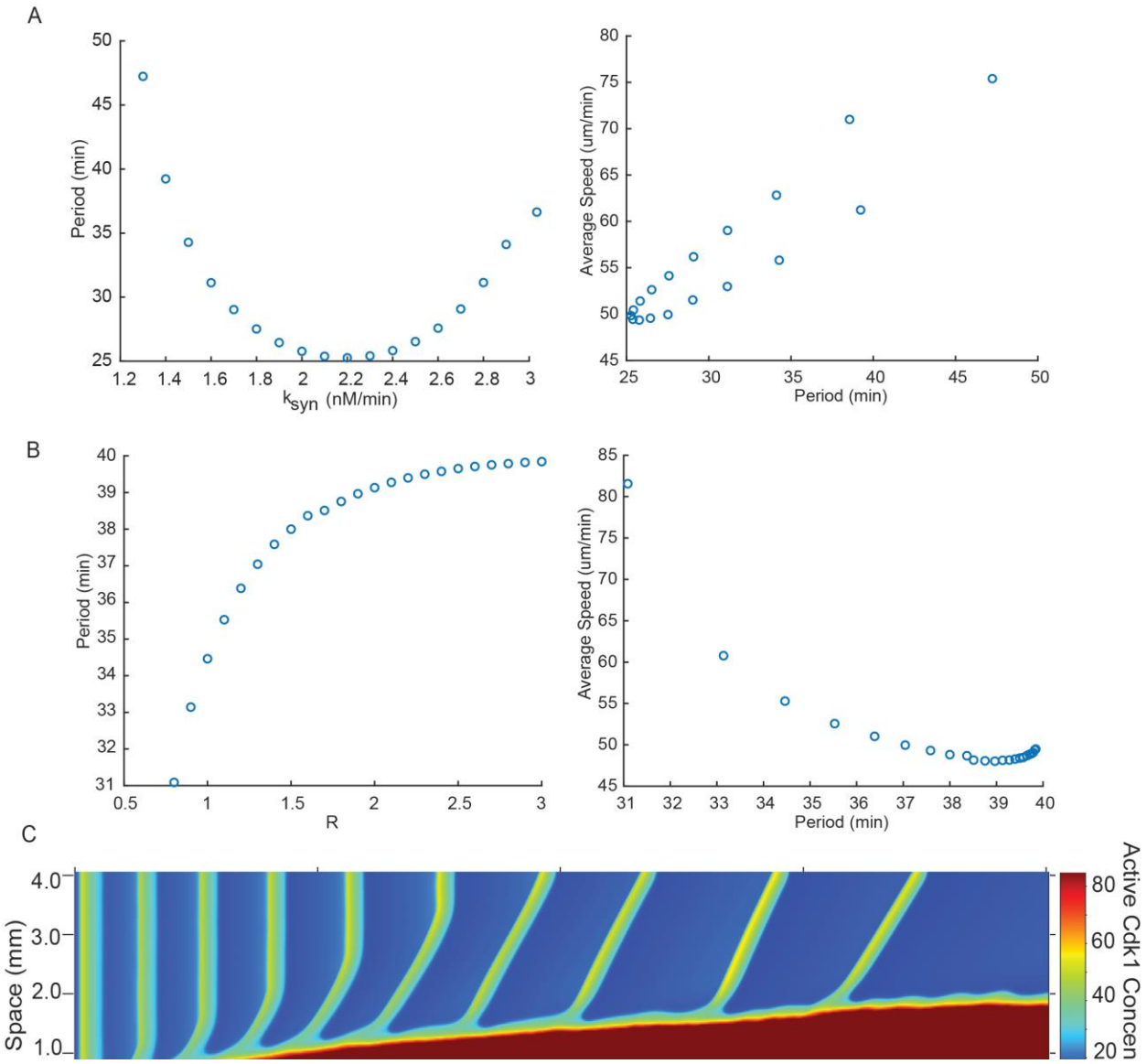

Figure 4.14 Simulations of CSF-Driven Waves do not Recapitulate Experimental Observations

A) Period as a function of the synthesis rate (Left) and the resulting dispersion relation (right). Changing the synthesis rate results in non-monotonic period dependence. As a result, the dispersion relation does not appear physical. B) The same as in A but for the positive-negative feedback ratio, R. While the period dependence displays monotonicity and the speed appears tunable, the period tunability range is small. This does not match what we observe experimentally. C) CSF-driven waves in the ATP depletion model from Guan et al., 2018. Although the period lengthens as before, we do not observe any significant change in the wave speed. The final cycle in the kymograph above does exhibit some discrepancy in speed, but repeated attempts to probe similar locations in phase space did not yield significant continued slowing.

Chapter 5

Discussion

Due to the complexity of living matter, communication and coordination of bioprocesses is of utmost importance. From patterns of firing neurons, to the flocking of birds, biological systems demonstrate this necessity on a regular basis. In this work, I probed the behavior and nature of one such coordination mechanism: mitotic waves.

In compiling the data acquired over the course of my graduate school career, we produced evidence for a unified picture of pattern formation in mitosis in *Xenopus*. While nuclei and other systems (CSF) may act as pacemakers for generating waves, the question of long-term behavior remained unanswered. Here I applied the idea of entrainment as an overarching mechanism to explain mitotic waves in *Xenopus* extracts in one-dimension. At early times, the system exhibits phase (or sweep) waves that lack definitive wavefronts and patterns. Over time, these transients give way to trigger waves, even without pacemakers. Nuclei and the CSF source, or pacemakers generally, expedite this entrainment, causing the system to decay more quickly to the trigger wave dispersion curve. Together, this work largely completes the picture of mitotic waves in *Xenopus* extracts, successfully explaining the long-term behavior of patterns as they develop over many cycles.

5.1 A Note Regarding Sweep Waves

This puts my work in dialogue with the existing literature regarding mitotic waves in *Drosohphila.* Hayden et al., proposed period lengthening as the main driver of a sweep-to-trigger transition (2022). While I observe something similar in unperturbed extracts, the addition of

nuclei and/or CSF-mediated driving indicates period lengthening is not required for directing this transition. Instead, it appears as though the phase waves we observe—whether they are sweep waves and/or what this distinction actually means remains a question—are simply transient patterns: if you wait long enough, the system will decay to trigger waves eventually. This seems to suggest sweep waves exist in a small range of conditions.

Furthermore, my and other work highlight that sweep waves do not appear to be robust to heterogeneity. In Hayden et al. (2022), the authors also perform experiments and simulations with embryos displaying a heterogenous distribution of nuclei in the syncytial embryo. They remark that disrupting homogeneity leads to trigger waves and a loss of synchrony (Hayden et al., 2022). I demonstrate a similar effect both by adding nuclei to the homogenous system, and by driving it explicitly with CSF. In all three cases, these trigger-wave-producing effects overtake underlying quasi-synchronous patterns. Together, these demonstrate trigger waves dominate sweep waves. In this way, the motivational modeling work from Chapter 2 is also illustrative. At small values of *r*, the system oscillates quasi-synchronously. These patterns appear to resemble sweep waves, as was shown. As *r* increases, however, local heterogeneity due to noise alone is sufficient to break quasi-synchrony and drive trigger waves. I would argue this transition does not represent a switch from one type of wave to another, rather a relative breakdown of the system's robustness to noise. As a result, I would also argue sweep waves exhibit limited, if any, robustness to non-homogeneous perturbations: the moment this balance breaks, whether through noise, the presence of a nucleus, or driving, trigger waves propagate.

What is more, simulating this system at larger length scales reveals sweep waves do not propagate over large distances, if they propagate at all. At most, these patterns persist for hundreds of microns. On the scale of some biological functions, this is relevant. However, for the

specific purpose of coordinating function, this seems insufficient. Trigger waves, as made evident by our work here, conversely, transmit signals orders of magnitude farther in distance. This questions the physiological relevance of sweep waves. At most, one could argue for a tradeoff between speed and distance. For mitosis, in particular, it could be reasonable that nature would select for trigger waves in larger embryos such as *Xenopus*, where coordinating over large distances is more relevant than in *Drosophila*.

However, this short length-scale, coupled with their apparent lack of robustness, suggests sweep waves may not actively perform their proposed function of signal transduction. Instead, they may simply reflect the reality that the *Droshopila* embryo undergoes quasi-synchronous oscillations prior to MBT precisely because it exists in a quasi-homogenous state. In this author's opinion, sweep waves should be viewed as artifacts of a system on the edge of synchrony: phase waves by another name.

5.2 Outlook and Future Work

Regardless, outside the question of sweep waves, future experiments could expand on this work by pursuing other forms of perturbations by inhibiting the feedback loops in the network. The field already demonstrated the importance of Wee1 for "forming the trigger" (Chang and Ferrell, 2013), but with our setup and analysis framework, one could quantify the effect and provide stronger evidence in either direction. The same applies for Cdc25. Canonically thought of as equal-but-opposite inputs, it would be interesting to observe whether or not Wee1 and Cdc25 affect this time dependence in similar manners. Moreover, we know that these inputs also translocate in and out of the nucleus throughout one cycle, at different times (Baldin and Ducommun, 1995; Trunnel et al., 2011). It stands to reason that inhibition thereof could change in the presence of nuclei, and thus, we might see a nuclei-dependent effect on how

inhibition perturbs this transition. Clearly, much work remains on elucidating the details of time-dependent wave behavior.

Additionally, I demonstrated the use of the CSF driving setup to offer a mechanistic way of probing mitotitc trigger waves directly. I took advantage of this feasibility and used mitotic oscillator-specific drugs to modulate the period systematically by both inihibitng Cdk1 and degrading endogenous cyclin B with morpholinos. In the future, this system could be used to expand on this study, including inhibitors for other clock constituents such as Cdc25, Wee1, PP2A, and many others. Our modeling work with our collaborators provides a framework within which such manipulations should be viewed, and more data supporting this theory would be welcome. Additionally, although I provide some numerical work in this publication on the effect of changing the diffusive properties of the extract, certainly experimental data on this topic should be recorded to confirm the theoretical predictions.

Moving forward, as in the undriven case, I envision this project delving deeper into the perturbability of clock properties and resultant wave propagation. I believe the CSF-driven system presents a novel and useful tool for studying traveling waves *in vitro*, not limited to oscillatory systems. As demonstrated in the proof-of-concept experiment described in the previous chapter, interphase extracts provide a medium in which to study purely bistable fronts. By eliminating the complexity of oscillations—lifetime, period, etc.—these experiments would focus on the role of activation alone, similar to what was demonstrated in *Drosophila* (Vergassola et al., 2018). Furthermore, interphase extracts, much like CSF extracts, maintain activity over many months while frozen, opening them up to much easier and more rapid data acquisition than involving the cycling system. In reality, such experiments could stand as a

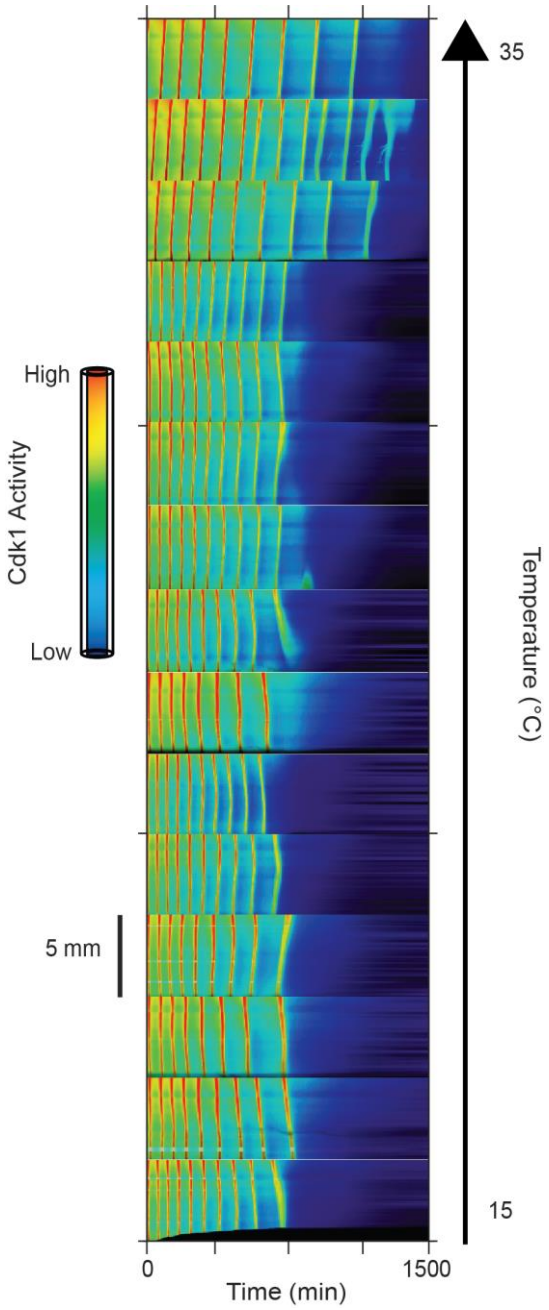

Figure 5.1 Temperature-dependent Wave Behavior

Kymographs for tubes along a gradient in temperature. While temperature clearly affects the frequency, any effect on wave propagation would require further experiments and careful analysis. Such an experiment represents one of many future directions for this wave project.

cleaner method for testing the all of the perturbations mentioned above: clock inhibitors, glycerol (diffusion), etc. In particular, this would provide a direct test for whether nuclei actually pertub wave propagation as it would eliminate their role as a pacemaker. In total, this setup offers a

welath of opportunity to probe bistable waves, arguably the more relevant topic for *in vivo* embryogenesis in *Xenopus*.

Additionally, one can imagine perturbing the source itself. As metnioned, theory predicts the wave speed to depend on the difference between the pacemaker and bulk frequency (Rombouts and Gelens, 2020). Either through dilution or inhibitors, it is plausible that the driving frequency of the CSF source could be modulated, thus providing a direct test of these theoretical predictions. Admittedly, the interplay between CSF arrest and its driving force are not known, so it is likely this set of perturbations would be more complicated to explain. Accurate modeling work could assist with this. Nevertheless, as we have demonstrated the efficacy of driving waves *in vitro*, understanding this interaction is important.

Moreover, current members of our lab plan to implement additional pertubations to the oscillator in our droplet system, effects that would be interesting to study in the wave context. For example, one member constructed a temperature gradient device and generated preliminary data on the effect of temperature on the clock. As a first attempt, we used this gradient to image our wave setup (Figure 5.1). Without analysis, it is impossible to quantify what, if any, effect temperature has on wave propagation. However, there is a readily apparent visual change in frequency across the temperature range, suggesting a plasubile effect.

While more complicated when considering waves—temperature would affect both diffusion and the clock itself—temperature dependence for the wave speed would be an interesting result. Furthermore, considering the existant work on the temperature dependence of sweep waves, such an experiment would dovetail nicely (Hayden, et al. 2022). In fact, with a method for increasing the frequency of oscillations, coupled with higher time resolution, one could accurately determine the activation-time scaling law for mitotic waves in *Xenopus*, as in

the work in *Drosphila* (Vergassola, et al., 2018). Taken together, this future work would help further solidify the field's detailed knowledge of how organisms transmit mitotic information across great lengths, but also provide fundamental information regarding the nature of biochemical waves generally, trigger or otherwise.

5.3 Conclusion

Together, in addition to offering the first look into time-dependent wave behavior, this work sets the stage for countless further experiments. Unfortunately, due to the ongoing pandemic, resulting supply chain issues, and, not least of all, time, I was unable to perform this wide array of work. Nonetheless, I look forward to future lab members tackling this challenge and am excited to read about these advancements in the near future.

Bibliography

Afanzar, O., Buss, G. K., Stearns, T., & Ferrell, J. E., Jr. (2020). The nucleus serves as the pacemaker for the cell cycle. *ELife*, *9*, e59989. https://doi.org/10.7554/eLife.59989

Ainsworth, M., Lee, S., Cunningham, M. O., Traub, R. D., Kopell, N. J., & Whittington, M. A. (2012). Rates and Rhythms: A Synergistic View of Frequency and Temporal Coding in Neuronal Networks. *Neuron*, *75*(4), 572–583. https://doi.org/10.1016/j.neuron.2012.08.004

Anderson, G. A., Gelens, L., Baker, J. C., & Ferrell, J. E. (2017). Desynchronizing Embryonic Cell Division Waves Reveals the Robustness of Xenopus laevis Development. *Cell Reports*, *21*(1), 37–46. https://doi.org/10.1016/j.celrep.2017.09.017

Baldin, V., & Ducommun, B. (1995). Subcellular localisation of human wee1 kinase is regulated during the cell cycle. *Journal of Cell Science*, *108*(6), 2425–2432. https://doi.org/10.1242/jcs.108.6.2425

Bell-Pedersen, D., Cassone, V. M., Earnest, D. J., Golden, S. S., Hardin, P. E., Thomas, T. L., & Zoran, M. J. (2005). Circadian rhythms from multiple oscillators: Lessons from diverse organisms. *Nature Reviews. Genetics*, *6*(7), 544–556. https://doi.org/10.1038/nrg1633

Bement, W. M., Leda, M., Moe, A. M., Kita, A. M., Larson, M. E., Golding, A. E., Pfeuti, C., Su, K.-C., Miller, A. L., Goryachev, A. B., & von Dassow, G. (2015). Activator–inhibitor coupling between Rho signalling and actin assembly makes the cell cortex an excitable medium. *Nature Cell Biology*, *17*(11), Article 11. https://doi.org/10.1038/ncb3251

Bernitt, E., Döbereiner, H.-G., Gov, N. S., & Yochelis, A. (2017). Fronts and waves of actin polymerization in a bistability-based mechanism of circular dorsal ruffles. *Nature Communications*, *8*(1), Article 1. https://doi.org/10.1038/ncomms15863

Beta, C., & Kruse, K. (2017). Intracellular Oscillations and Waves. *Annual Review of Condensed Matter Physics*, *8*(1), 239–264. https://doi.org/10.1146/annurev-conmatphys-031016-025210

Bonnet, J., Coopman, P., & Morris, M. C. (2008). Characterization of centrosomal localization and dynamics of Cdc25C phosphatase in mitosis. *Cell Cycle*, *7*(13), 1991–1998. https://doi.org/10.4161/cc.7.13.6095

Brown, H., Difrancesco, D., & Noble, S. (1979). Cardiac pacemaker oscillation and its modulation by autonomic transmitters. *The Journal of Experimental Biology*, *81*, 175–

204. https://doi.org/10.1242/jeb.81.1.175

Bub, G., Shrier, A., & Glass, L. (2002). Spiral Wave Generation in Heterogeneous Excitable Media. *Physical Review Letters*, *88*(5), 058101. https://doi.org/10.1103/PhysRevLett.88.058101

Bub, G., Shrier, A., & Glass, L. (2005). Global Organization of Dynamics in Oscillatory Heterogeneous Excitable Media. *Physical Review Letters*, *94*(2), 028105. https://doi.org/10.1103/PhysRevLett.94.028105

Bugrim, A. E., Dolnik, M., Zhabotinsky, A. M., & Epstein, I. R. (1996). Heterogeneous Sources of Target Patterns in Reaction−Diffusion Systems. *The Journal of Physical Chemistry*, *100*(49), 19017–19022. https://doi.org/10.1021/jp961603t

Cai, L., Dalal, C. K., & Elowitz, M. B. (2008). Frequency-modulated nuclear localization bursts coordinate gene regulation. *Nature*, *455*(7212), 485–490. https://doi.org/10.1038/nature07292

Carlson, E. D., Gan, R., Hodgman, C. E., & Jewett, M. C. (2012). Cell-free protein synthesis: Applications come of age. *Biotechnology Advances*, *30*(5), 1185–1194. https://doi.org/10.1016/j.biotechadv.2011.09.016

Chang, J. B., & Ferrell, J. E. (2018). Robustly Cycling Xenopus laevis Cell-Free Extracts in Teflon Chambers. *Cold Spring Harbor Protocols*, *2018*(8), pdb.prot097212. https://doi.org/10.1101/pdb.prot097212

Chang, J. B., & Ferrell Jr, J. E. (2013). Mitotic trigger waves and the spatial coordination of the Xenopus cell cycle. *Nature*, *500*(7464), Article 7464. https://doi.org/10.1038/nature12321

Cheng, X., & Ferrell, J. E. (2018). Apoptosis propagates through the cytoplasm as trigger waves. *Science*, *361*(6402), 607–612. https://doi.org/10.1126/science.aah4065

Cheng, X., & Ferrell, J. E. (2019). Spontaneous emergence of cell-like organization in Xenopus egg extracts. *Science*, *366*(6465), 631–637. https://doi.org/10.1126/science.aav7793

Cicenas, J., Kalyan, K., Sorokinas, A., Stankunas, E., Levy, J., Meskinyte, I., Stankevicius, V., Kaupinis, A., & Valius, M. (2015). Roscovitine in cancer and other diseases. *Annals of Translational Medicine*, *3*(10), 135. https://doi.org/10.3978/j.issn.2305-5839.2015.03.61

Cross, M. C., & Hohenberg, P. C. (1993). Pattern formation outside of equilibrium. *Reviews of Modern Physics*, *65*(3), 851–1112. https://doi.org/10.1103/RevModPhys.65.851

Dawson, S. P., Keizer, J., & Pearson, J. E. (1999). Fire–diffuse–fire model of dynamics of intracellular calcium waves. *Proceedings of the National Academy of Sciences*, *96*(11), 6060–6063. https://doi.org/10.1073/pnas.96.11.6060

Deming, P., & Kornbluth, S. (2006). Study of Apoptosis In Vitro Using the Xenopus Egg Extract

Reconstitution System. In X. J. Liu (Ed.), *Xenopus Protocols: Cell Biology and Signal Transduction* (pp. 379–393). Humana Press. https://doi.org/10.1007/978-1-59745-000-3_27

Deneke, V. E., & Di Talia, S. (2018). Chemical waves in cell and developmental biology. *Journal of Cell Biology*, *217*(4), 1193–1204. https://doi.org/10.1083/jcb.201701158

Deneke, V. E., Melbinger, A., Vergassola, M., & Di Talia, S. (2016). Waves of Cdk1 Activity in S Phase Synchronize the Cell Cycle in Drosophila Embryos. *Developmental Cell*, *38*(4), 399–412. https://doi.org/10.1016/j.devcel.2016.07.023

Deneke, V. E., Puliafito, A., Krueger, D., Narla, A. V., De Simone, A., Primo, L., Vergassola, M., De Renzis, S., & Di Talia, S. (2019). Self-Organized Nuclear Positioning Synchronizes the Cell Cycle in Drosophila Embryos. *Cell*, *177*(4), 925-941.e17. https://doi.org/10.1016/j.cell.2019.03.007

Dunphy, W. G., Brizuela, L., Beach, D., & Newport, J. (1988). The Xenopus cdc2 protein is a component of MPF, a cytoplasmic regulator of mitosis. *Cell*, *54*(3), 423–431. https://doi.org/10.1016/0092-8674(88)90205-X

Evans, T., Rosenthal, E. T., Youngblom, J., Distel, D., & Hunt, T. (1983). Cyclin: A protein specified by maternal mRNA in sea urchin eggs that is destroyed at each cleavage division. *Cell*, *33*(2), 389–396. https://doi.org/10.1016/0092-8674(83)90420-8

Ferrell, J. E. (2008). Feedback regulation of opposing enzymes generates robust, all-or-none bistable responses. *Current Biology*, *18*(6), R244–R245. https://doi.org/10.1016/j.cub.2008.02.035

Field, C. M., Pelletier, J. F., & Mitchison, T. J. (2017). Xenopus extract approaches to studying microtubule organization and signaling in cytokinesis. *Methods in Cell Biology*, *137*, 395–435. https://doi.org/10.1016/bs.mcb.2016.04.014

FitzHugh, R. (1961). Impulses and Physiological States in Theoretical Models of Nerve Membrane. *Biophysical Journal*, *1*(6), 445–466. https://doi.org/10.1016/S0006-3495(61)86902-6

Foe, V. E., & Alberts, B. M. (1983). Studies of nuclear and cytoplasmic behaviour during the five mitotic cycles that precede gastrulation in Drosophila embryogenesis. *Journal of Cell Science*, *61*(1), 31–70. https://doi.org/10.1242/jcs.61.1.31

Fontanilla, R. A., & Nuccitelli, R. (1998). Characterization of the Sperm-Induced Calcium Wave in Xenopus Eggs Using Confocal Microscopy. *Biophysical Journal*, *75*(4), 2079–2087. https://doi.org/10.1016/S0006-3495(98)77650-7

Forger, D. B. (2017). *Biological clocks, rhythms, and oscillations: The theory of biological timekeeping*. The MIT Press.

Forger, D. B., & Peskin, C. S. (2003). A detailed predictive model of the mammalian circadian

clock. *Proceedings of the National Academy of Sciences*, *100*(25), 14806–14811. https://doi.org/10.1073/pnas.2036281100

Fukujin, F., Nakajima, A., Shimada, N., & Sawai, S. (2016). Self-organization of chemoattractant waves in Dictyostelium depends on F-actin and cell–substrate adhesion. *Journal of The Royal Society Interface*, *13*(119), 20160233. https://doi.org/10.1098/rsif.2016.0233

Gautier, J., Minshull, J., Lohka, M., Glotzer, M., Hunt, T., & Maller, J. L. (1990). Cyclin is a component of maturation-promoting factor from Xenopus. *Cell*, *60*(3), 487–494. https://doi.org/10.1016/0092-8674(90)90599-a

Gautier, J., Norbury, C., Lohka, M., Nurse, P., & Maller, J. (1988). Purified maturation-promoting factor contains the product of a Xenopus homolog of the fission yeast cell cycle control gene cdc2+. *Cell*, *54*(3), 433–439. https://doi.org/10.1016/0092-8674(88)90206-1

Gavet, O., & Pines, J. (2010). Activation of cyclin B1–Cdk1 synchronizes events in the nucleus and the cytoplasm at mitosis. *Journal of Cell Biology*, *189*(2), 247–259. https://doi.org/10.1083/jcb.200909144

Gelens, L., Anderson, G. A., & Ferrell, J. E. (2014). Spatial trigger waves: Positive feedback gets you a long way. *Molecular Biology of the Cell*, *25*(22), 3486–3493. https://doi.org/10.1091/mbc.e14-08-1306

Gelens, L., Huang, K. C., & Ferrell, J. E. (2015). How Does the Xenopus laevis Embryonic Cell Cycle Avoid Spatial Chaos? *Cell Reports*, *12*(5), 892–900. https://doi.org/10.1016/j.celrep.2015.06.070

Gerhart, J. C. (1980). Mechanisms Regulating Pattern Formation in the Amphibian Egg and Early Embryo. In R. F. Goldberger (Ed.), *Biological Regulation and Development: Molecular Organization and Cell Function* (pp. 133–316). Springer US. https://doi.org/10.1007/978-1-4684-9933-9_4

Gerhart, J., Wu, M., Cyert, M., & Kirschner, M. (1985). M-phase promoting factors from eggs of Xenopus laevis. *Cytobios*, *43*(174S), 335–347.

Good, M. C., & Heald, R. (2018). Preparation of Cellular Extracts from Xenopus Eggs and Embryos. *Cold Spring Harbor Protocols*, *2018*(6), 10.1101/pdb.prot097055. https://doi.org/10.1101/pdb.prot097055

Grieger, J. A., & Norman, R. J. (2020). Menstrual Cycle Length and Patterns in a Global Cohort of Women Using a Mobile Phone App: Retrospective Cohort Study. *Journal of Medical Internet Research*, *22*(6), e17109. https://doi.org/10.2196/17109

Guan, Y., Li, Z., Wang, S., Barnes, P. M., Liu, X., Xu, H., Jin, M., Liu, A. P., & Yang, Q. (2018). A robust and tunable mitotic oscillator in artificial cells. *ELife*, *7*, e33549. https://doi.org/10.7554/eLife.33549

Hagan, P. S. (1981). Target patterns in reaction-diffusion systems. *Advances in Applied Mathematics*, *2*(4), 400–416. https://doi.org/10.1016/0196-8858(81)90042-7

Haim, D., Li, G., Ouyang, Q., McCormick, W. D., Swinney, H. L., Hagberg, A., & Meron, E. (1996). Breathing Spots in a Reaction-Diffusion System. *Physical Review Letters*, *77*(1), 190–193. https://doi.org/10.1103/PhysRevLett.77.190

Hartwell, L. H. (1971). Genetic control of the cell division cycle in yeast: II. Genes controlling DNA replication and its initiation. *Journal of Molecular Biology*, *59*(1), 183–194. https://doi.org/10.1016/0022-2836(71)90420-7

Hartwell, L. H., Mortimer, R. K., Culotti, J., & Culotti, M. (1973). GENETIC CONTROL OF THE CELL DIVISION CYCLE IN YEAST: V. GENETIC ANALYSIS OF cdc MUTANTS. *Genetics*, *74*(2), 267–286. https://doi.org/10.1093/genetics/74.2.267

Hayden, L., Hur, W., Vergassola, M., & Di Talia, S. (2022). Manipulating the nature of embryonic mitotic waves. *Current Biology*, *32*(22), 4989-4996.e3. https://doi.org/10.1016/j.cub.2022.10.014

Hu, Z., & Lutkenhaus, J. (1999). Topological regulation of cell division in Escherichia coli involves rapid pole to pole oscillation of the division inhibitor MinC under the control of MinD and MinE. *Molecular Microbiology*, *34*(1), 82–90. https://doi.org/10.1046/j.1365-2958.1999.01575.x

Huang, J., & Raff, J. W. (1999). The disappearance of cyclin B at the end of mitosis is regulated spatially in Drosophila cells. *The EMBO Journal*, *18*(8), 2184–2195. https://doi.org/10.1093/emboj/18.8.2184

Ishihara, K., Nguyen, P. A., Wühr, M., Groen, A. C., Field, C. M., & Mitchison, T. J. (2014). Organization of early frog embryos by chemical waves emanating from centrosomes. *Philosophical Transactions of the Royal Society B: Biological Sciences*, *369*(1650), 20130454. https://doi.org/10.1098/rstb.2013.0454

Isomura, A., & Kageyama, R. (2014). Ultradian oscillations and pulses: Coordinating cellular responses and cell fate decisions. *Development (Cambridge, England)*, *141*(19), 3627–3636. https://doi.org/10.1242/dev.104497

Jakubith, S., Rotermund, H. H., Engel, W., von Oertzen, A., & Ertl, G. (1990). Spatiotemporal concentration patterns in a surface reaction: Propagating and standing waves, rotating spirals, and turbulence. *Physical Review Letters*, *65*(24), 3013–3016. https://doi.org/10.1103/PhysRevLett.65.3013

Jin, M., Tavella, F., Wang, S., & Yang, Q. (2022). In vitro cell cycle oscillations exhibit a robust and hysteretic response to changes in cytoplasmic density. *Proceedings of the National Academy of Sciences*, *119*(6), e2109547119. https://doi.org/10.1073/pnas.2109547119

Kheowan, O.-U., Mihaliuk, E., Blasius, B., Sendiña-Nadal, I., & Showalter, K. (2007). Wave Mediated Synchronization of Nonuniform Oscillatory Media. *Physical Review Letters*,

98(7), 074101. https://doi.org/10.1103/PhysRevLett.98.074101

Kim, S. Y., & Ferrell, J. E. (2007). Substrate Competition as a Source of Ultrasensitivity in the Inactivation of Wee1. *Cell*, *128*(6), 1133–1145. https://doi.org/10.1016/j.cell.2007.01.039

Kopell, N. (1981). Target pattern solutions to reaction-diffusion equations in the presence of impurities. *Advances in Applied Mathematics*, *2*(4), 389–399. https://doi.org/10.1016/0196-8858(81)90041-5

Kumagai, A., & Dunphy, W. G. (1992). Regulation of the cdc25 protein during the cell cycle in Xenopus extracts. *Cell*, *70*(1), 139–151. https://doi.org/10.1016/0092-8674(92)90540-S

Kuramoto, Y. (1984). Chemical Waves. In Y. Kuramoto (Ed.), *Chemical Oscillations, Waves, and Turbulence* (pp. 89–110). Springer. https://doi.org/10.1007/978-3-642-69689-3_6

Lakhia, R., Mishra, A., & Patel, V. (2019). Chapter 7—Manipulation of renal gene expression using oligonucleotides. In T. Weimbs (Ed.), *Methods in Cell Biology* (Vol. 154, pp. 109–120). Academic Press. https://doi.org/10.1016/bs.mcb.2019.05.006

Lechleiter, J., Girard, S., Peralta, E., & Clapham, D. (1991). Spiral Calcium Wave Propagation and Annihilation in Xenopus laevis Oocytes. *Science*, *252*(5002), 123–126. https://doi.org/10.1126/science.2011747

Lee, K. J., Cox, E. C., & Goldstein, R. E. (1996). Competing Patterns of Signaling Activity in Dictyostelium Discoideum. *Physical Review Letters*, *76*(7), 1174–1177. https://doi.org/10.1103/PhysRevLett.76.1174

Li, Z., Wang, S., Sun, M., Jin, M., Khain, D., & Yang, Q. (2021). *High-resolution mapping of the period landscape reveals polymorphism in cell cycle frequency tuning* (p. 2021.05.10.442602). bioRxiv. https://doi.org/10.1101/2021.05.10.442602

Li, Z., & Yang, Q. (2018). Systems and synthetic biology approaches in understanding biological oscillators. *Quantitative Biology (Beijing, China)*, *6*(1), 1–14. https://doi.org/10.1007/s40484-017-0120-7

Lohka, M. J., Hayes, M. K., & Maller, J. L. (1988). Purification of maturation-promoting factor, an intracellular regulator of early mitotic events. *Proceedings of the National Academy of Sciences*, *85*(9), 3009–3013. https://doi.org/10.1073/pnas.85.9.3009

Lohka, M. J., & Maller, J. L. (1985). Induction of nuclear envelope breakdown, chromosome condensation, and spindle formation in cell-free extracts. *Journal of Cell Biology*, *101*(2), 518–523. https://doi.org/10.1083/jcb.101.2.518

Luther, R. (1906). II. Sitzung am Dienstag, den 22. Mai, vormittags 9 Uhr, im grossen Auditorium des chemischen Laboratoriums der Technischen Hochschule. Räumliche Fortpflanzung chemischer Reaktionen. *Zeitschrift Für Elektrochemie Und Angewandte Physikalische Chemie*, *12*(32), 596–600. https://doi.org/10.1002/bbpc.19060123208

Maryu, G., & Yang, Q. (2022). Nuclear-cytoplasmic compartmentalization of cyclin B1-Cdk1 promotes robust timing of mitotic events. *Cell Reports*, *41*(13), 111870. https://doi.org/10.1016/j.celrep.2022.111870

Masui, Y., & Markert, C. L. (1971). Cytoplasmic control of nuclear behavior during meiotic maturation of frog oocytes. *Journal of Experimental Zoology*, *177*(2), 129–145. https://doi.org/10.1002/jez.1401770202

McNamara, H. M., Zhang, H., Werley, C. A., & Cohen, A. E. (2016). Optically Controlled Oscillators in an Engineered Bioelectric Tissue. *Physical Review X*, *6*(3), 031001. https://doi.org/10.1103/PhysRevX.6.031001

Mikhailov, A. S., & Engel, A. (1986). Multiple target pattern creation and synchronization phenomena. *Physics Letters A*, *117*(5), 257–260. https://doi.org/10.1016/0375-9601(86)90088-5

Mueller, P. R., Coleman, T. R., & Dunphy, W. G. (1995). Cell cycle regulation of a Xenopus Wee1-like kinase. *Molecular Biology of the Cell*, *6*(1), 119–134. https://doi.org/10.1091/mbc.6.1.119

Murray, A. W. (1991). Chapter 30 Cell Cycle Extracts. In B. K. Kay & H. B. Peng (Eds.), *Methods in Cell Biology* (Vol. 36, pp. 581–605). Academic Press. https://doi.org/10.1016/S0091-679X(08)60298-8

Murray, A. W., & Kirschner, M. W. (1989). Cyclin synthesis drives the early embryonic cell cycle. *Nature*, *339*(6222), Article 6222. https://doi.org/10.1038/339275a0

Murray, A. W., Solomon, M. J., & Kirschner, M. W. (1989). The role of cyclin synthesis and degradation in the control of maturation promoting factor activity. *Nature*, *339*(6222), Article 6222. https://doi.org/10.1038/339280a0

Nakajima, M., Imai, K., Ito, H., Nishiwaki, T., Murayama, Y., Iwasaki, H., Oyama, T., & Kondo, T. (2005). Reconstitution of Circadian Oscillation of Cyanobacterial KaiC Phosphorylation in Vitro. *Science*, *308*(5720), 414–415. https://doi.org/10.1126/science.1108451

Newmeyer, D. d., Lucocq, J. m., Bürglin, T. r., & De Robertis, E. m. (1986). Assembly in vitro of nuclei active in nuclear protein transport: ATP is required for nucleoplasmin accumulation. *The EMBO Journal*, *5*(3), 501–510. https://doi.org/10.1002/j.1460-2075.1986.tb04239.x

Nolet, F. E., & Gelens, L. (2021). Mitotic waves in an import-diffusion model with multiple nuclei in a shared cytoplasm. *Biosystems*, *208*, 104478. https://doi.org/10.1016/j.biosystems.2021.104478

Nolet, F. E., Rombouts, J., & Gelens, L. (2020). Synchronization in reaction–diffusion systems with multiple pacemakers. *Chaos: An Interdisciplinary Journal of Nonlinear Science*, *30*(5), 053139. https://doi.org/10.1063/5.0002251

Nolet, F. E., Vandervelde, A., Vanderbeke, A., Piñeros, L., Chang, J. B., & Gelens, L. (2020). Nuclei determine the spatial origin of mitotic waves. *ELife*, *9*, e52868. https://doi.org/10.7554/eLife.52868

Novak, B., & Tyson, J. J. (1993a). Modeling the Cell Division Cycle: M-phase Trigger, Oscillations, and Size Control. *Journal of Theoretical Biology*, *165*(1), 101–134. https://doi.org/10.1006/jtbi.1993.1179

Novak, B., & Tyson, J. J. (1993b). Numerical analysis of a comprehensive model of M-phase control in Xenopus oocyte extracts and intact embryos. *Journal of Cell Science*, *106*(4), 1153–1168. https://doi.org/10.1242/jcs.106.4.1153

Novák, B., & Tyson, J. J. (2008). Design principles of biochemical oscillators. *Nature Reviews Molecular Cell Biology*, *9*(12), Article 12. https://doi.org/10.1038/nrm2530

Nurse, P. (1975). Genetic control of cell size at cell division in yeast. *Nature*, *256*(5518), Article 5518. https://doi.org/10.1038/256547a0

Nurse, P. (1985). Cell cycle control genes in yeast. *Trends in Genetics*, *1*, 51–55. https://doi.org/10.1016/0168-9525(85)90023-X

O'Farrell, P. H. (2015). Growing an Embryo from a Single Cell: A Hurdle in Animal Life. *Cold Spring Harbor Perspectives in Biology*, *7*(11), a019042. https://doi.org/10.1101/cshperspect.a019042

O'Farrell, P. H., Stumpff, J., & Tin Su, T. (2004). Embryonic Cleavage Cycles: How Is a Mouse Like a Fly? *Current Biology*, *14*(1), R35–R45. https://doi.org/10.1016/j.cub.2003.12.022

Paydarfar, D., & Eldridge, F. L. (1987). Phase resetting and dysrhythmic responses of the respiratory oscillator. *American Journal of Physiology-Regulatory, Integrative and Comparative Physiology*, *252*(1), R55–R62. https://doi.org/10.1152/ajpregu.1987.252.1.R55

Perez-Mongiovi, D., Chang, P., & Houliston, E. (1998). A propagated wave of MPF activation accompanies surface contraction waves at first mitosis in Xenopus. *Journal of Cell Science*, *111*(3), 385–393. https://doi.org/10.1242/jcs.111.3.385

Pomerening, J. R., Sontag, E. D., & Ferrell, J. E. (2003). Building a cell cycle oscillator: Hysteresis and bistability in the activation of Cdc2. *Nature Cell Biology*, *5*(4), Article 4. https://doi.org/10.1038/ncb954

Preibisch, S., Saalfeld, S., & Tomancak, P. (2009). Globally optimal stitching of tiled 3D microscopic image acquisitions. *Bioinformatics*, *25*(11), 1463–1465. https://doi.org/10.1093/bioinformatics/btp184

Puls, O., & Yang, Q. (2018). The Rise of Ultrafast Waves. *Developmental Cell*, *47*(5), 532–534. https://doi.org/10.1016/j.devcel.2018.11.026

Rabinovitch, A., Gutman, M., & Aviram, I. (2001). Inwards Propagating Waves in a Limit Cycle Medium. *Physical Review Letters*, *87*(8), 084101. https://doi.org/10.1103/PhysRevLett.87.084101

Rankin, S., & Kirschner, M. W. (1997). The surface contraction waves of Xenopus eggs reflect the metachronous cell-cycle state of the cytoplasm. *Current Biology*, *7*(6), 451–454. https://doi.org/10.1016/S0960-9822(06)00192-8

Reimann, J. D. R., & Jackson, P. K. (2002). Emi1 is required for cytostatic factor arrest in vertebrate eggs. *Nature*, *416*(6883), Article 6883. https://doi.org/10.1038/416850a

Rombouts, J., & Gelens, L. (2020). Synchronizing an oscillatory medium: The speed of pacemaker-generated waves. *Physical Review Research*, *2*(4), 043038. https://doi.org/10.1103/PhysRevResearch.2.043038

Rombouts, J., & Gelens, L. (2021a). Analytical approximations for the speed of pacemaker-generated waves. *Physical Review E*, *104*(1), 014220. https://doi.org/10.1103/PhysRevE.104.014220

Rombouts, J., & Gelens, L. (2021b). Dynamic bistable switches enhance robustness and accuracy of cell cycle transitions. *PLOS Computational Biology*, *17*(1), e1008231. https://doi.org/10.1371/journal.pcbi.1008231

Rombouts, J., Gelens, L., & Erneux, T. (2019). Travelling fronts in time-delayed reaction–diffusion systems. *Philosophical Transactions of the Royal Society A: Mathematical, Physical and Engineering Sciences*, *377*(2153), 20180127. https://doi.org/10.1098/rsta.2018.0127

Russell, P., & Nurse, P. (1986). Cdc25+ functions as an inducer in the mitotic control of fission yeast. *Cell*, *45*(1), 145–153. https://doi.org/10.1016/0092-8674(86)90546-5

Russell, P., & Nurse, P. (1987). Negative regulation of mitosis by wee1+, a gene encoding a protein kinase homolog. *Cell*, *49*(4), 559–567. https://doi.org/10.1016/0092-8674(87)90458-2

Rust, M. J., Markson, J. S., Lane, W. S., Fisher, D. S., & O'Shea, E. K. (2007). Ordered Phosphorylation Governs Oscillation of a Three-Protein Circadian Clock. *Science*, *318*(5851), 809–812. https://doi.org/10.1126/science.1148596

Santos, S. D. M., Wollman, R., Meyer, T., & Ferrell, J. E. (2012). Spatial Positive Feedback at the Onset of Mitosis. *Cell*, *149*(7), 1500–1513. https://doi.org/10.1016/j.cell.2012.05.028

Schindelin, J., Arganda-Carreras, I., Frise, E., Kaynig, V., Longair, M., Pietzsch, T., Preibisch, S., Rueden, C., Saalfeld, S., Schmid, B., Tinevez, J.-Y., White, D. J., Hartenstein, V., Eliceiri, K., Tomancak, P., & Cardona, A. (2012). Fiji: An open-source platform for biological-image analysis. *Nature Methods*, *9*(7), Article 7. https://doi.org/10.1038/nmeth.2019

Schmidt, A., Duncan, P. I., Rauh, N. R., Sauer, G., Fry, A. M., Nigg, E. A., & Mayer, T. U. (2005). Xenopus polo-like kinase Plx1 regulates XErp1, a novel inhibitor of APC/C activity. *Genes & Development*, *19*(4), 502–513. https://doi.org/10.1101/gad.320705

Schmidt, A., Rauh, N. R., Nigg, E. A., & Mayer, T. U. (2006). Cytostatic factor: An activity that puts the cell cycle on hold. *Journal of Cell Science*, *119*(7), 1213–1218. https://doi.org/10.1242/jcs.02919

Sha, W., Moore, J., Chen, K., Lassaletta, A. D., Yi, C.-S., Tyson, J. J., & Sible, J. C. (2003). Hysteresis drives cell-cycle transitions in Xenopus laevis egg extracts. *Proceedings of the National Academy of Sciences*, *100*(3), 975–980. https://doi.org/10.1073/pnas.0235349100

Shinagawa, A., Konno, S., Yoshimoto, Y., & Hiramoto, Y. (1989). Nuclear Involvement in Localization of the Initiation Site of Surface Contraction Waves in Xenopus Eggs. *Development, Growth & Differentiation*, *31*(3), 249–255. https://doi.org/10.1111/j.1440-169X.1989.00249.x

Smith, L. D., & Ecker, R. E. (1971). The interaction of steroids with Rana pipiens oocytes in the induction of maturation. *Developmental Biology*, *25*(2), 232–247. https://doi.org/10.1016/0012-1606(71)90029-7

Solomon, M. J., Glotzer, M., Lee, T. H., Philippe, M., & Kirschner, M. W. (1990). Cyclin activation of p34cdc2. *Cell*, *63*(5), 1013–1024. https://doi.org/10.1016/0092-8674(90)90504-8

Spirin, A. S., Baranov, V. I., Ryabova, L. A., Ovodov, S., & Alakhov, Y. B. (1988). A Continuous Cell-Free Translation System Capable of Producing Polypeptides in High Yield. *Science*, *242*(4882), 1162–1164. https://doi.org/10.1126/science.3055301

Stich, M., & Mikhailov, A. S. (2006). Target patterns in two-dimensional heterogeneous oscillatory reaction–diffusion systems. *Physica D: Nonlinear Phenomena*, *215*(1), 38–45. https://doi.org/10.1016/j.physd.2006.01.011

Stricker, S. A. (1999). Comparative Biology of Calcium Signaling during Fertilization and Egg Activation in Animals. *Developmental Biology*, *211*(2), 157–176. https://doi.org/10.1006/dbio.1999.9340

Swadlow, H. A., & Waxman, S. G. (2012). Axonal conduction delays. *Scholarpedia*, *7*(6), 1451. https://doi.org/10.4249/scholarpedia.1451

Takagi, J., & Shimamoto, Y. (2017). High-quality frozen extracts of Xenopus laevis eggs reveal size-dependent control of metaphase spindle micromechanics. *Molecular Biology of the Cell*, *28*(16), 2170–2177. https://doi.org/10.1091/mbc.E17-03-0174

Tang, Z., Coleman, T. r., & Dunphy, W. g. (1993). Two distinct mechanisms for negative regulation of the Wee1 protein kinase. *The EMBO Journal*, *12*(9), 3427–3436. https://doi.org/10.1002/j.1460-2075.1993.tb06017.x

Thron, C. D. (1996). A model for a bistable biochemical trigger of mitosis. *Biophysical Chemistry*, *57*(2), 239–251. https://doi.org/10.1016/0301-4622(95)00075-5

Tomchik, K. J., & Devreotes, P. N. (1981). Adenosine 3′,5′-Monophosphate Waves in Dictyostelium discoideum: A Demonstration by Isotope Dilution—Fluorography. *Science*, *212*(4493), 443–446. https://doi.org/10.1126/science.6259734

Trunnell, N. B., Poon, A. C., Kim, S. Y., & Ferrell, J. E. (2011). Ultrasensitivity in the Regulation of Cdc25C by Cdk1. *Molecular Cell*, *41*(3), 263–274. https://doi.org/10.1016/j.molcel.2011.01.012

Tsai, T. Y.-C., Theriot, J. A., & Jr, J. E. F. (2014). Changes in Oscillatory Dynamics in the Cell Cycle of Early Xenopus laevis Embryos. *PLOS Biology*, *12*(2), e1001788. https://doi.org/10.1371/journal.pbio.1001788

Tuck, C., Zhang, T., Potapova, T., Malumbres, M., & Novák, B. (2013). Robust mitotic entry is ensured by a latching switch. *Biology Open*, *2*(9), 924–931. https://doi.org/10.1242/bio.20135199

Tunquist, B. J., & Maller, J. L. (2003). Under arrest: Cytostatic factor (CSF)-mediated metaphase arrest in vertebrate eggs. *Genes & Development*, *17*(6), 683–710. https://doi.org/10.1101/gad.1071303

Tyson, J. J., & Fife, P. C. (1980). Target patterns in a realistic model of the Belousov–Zhabotinskii reaction. *The Journal of Chemical Physics*, *73*(5), 2224–2237. https://doi.org/10.1063/1.440418

Tyson, J. J., & Keener, J. P. (1988). Singular perturbation theory of traveling waves in excitable media (a review). *Physica D: Nonlinear Phenomena*, *32*(3), 327–361. https://doi.org/10.1016/0167-2789(88)90062-0

Tyson, J. J., & Novak, B. (2015). Bistability, Oscillations, and Traveling Waves in Frog Egg Extracts. *Bulletin of Mathematical Biology*, *77*(5), 796–816. https://doi.org/10.1007/s11538-014-0009-9

Vergassola, M., Deneke, V. E., & Di Talia, S. (2018). Mitotic waves in the early embryogenesis of Drosophila: Bistability traded for speed. *Proceedings of the National Academy of Sciences*, *115*(10), E2165–E2174. https://doi.org/10.1073/pnas.1714873115

Wagner, J., Li, Y.-X., Pearson, J., & Keizer, J. (1998). Simulation of the Fertilization Ca2+ Wave in Xenopus laevis Eggs. *Biophysical Journal*, *75*(4), 2088–2097. https://doi.org/10.1016/S0006-3495(98)77651-9

Walgraef, D., Dewel, G., & Borckmans, P. (1983). Chemical waves in a two-dimensional oscillating system. *The Journal of Chemical Physics*, *78*(6), 3043–3051. https://doi.org/10.1063/1.445266

Winfree, A. T. (1974). Two kinds of wave in an oscillating chemical solution. *Faraday Symposia*

of the Chemical Society, *9*(0), 38–46. https://doi.org/10.1039/FS9740900038

Winfree, A. T., & Tyson, J. J. (1988). When Time Breaks Down: The Three-Dimensional Dynamics of Electrochemical Waves and Cardiac Arrhythmias. *Physics Today*, *41*(12), 107–109. https://doi.org/10.1063/1.2811674

Yamamoto, T. M., Iwabuchi, M., Ohsumi, K., & Kishimoto, T. (2005). APC/C-Cdc20-mediated degradation of cyclin B participates in CSF arrest in unfertilized Xenopus eggs. *Developmental Biology*, *279*(2), 345–355. https://doi.org/10.1016/j.ydbio.2004.12.025

Yang, Q., & Ferrell, J. E. (2013). The Cdk1–APC/C cell cycle oscillator circuit functions as a time-delayed, ultrasensitive switch. *Nature Cell Biology*, *15*(5), Article 5. https://doi.org/10.1038/ncb2737

Zaikin, A. N., & Zhabotinsky, A. M. (1970). Concentration Wave Propagation in Two-dimensional Liquid-phase Self-oscillating System. *Nature*, *225*(5232), Article 5232. https://doi.org/10.1038/225535b0

Zhabotinskii, A. M. (1964). [PERIODIC COURSE OF THE OXIDATION OF MALONIC ACID IN A SOLUTION (STUDIES ON THE KINETICS OF BEOLUSOV'S REACTION)]. *Biofizika*, *9*, 306–311.

Zhabotinsky, A. M., & Zaikin, A. N. (1973). Autowave processes in a distributed chemical system. *Journal of Theoretical Biology*, *40*(1), 45–61. https://doi.org/10.1016/0022-5193(73)90164-1

Zieske, K., Chwastek, G., & Schwille, P. (2016). Protein Patterns and Oscillations on Lipid Monolayers and in Microdroplets. *Angewandte Chemie International Edition*, *55*(43), 13455–13459. https://doi.org/10.1002/anie.201606069

Zieske, K., & Schwille, P. (2014). Reconstitution of self-organizing protein gradients as spatial cues in cell-free systems. *ELife*, *3*, e03949. https://doi.org/10.7554/eLife.03949

Zwicker, D. (2020). py-pde: A Python package for solving partial differential equations. *Journal of Open Source Software*, *5*(48), 2158. https://doi.org/10.21105/joss.02158